12-2020

IDENTIFICATION OF MICRORNAs RELATED TO TYPE 2 DIABETIC OSTEOPATH

Mouza Mohammed Saeed Alfashti Alaleeli

United Arab Emirates University

College of Medicine and Health Sciences

Department of Biochemistry

IDENTIFICATION OF MICRORNAs RELATED TO TYPE 2
DIABETIC OSTEOPATHY

Mouza Mohammed Saeed Alfashti Alaleeli

This thesis is submitted in partial fulfilment of the requirements for the degree of
Master of Medical Sciences (Biochemistry and Molecular Biology)

Under the Supervision of Dr. Sahar Mohsin

December 2020

Declaration of Original Work

I, Mouza Mohammed Saeed Alfashti Alaleeli, the undersigned, a graduate student at the United Arab Emirates University (UAEU), and the author of this thesis entitled *"Identification of MicroRNAs Related to Type 2 Diabetic Osteopathy"*, hereby, solemnly declare that this thesis is my own original research work that has been done and prepared by me under the supervision of Dr. Sahar Mohsin, in the College of Medicine and Health Sciences at UAEU. This work has not previously been presented or published, or formed the basis for the award of any academic degree, diploma or a similar title at this or any other university. Any materials borrowed from other sources (whether published or unpublished) and relied upon or included in my thesis have been properly cited and acknowledged in accordance with appropriate academic conventions. I further declare that there is no potential conflict of interest with respect to the research, data collection, authorship, presentation and/ or publication of this thesis.

Student's Signature: _____   Date: 14-October-2020

Advisory Committee

1) Advisor: Sahar Mohsin

Title: Assistant Professor

Department of Anatomy

College of Medicine and Health Sciences

2) Member: Farah Mustafa

Title: Associate Professor

Department of Biochemistry

College of Medicine and Health Sciences

3) Member: Suraiya Ansari

Title: Associate Professor

Department of Biochemistry

College of Medicine and Health Sciences

Approval of the Master Thesis

This Master Thesis is approved by the following Examining Committee Members:

1) Advisor (Committee Chair): Sahar Mohsin

   Title: Assistant Professor

   Department of Anatomy

   College of Medicine and Health Sciences

   Signature _____   Date 16/12/2020

2) Member: Ernest A. Adeghate

   Title: Professor

   Department of Anatomy

   College of Medicine and Health Sciences

   Signature _____   Date 16/12/2020

3) Member (External Examiner): Alam Nur-E-Kamal

   Title: Professor

   Department of Biology
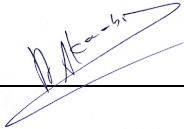
   Institution: The City University of New York, USA

   Signature _____   Date 16/12/2020

This Master Thesis is accepted by:

Acting Dean of the College of Medicine and Health Sciences: Professor Juma Alkaabi

Signature _____   Date 25 January 2021

Dean of the College of Graduate Studies: Professor Ali Al-Marzouqi

Signature _____   Date   25 January 2021

Copy _____ of _____

Abstract

T2DM is linked to an increase in the fracture rate as compared to the non-diabetic population even with normal or raised Bone Mineral Density (BMD). Previous studies have addressed the question of how T2DM induces osteoporosis; the exact underlying mechanism is still elusive. Bones undergo continuous remodeling throughout life. Bone remodeling implicates the coupling of osteoclastic bone resorption and osteoblastic bone formation. This process is controlled by numerous genetic, hormonal, and neurogenic mechanisms. Osteoporosis is a result of bone loss that occurs by uncoupled remodeling. The existing evidence indicates that short non-coding RNAs known as microRNAs (miRNAs), are the key post-transcriptional repressors of gene expression, and growing numbers of novel miRNAs have been verified to play vital roles in the regulation of osteogenesis, osteoclastogenesis, and adipogenesis, revealing how they interact with signaling molecules to control these processes. This study aims to identify the changes in miRNAs levels related to the bone remodeling cycle in bones of type 2 diabetic rats. Three-month-old female Wistar rats (n=24) were obtained from the animal house facility at United Arab Emirates University for this study. All animal procedures were approved by the animal ethical committee at United Arab Emirates University (ERA_2017_5597). Animals (n=12) were fed with a high-calorie diet (D12492 diet; Research Diets, Inc, USA) for 3 weeks followed by injection of two lower doses of STZ (30 mg/kg intraperitoneally) which was administered at weekly intervals. Rats having blood glucose >15 mmol/liter were considered as diabetic and were used for this study. The animals were sacrificed after 8, 10, and 14 weeks of the onset of diabetes. The tibia was dissected out and used for the extraction of miRNAs using the mirVana™miRNA isolation kit provided by Ambion (AM 1560). miRNAs known to be related to bone metabolism were assayed by quantitative RT-PCR using Taqman probes and primers (4427975, Thermofisher Scientific) in the serum and bone tissue samples. This study revealed that in 8 weeks of the duration of T2DM, the dysregulation of miR-20a, miR-21, miR-29a, miR-31, and miR-155 affects the bone remodeling cycle by promoting osteoclastogenesis and suppressing osteoblast differentiation. In 10 weeks of the duration of T2DM, the dysregulation of miR-20a, miR-21, miR-29a, miR-31, and miR-155 affects the bone remodeling cycle by suppressing osteoclastogenesis, and suppressing bone formation.

In 14 weeks of the duration of T2DM, the dysregulation of miR-20a, miR-21, miR-29a, miR-31, and miR-155 affects the bone remodeling cycle by suppressing both osteoclastogenesis and osteoblast differentiation. Moreover, miR-21 and miR-155 could be used as potential serum biomarkers.

The study concludes that the longer duration of T2DM adversely affects the bone, indicating an increased bone fragility. The research project resulted in a novel and innovative perspective in defining the mechanism of osteoporosis in type 2 diabetes mellitus through miRNAs with the potential to be used as diagnostic biomarkers to assess fracture risk or therapeutic targets for type 2 diabetic osteopathy.

Keywords: Type 2 diabetes mellitus, osteoporosis, bone remodeling cycle, microRNAs.

Title and Abstract (in Arabic)

تحديد المايكرو آر إنات (microRNAs) المرتبطة بأمراض العظام في مرض السكري النوع الثاني

الملخص

مرض السكري النوع الثاني مرتبط بعلو في نسبة الكسور مقارنة بالسكان الذين لا يعانون من مرض السكري حتى مع كثافة طبيعية أو عالية في معادن العظام. الدراسات السابقة تطرقت إلى السؤال في كيف لمرض السكري النوع الثاني أن يسبب مرض هشاشة العظام؛ الآلية الأساسية الدقيقة لهذا الشيء .لاال مبهمة. تخضع العظام لعملية إعادة تشكيل مستمرة طوال الحياة. تنطوي عملية إعادة تشكيل العظام على اقتران عملية امتصاص العظم و تكوين العظم. يتم التحكم في هذه العملية من خلال العديد من الآليات الجينية و الهرمونية و العصبية. مرض هشاشة العظام هي نتاج لفقد العظام الذي يحدث من خلال عملية إعادة تشكيل العظام الغير مقترنةالألياً الأدلة الموجودة إلى أن الألألأاض النووية الرايبوزية القصيرة و الغير مشفرة المعروفة باسم المايكرو آر إنات (microRNAs)، هي المثبطات الرئيسية للتعبير الجيني بعد عملية النسخ-post) (transcription، و قد تم الـ تحقق من أعداد متزايدة من المايكرو آر إنات الجديدة لتلعب أدواراً حيوية في تنظيم تكون خلايا تكوين العظم (osteogenesis)، تكون خلايا امتصاص العظم (osteoclastogenesis)، تكون خلايا تكوين الشحم (adipogenesis)، يكشف عن كيفية تفاعلها مع جزيئات الإشارة (signaling molecules) للتحكم في هذه العـلليات التنظيمية. الهدف من هذه الدراسة هي تحديد التغيرات في مستوياتالمايكرو آر إنات المتعلقة بدورة إعادة تشكيل العظام في عظام الفئران المصابة بمرض السكري النوع الثاني. تم الحصول على إناث فئران الويستار (Wistar rats) البالغة من العمر ثلاثة أشهر (العدد=24) من مرفق جامعة الإمارات العربية المتحدة لهذه الدر ا... تمت الموافقة على جميع الإجراءات المتعلقة بالحيوانات من قبل لجنة أخلاقيات التعامل مع الحيوان بجامعة الإمارات العربية المتحدة (ERA_2017_5597). تم تغذية الحيوانات (العدد=12) بنظام غذائي (D12492diet; Research Diets, Inc, USA) عالي السعرات الحرارية لمدة 3 أسابيع متبوعاً بحقن جرعتين مخفضتين من الـSTZ (30 mg/kg intraperitoneally) و التي تم إعطاؤها على فترات أسبوعية. اعتبرت الفئران التي تحتوي على نسبة السكر في الدم أكثر من 15 ملي مول/لتر مصابة بمرض السكري و استخدمت في دراستنا. تم التضحية بالحيوانات بعد

8، 10 و 44 أسبوعاً من ظهور مرض السكري. تم تشريح عظمة الظنبوب (tibia) و تم استلالالا لاستخراج المايكرو آر إنات باستخدام طقم عزل المايكرو آر إنات من مولانا (mirVana) المقدمة من (Ambion (AM 1560. تم تقييم تعبير المايكرو آر إنات المتعلقة عملية الأيض العظمية بواسطة تحليل البي سي آر-الوقت الحقيقي الكمي (quantitative RT-PCR) باستخدام مسابير و بادئات تاق مان (Taqman probes and primers) في عينات ا لمصل و أنسجة العظم. نتج عن هذا المشروع البحثي منظور جديد و مبتكر في تحديد آلية مرض هشاشة العظام في مرض السكري النوع الثاني من خلال المايكرو آر إنات مع إمكانية استخدامها كمؤشرات بيولوجية تشخيصية لتقييم مخاطر الكسر أو الأهداف العلاجية لأمراض العظام في مرض السكري النوع الثا ني. كشفت هذه الدراسة أنه في 8 أسابيع من مدة الإصابة بمرض السكري النوع الثا ني، التنظيم المختل في المايكرو آر إن إيه-20a، المايكرو آر إن أيه-21، المايكرو آر إن أيه-29a، المايكرو آر إن أيه-31، و المايكرو آر إن أيه-155 أثر على دورة إعادة تش كيل العظام عن طريق قمع خلايا تكوين امتصاص العظم و خلايا تكوين العظم. في ال 10 أسابيع من مدة الإصابة بمرض السكري النوع الثا اني، التنظيم المختل في المايكرو آر إن إيه-20a، المايكرو آر إن أيه-21، المايكرو آر إن أيه-29a، المايكرو آر إن أيه-31، و المايكرو آر إن أيه-155 أثرعلى دورة إعادة تشكيل العظام عن طريق قمع خلايا تكوين امتصاص العظم و خلايا تكوين العظم. في ال 44 أسبوع من مدة الإصابة بمرض السكري النوع الثاني، التنظيم المختل في المايكرو آر إن إيه-20a، المايكرو آر إن أيه-21، المايكرو آر إن أيه-29a، المايكرو آر إن أيه-31، و المايكرو آر إن أيه-155 أثر على دورة إعادة تشكيل العظام عن طريق قمع خلايا تكوين امتصاص العظم و خلايا تكوين العظم. علاوة على ذلك، يمكن استخدام مايكرو آر إن أيه-21 و مايكرو آر إن أيه-155 كمؤشرات حيوية محتملة في مصل الدم. تشير الدراسة أيضاً إلى أن طول مدة الإصابة بمرض السكري النوع الثاني يؤثر سلباً على العظام، مما يشير إلى زيادة هشاشة العظام.

مفاهيم البحث الرئيسية: مرض السكري النوع الثاني، مرض هشاشة العظام، دورة إعادة تشكيل العظام، مايكرو آر إنات.

Acknowledgments

Dedication

To my beloved late grandmother (Sallma Salem AlAleeli)

Table of Contents

List of Tables

List of Figures

List of Abbreviations

ACTB	Actin-Beta
ATG16L1	Autophagy Related 16 Like 1
BAMBI	Bone Morphogenetic Proteins and Activin Membrane-Bound Inhibitor
BMD	Bone Mineral Density
BMP2	Bone Morphogenetic Protein 2
BMP3	Bone Morphogenetic Protein 3
CALCA	Calcitonin Related Polypeptide Alpha
CRIM1	Cysteine-Rich Motor Neuron 1
CTD	Carboxyl-Terminal Domain
CTSK	Cathepsin K
DKK1	Dikkopf 1
DEXA	Dual-Energy X-Ray Absorptiometry
ELISA	Enzyme-Linked Immunosorbent Assay
GI tract	Gastrointestinal Tract
HDAC4	Histone Deacetylase 4
KDM6B	Lysine-Specific Demethylase 6b
KREMEN2	Kringle Containing Transmembrane Protein 2
M-CSF	Macrophage Colony-Stimulating Factor
MiR/MiRNA	MicroRNA
MITF	Microphthalmia-Associated Transcription Factor
OC	Osteocalcin
ON	Osteonectin

OPG	Osteoprotegerin
PDCD4	Programmed Cell Death Protein 4
PP Cells	Pancreatic Polypeptide Cells
PPARG	Peroxisome Proliferator-Activated Receptor Gamma
RANKL	Receptor Activator of Nuclear Factor-Kappa-B Ligand
RhoA	Ras Homolog Family Member A
RISC	RNA Induced Silencing Complex
RUNX2	Runt-Related Transcription Factor 2
SATB2	Sequence-Binding Protein 2
SFRP2	Secreted Frizzled-Related Protein 2
SMAD7	Small Mothers Against Decapentaplegic 7
SOCS1	Suppressor of Cytokine Signaling 1
SOST	Sclerostin
SP7	Osterix
SPRY1	Sprouty Homolog 1
SRF	Serum Response Factor
StRNAs	Small Temporal Rnas
T2DM	Type 2 Diabetes Mellitus
TGFB1	Transforming Growth Factor-Beta 1
TGFBR2	TGF-B Receptor 2
TRAP	Tartrate-Resistant Acid Phosphatase
TUNEL	Terminal Deoxynucleotidyl Transferase dUTP Nick End Labeling

Chapter 1: Introduction

1.1 Background

A healthy skeleton is maintained by being remodeled constantly; since the bone is an active tissue (Feng & McDonald, 2011). The bone serves as a reservoir for calcium and phosphate, protector of the vital organs, and support provider for the muscle's attachment sites (Feng & McDonald, 2011). The type of bone that provides protection and responsible for the mechanical function is the cortical bone, which is stiffer with high resistance to bending, whereas the other type of bone that provides strength and responsible for the metabolic function is the trabecular bone, which is spongy and has good absorbing forces (Feng & McDonald, 2011).

1.1.1 Anatomy of the Bone

Bones can be classified according to their shapes as long bones, short bones, flat bones, and irregular bones are the main four categories of the bones (Clarke, 2008). Overall of 80% of cortical bone and 20% of cancellous bone [trabecular bone] is the composition of the adult human skeleton (Clarke, 2008). Figure 1 illustrates an example of a long bone showing the cortical and cancellous bone. The cortical and cancellous bone is what the adult human skeleton is composed of, and according to the skeletal site, their proportions vary (Compston et al., 2019). The diaphysis of the long bones generally contains cortical bone and epiphysis has a predominantly trabecular bone (Compston et al., 2019).
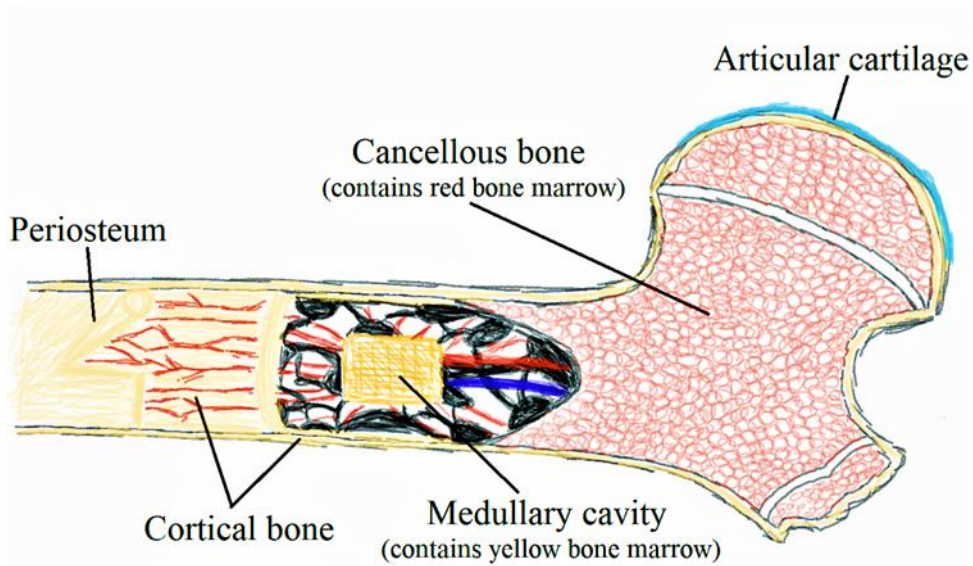
Figure 1: A cross-section of a proximal femur (posterior view).
Articular cartilage is a thin layer of hyaline cartilage that covers the end part of a long bone, which functions by acting as a shock absorber; to reduce friction (OpenStax, 2013a). The outer surface of the cortical bone is surrounded by a fibrous connective tissue sheath called the periosteum (OpenStax, 2013a).

The functional building block of a bone is the osteon (Clarke, 2008). The osteon is formed as an end-product of a bone remodeling cycle (Clarke, 2008). The bone remodeling cycle benefits the bone by preserving its mechanical strength, and that is achieved by replacing the bones which are old and have microdamage with new healthy bones, as well as maintaining the calcium and phosphate homeostasis (Clarke, 2008). Osteoclasts and osteoblasts are the key players in the bone remodeling cycle (Clarke, 2008). Simply, the osteoclasts are defined as the cells that are capable of resorbing the bone, while the osteoblasts are defined as the cells that are capable of forming the bone (Clarke, 2008).

1.2 Bone Remodeling Cycle

The process of bone remodeling works by replacing an old or damaged bone with a new bone, and that results in every 10 years a continuous renewal of the skeleton

(Compston et al., 2019). A Bone Remodeling Unit (BRU) or Basic Multicellular Unit (BMU) is defined as a group of bone cells that removes and replaces one bone structural unit (osteon) (Compston et al., 2019). At the bone remodeling units, bone resorption takes place, bone resorption is the process by which osteoclasts break down the bone tissue (Compston et al., 2019). This process is critical in the maintenance of blood calcium levels. Abnormal increases in the activity of osteoclasts that produce an increase in bone resorption cause osteoporosis and other bone loss-associated diseases (Compston et al., 2019). Simultaneously within the resorption cavity, the bone formation and mineralization of the new bone is a function of the osteoblasts (Compston et al., 2019). These events are always sequenced as bone resorption followed by bone formation, and these two processes are both specific to the site and specific for a fixed time (Compston et al., 2019). Remodeling balance is defined as the equal quantities of the bone resorbed compared to the bone formed, as observed in the young adult skeleton (Compston et al., 2019). During skeletal development, the bones are structured by the process of bone modeling for the optimization of their structure to fight against any mechanical stress (Compston et al., 2019).

1.2.1 Phases of Bone Remodeling Cycle

1.2.1.1 Activation

Certain trauma like bone injury or bone damage may trigger the activation of the bone remodeling cycle via various initiation factors that recruit the precursors of osteoclast and osteoblast (Kenkre & Bassett, 2018). The initiation factors can be paracrine factors which are released when the osteocytes undergo apoptosis and travel through the dendritic processes of the apoptotic osteocytes (Kenkre & Bassett, 2018).

After initiation, numerous mononuclear pre-osteoclasts [come from the monocyte/macrophage lineage] fuse together to make multinucleated preosteoclasts which will bind to the area of resorption (Walsh, 2017). M-CSF [macrophage colony-stimulating factor] and RANKL [receptor activator of nuclear factor-kappa-B ligand] act as an activator to initiate the multinucleated preosteoclasts mediated dissolution of bone (Walsh, 2017). These multinucleated cells secrete hydrochloric acid to dissolve the bone mineral and cathepsin K to digest the bone matrix (Hadjidakis & Androulakis, 2006).

1.2.1.2 Resorption

Once the multinucleated preosteoclasts got activated by M-CSF and RANKL, they will differentiate into osteoclasts [bone resorption cells] that will bind to the site of resorption and form a ruffled border, which then starts the secretion of the acids and the proteolysis enzymes (Hadjidakis & Androulakis, 2006). The duration of the resorption phase is regulated; so that there is no excess of resorption, and that's by apoptosis of the osteoclasts (Kenkre & Bassett, 2018).

1.2.1.3 Reversal

It is the phase when the switch happens from bone resorption to bone formation (Kenkre & Bassett, 2018). Osteoclasts release osteogenic signals to trigger the mesenchymal cells [known as the reversal cells] to form cement lines, which are the bridge that connects the resorbing osteoclasts and the bone-forming osteoblasts (Delaisse, 2014). However, the mechanism of the reversal phase is not fully understood (Kenkre & Bassett, 2018).

1.2.1.4 Formation

Osteoblasts are differentiated from the mesenchymal stem cell lineage and have two main functions: 1) synthesis of osteoid matrix [type 1 collagen-rich] and 2) regulation of matrix mineralization (Kenkre & Bassett, 2018). The canonical Wnt signaling pathway is the one controlling the osteoblastogenesis. In this phase, osteoid covers the site of resorption, and osteoid mineralization [in form of hydroxyapatite crystals] is started (Crockett et al., 2011).

1.2.1.5 Termination

The complete osteoid matrix mineralization triggers the osteoblasts either to be trapped into their mineralized matrix and differentiate into osteocytes or to be changed into bone-lining cells by undergoing programmed cell death (Crockett et al., 2011).

1.3 Disorders of Bone Remodeling

1.3.1 Osteoporosis

Osteoporosis is a skeletal disorder in which the patient's bone quantity and quality are affected (Dougherty, 1996). Bone quantity measures bone mineral density whereas bone quality measures the adherence and microstructural deterioration of the bone's internal architecture (Dougherty, 1996). Osteoporosis can be defined as a systemic skeletal disease, resulting in micro-architectural deterioration (Eastell, 2013). Some of the key characteristics are low bone mass, notable elevation in bone fragility, and vulnerability to fractures (Eastell, 2013). The most severely affected regions are the pelvic region, vertebral column, and limbs (Eastell, 2013). Moreover, it is also defined based on the bone mineral density [BMD] as such the comparison of the bone mineral density between an older person and a younger person is measured by

determining the standard deviation units by Dual-energy X-ray absorptiometry (DEXA) [T-score $\leq$ - 2.5 is considered as having osteoporosis] (Eastell, 2013). The fractures of osteoporotic individuals cause noticeable morbidity and mortality [in the first year following a hip fracture, the mortality rate is elevated by 20%] (Eastell, 2013). Kyphosis, abdominal protrusion, and loss of height are deformities that result from osteoporosis (Eastell, 2013). The imbalance of the rates between bone resorption and bone formation is the cause of the bone loss, which ends up in the perforation and the thinning of the bones that modify its architecture and losing its strength (Eastell, 2013). There are two mechanisms by which osteoporosis roles: 1) high turnover osteoporosis that is defined by significantly elevated levels of bone resorption and bone formation, and 2) low turnover osteoporosis that is known by a notably drop in the levels of bone resorption and bone formation (Heinz, 1992). Scientists have classified osteoporosis into primary type 1 osteoporosis and primary type 2 osteoporosis according to the bone turnover rate. Primary type 1 is post-menopausal osteoporosis in females that is categorized as high bone turnover, which is caused by a deficiency in estrogen or androgen levels in the blood, and primary type 2 is senile osteoporosis in both sexes that is recognized by low bone turnover, which results from aging, or in scientific words, senescence of body cells (Heinz, 1992). Secondary Osteoporosis develops when certain medical conditions and medications increase bone remodeling leading to disruption of bone reformation (Heinz, 1992). The loss of bone mass occurs due to the imbalance between the production of new bone and the loss of old bone, leading to lower bone turnover rate (Heinz, 1992). In other words, some of drugs and diseases may lead to osteoporosis as a side effect, it is known as secondary osteoporosis, and its mechanism of action is not clearly understood, whether it is a high or low bone turnover which differs specifically in each disorder (Heinz, 1992).

1.3.2 Examples of Secondary Osteoporosis

Rheumatoid arthritis, asthma, and multiple sclerosis are treated commonly with immunomodulatory drugs called "Glucocorticoids" (Feng & McDonald, 2011). Low bone mass and increased fracture risk are the most significant complications of the prolonged therapeutic use of glucocorticoids, which then leads to secondary osteoporosis called glucocorticoid-induced osteoporosis (Feng & McDonald, 2011). Those glucocorticoids inhibit osteoblast differentiation that leads to suppression of bone formation, and elevation in bone resorption, which results in an imbalance of the bone remodeling cycle leading to a decrease in bone mass (Feng & McDonald, 2011).

Another example of secondary osteoporosis is immobilization-induced osteoporosis, which is defined as the prolonged decrease in mechanical demands results in impaired mechanical strength of the bones, which affects its mechanical loading or weight-bearing (Feng & McDonald, 2011). However, the mechanism of immobilization-induced osteoporosis is not completely understood (Feng & McDonald, 2011).

1.4 Epidemiology of Osteoporosis in Type 2 Diabetic Individuals

1.4.1 Type 2 Diabetes Mellitus

The endocrine portion of the pancreas is represented by the islets of Langerhans, and those secrete hormones directly into the bloodstream without going through a duct (OpenStax, 2013b). There are four types of islets of Langerhans: 1) alpha cells [secrete glucagon], 2) beta cells [secrete insulin], 3) delta cells [secrete somatostatin] and 4) PP cells [secrete pancreatic polypeptide hormone] (OpenStax, 2013b). The elevated levels of blood glucose, blood amino acids, blood fatty acids,

and gastrointestinal hormones from the upper gastrointestinal (GI) tract stimulate the somatostatin secretion, while insulin and catecholamines inhibit the somatostatin secretion (OpenStax, 2013b). Somatostatin inhibits gastrointestinal, endocrine, exocrine, pancreatic, and pituitary secretions (OpenStax, 2013b). The pancreatic polypeptide hormone regulates the pancreatic exocrine and endocrine secretions and plays a major role in appetite (OpenStax, 2013b).

The molecular weight of the insulin is around 6000 Daltons, which is a relatively small protein that has two chains kept united by disulfide bonds, and among vertebrates, the sequence of the amino acid is highly conserved (Humbel, 1966). Preproinsulin is a single chain precursor that is translated from the insulin mRNA, and during the insertion of the preproinsulin into the endoplasmic reticulum, it gets cleaved to become proinsulin (Humbel, 1966). In addition, the proinsulin is further cleaved within the endoplasmic reticulum by endopeptidases to form insulin [the mature form] and free C peptide, which then packaged into secretory granules in the Golgi and accumulates in the cytoplasm (Humbel, 1966). When an appropriate stimulus is present, the beta cells secrete insulin along with free C peptide by exocytosis, and insulin binds to the receptors of the target cells (Humbel, 1966). The secretion of insulin is regulated through four different factors: 1) hyperglycemia [the insulin will be secreted to return the body to normoglycemia], 2) hyperaminoacidemia [the beta cells are stimulated by arginine and lysine; to elevate the secretion of insulin, and the insulin will lower the number of amino acids in the plasma by promoting their entry into the cells and enhancing protein synthesis], 3) the insulin level is increased in the presence of the fatty acids and ketone bodies, and 4) hormones as well increase the level of insulin [for instance, glucagon, gastrin, cortisol, growth hormone, gastric inhibitory peptide, secretin and cholecystokinin] (OpenStax, 2013b). The insulin

affects carbohydrate metabolism by storing the glucose as glycogen in the liver, making more of stored glycogen in the liver [glycogenesis], inhibiting glycogenolysis and gluconeogenesis, and converting the increased glucose in the liver to fatty acids (OpenStax, 2013b). Insulin has a role in fat metabolism by suppressing the hormone-sensitive lipase from breaking down the fats and promoting glucose transport into the adipocytes (OpenStax, 2013b). Insulin has a crucial part on protein metabolism by lowering the gluconeogenesis rate in the liver, halting the protein catabolism, rising the transcription rate of DNA and the translation rate of mRNA to synthesize new proteins, and enabling an active transport of a lot of amino acids into the cells (OpenStax, 2013b).

Type 2 diabetes mellitus is characterized by chronic hyperglycemia, which is caused by insulin resistance along with defective insulin secretion (Ling et al., 2019). Moreover, aging, unhealthy lifestyle, and obesity are well-established cause for insulin resistance, and the impaired insulin secretion happened due to the long-term exposure of hyperglycemia, which altered the ability of the pancreatic β-cells to secrete insulin (Chatterjee et al., 2017; Davegårdh et al., 2018; Ling & Ronn, 2019). Studies have shown that the pancreatic β-cells dysfunction is due to its destruction by the ongoing apoptosis (Taylor et al., 2019). Furthermore, type 2 diabetic patients will develop some complications such as osteoporosis, which makes them more susceptible to fractures and thus take more than the normal time of healing (Bhamb et al., 2019). Type 2 diabetes mellitus may lead to osteoporosis; since it disturbs the bone remodeling cycle (Bhamb et al., 2019).

1.4.2 Prevalence of Fracture Risk in Type 2 Diabetes Mellitus

A meta-analysis was conducted for 16 epidemiologic studies; to find an

association between diabetes and bone fractures, this systematic review revealed that there was a strong association between type 2 diabetes mellitus and elevated risk of hip fractures in both men and women (Janghorbani et al., 2007). Another meta-analysis was performed for 30 epidemiologic studies; to detect an association between diabetes mellitus and bone fractures, this systematic review reported that there was a strong association between T2DM and increased overall fracture risk, emphasizing that strategies should be implemented to prevent fractures in type 2 diabetic patients (Moayeri et al., 2017).

A cross-sectional, single-center study was done by the Heidelberg Study Center in collaboration with the European Vertebral Osteoporosis Study for the diabetic patients from the outpatient clinic at the University of Heidelberg revealed that out of 325 diabetic patients, 12 of them had serious-traumatic bone fractures and 17 of them had low-traumatic bone fractures (Leidig-Bruckner et al., 2014). Furthermore, a cross-sectional study was done from 24 tertiary hospital diabetes clinics in Korea stated that 43.3% of post-menopausal women with T2DM had vertebral fractures (Chung et al., 2013).

A historical cohort study was performed on the Rochester residents with T2DM stated that 1369 bone fractures were experienced by 700 diabetic residents, emphasizing that among the diabetic Rochester residents, the overall fracture risk was increased (Melton et al., 2008). In addition to that, a retrospective cohort study stated that patients with T2DM who received insulin as a treatment, are at a high risk of getting bone fractures (Monami et al., 2008). It's been reported that 30% of T2DM patients got low-traumatic bone fractures, based on a questionnaire from a Moscow outpatient clinic (Yalochkina et al., 2016).

Recent research by Dr. Sahar's research group at UAEU has shown a suggestion that T2DM affects the trabecular structure within a rat's femoral heads negatively and changes are most significant at a longer duration of T2DM, increasing the risk of hip fractures (Mohsin et al., 2019).

1.5 Statement of the Problem

Currently, a widely used clinical technique for the diagnosis of osteoporosis is the DEXA scan where bone density/quantity is measured (Rossini et al., 2016). Additionally, some of the biochemical tests available as a biomarker for osteoporosis are non-specific (Lorentzon & Cummings, 2015). The available biomarkers have poor sensitivity and specificity for several reasons. For instance, alkaline phosphatase, osteocalcin, pro-peptides of type I procollagen are considered as bone formation markers, and pyridinoline, deoxypyridinoline, N- and C-terminal telopeptides of type I collagen are considered as bone resorption markers (Rossini et al., 2016). But these biomarker levels are altered due to several other disorders and diseases. For example, elevated serum alkaline phosphatase does not always mean that the patient has a bone disease since the alkaline phosphatase is also considered as a hepatic marker (Mukaiyama et al., 2015). Moreover, osteocalcin is mainly produced by osteoblasts, its carboxylated form regulates mineralization by acting in the bone matrix (Zoch et al., 2016). But, the undercarboxylated form of osteocalcin acts in the β-cells of the pancreas to enhance the production and secretion of insulin, acts in the brain to enhance the production of neurotransmitters, acts in the adipose tissue to enhance insulin sensitivity, and acts in the testes to start the production of testosterone (Zoch et al., 2016). Although its carboxylated form might be useful for the diagnosis of osteoporosis, it cannot be used exclusively to rule out osteoporosis without DXA (Singh et al., 2015). In addition, pro-peptides of type I procollagen, pyridinoline,

deoxypyridinoline, N- and C-terminal telopeptides of type I collagen are well-known biochemical markers for bone, but because of their poor specificity, they cannot be used to screen for osteoporosis, rather they are used to for monitoring purposes of antiresorptive therapies (Zaitseva et al., 2015).

Recent studies have shown that a new class of RNAs i.e. miRNA can also be used as a biomarker for various diseases such as liver disease, pancreatic cancer, viral diseases (Bandiera et al., 2015; Cui et al., 2020; Gokita et al., 2020; Huang, 2017). Recently their use as a biomarker in bone-related diseases is also being investigated like osteoporosis (Foessl et al., 2019). The purpose of this study is to investigate the altered expression of (if any) microRNAs that are known to have a role in bone formation and bone resorption in the bones and sera of type 2 diabetic rats. The current study will help in revealing the mechanisms of skeletal fragility in type 2 diabetes. The knowledge gained in this research will be beneficial in enriching the medical field with the potential to use microRNAs as diagnostic biomarkers or therapeutic targets for type 2 diabetic osteopathy.

1.6 The Role of MicroRNAs in Bone Resorption and Bone Formation
1.6.1 Definition of MicroRNAs

Micro-RNAs [miRNAs] are small RNAs [about 20 – 25 nucleotides long] that are called sometimes as small temporal RNAs [stRNAs]; because during development, their existence is temporary (Nelson & Cox, 2005). MiRNAs function as a post-transcriptional modulator, causing the silencing of its target known as RNA inference (Nelson & Cox, 2005). The 3` untranslated region (UTR) of the mRNA has some specific binding sites for various miRNAs, known as seed sequence (Nelson & Cox, 2005). Seed sequence is a region where the interaction takes place with 5' end of

miRNAs (Nelson & Cox, 2005). Consequently, the mRNA is halted from being translated as a result of mRNA degradation or translational inhibition, and the gene that produces the mRNA is silenced (Nelson & Cox, 2005).

1.6.2 Biogenesis of MicroRNAs

MiRNAs are synthesized in the nucleus by RNA polymerase II enzyme in a similar manner to mRNAs (Berg et al., 2015). RNA polymerase II requires two specific promoter regions to initiate the synthesis of genes (transcription) (Berg et al., 2015). The RNA polymerase II first binding site is upstream of the transcription start site, known as the TATA box and the second one is known as DPE (downstream promoter element), which can be coupled with CAAT box and GC Box (Berg et al., 2015). These are the regulatory sequences of the transcription initiation (Berg et al., 2015). The RNA polymerase II promoter has an enhancer element upstream of the start site, which stimulates the transcription (Berg et al., 2015).

The transcript is a primary microRNA, which will fold to form a typical stem and loop structure, it will become the final mature microRNA with its regulatory function after several steps of processing (Watson et al., 2014). First, the double-stranded stem is recognized by the protein DGCR8 [PASHA], an enzyme called DROSHA is associated with the protein DGCR8 [PASHA] to form a microprocessor complex, which can cleave the primary microRNA into a smaller precursor microRNA that can be exported into the cytoplasm where it will inactivate the mRNA of one or multiple genes (Watson et al., 2014). The precursor microRNA is carried out of the nucleus through a nuclear pore by a transporter molecule EXPORTIN 5 (Watson et al., 2014). In the cytoplasm, it is recognized by a large RNA protein called DICER, it chops the head of the stem and loop structure; to forms a short double-stranded

microRNA molecule (Watson et al., 2014). In the next step, an argonaute protein AGO 2 interacts with DICER; to bind the short double-stranded microRNA, which then is unwound and one strand is released, the remaining strand called the guide strand interacts with AGO 2 and some additional proteins to form the RISC [RNA induced silencing complex], it can be now guided to its target mRNA and inactivate one or multiple genes (Watson et al., 2014). The biogenesis of microRNAs is illustrated in Figure 2.
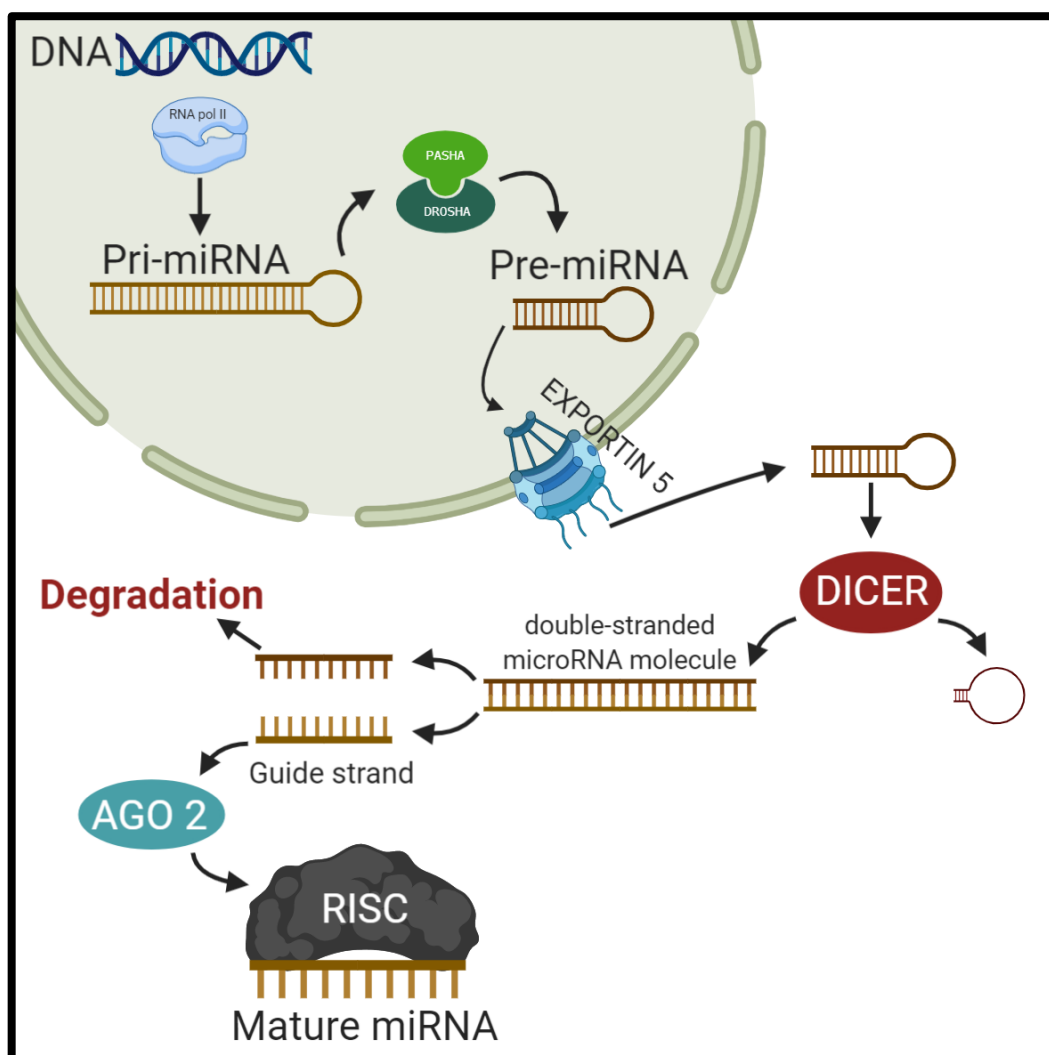
Figure 2: Biogenesis of microRNAs.

1.6.3 Gene Regulation by MicroRNAs

The mRNA of a target gene is complementary to the sequence of the microRNA that enables base pairing. Once bounds, there are two ways in which RISC can inactivate the mRNA, proteins in the complex can simply degrade the mRNA, which will be further destroyed by the cell (Watson et al., 2014). Blocking of translation is another mechanism, the RISC complex prevents the ribosome subunit from binding (Watson et al., 2014). In both cases, the mRNA will not be translated into a protein and the gene is silenced.

1.6.4 The Bone Remodeling Cycle is Regulated by MicroRNAs

Micro-RNAs activate bone remolding and regulation of osteoclast differentiation by controlling the signaling pathways that operate these events, for instance, the micro-RNAs can target the macrophage colony-stimulating factor [M-CSF] signaling pathway and the receptor activator of NF-κB ligand [RANKL] (Loh et al., 2018). Furthermore, there are micro-RNAs involve in bone formation as well by targeting the pathway that turns the mesenchymal stem cells into osteoblast lineage, which is the canonical Wnt/β-catenin signaling pathway (Loh et al., 2018). In order for the Wnt-responsive gene to be expressed, the β-catenin has to be stabilized for regulating the function of the osteoblast by targeting many Wnt-signaling pathway inhibitors; to act as a positive regulator of osteoblast differentiation (Loh et al., 2018).

1.7 Literature Review

1.7.1 MicroRNA-20a

Some of the miRNAs are involved in the regulation of the self-clearing of cells known as Autophagy (Che et al., 2019). For instance, miRNA-20a have a role in

hypoxia regulation, a research stated that upon HIF-1α (Hypoxia-inducible factor 1-alpha) accumulation, there was a significant drop in miR-20a expression. This study suggests that HIF-1α is targeted by miR-20a (Che et al., 2019). There is a negative correlation between the expression of miR-20a and HIF-1 α mediated autophagy/lysosome pathway (Che et al., 2019). Previous researches have established the direct targeting of ATG16L1 (Autophagy related 16 like 1) by miR-20a resulting in the defects of hypoxia-induced autophagy in osteoclast differentiation (Sun et al., 2015). ATG5 and FIP200 are two proteins that are essential for autophagosome formation, and it is noticed that the overexpression of miR-20a strongly decreases those two proteins and the mRNA levels (Che et al., 2019). Through increasing the expression of ATG5 and FIP200, the down-regulation of hypoxia-induced miR-20a is facilitated (Che et al., 2019). Another study shows that some of the members of the E2F family that are set of genes tangled with DNA synthesis and cell cycle regulation are targeted by miR-20a, which promotes proliferation, sustains cell survival, and increases angiogenesis (Che et al., 2019). Similarly, mir-20a is known to regulate cell growth (Torbati et al., 2019). Furthermore, the key regulatory mechanisms involved in osteoblastogenesis and differentiation are Wnt, BMP, and TGF-β signaling pathways (Bellavia et al., 2019). Interestingly, miR-20a is a regulatory factor for the Wnt, BMP, and TGF- β signaling pathways (Bellavia et al., 2019). In the Wnt signaling pathway, the expression of miR-20a inhibits the Peroxisome Proliferator-Activated Receptor Gamma [PPARG] that is involved in the differentiation of adipocytes, which will lead to the promotion of osteoblast differentiation (Bellavia et al., 2019). The Wnt signaling pathway is controlling osteoblasts formation by affecting the bone density through inactivating mutations in Wnt pathway components (Lodish et al., n.d.). In the BMP signaling pathway, the expression of miR-20a suppresses Bone Morphogenetic

Proteins and Activin Membrane-Bound Inhibitor [BAMBI] and Cysteine-Rich Motor Neuron 1 [CRIM1], which are controlling the signal transduction during developmental processes, and that's lead to the promotion of osteoblast differentiation (Bellavia et al., 2019). In the TGF-β signaling pathway, the expression of miR-20a blocks TGF-β Receptor 2 [TGFBR2] and Lysine-specific demethylase 6b [KDM6B], which the earlier involved in the regulation of cell proliferation and the latter involved in the cell differentiation, and that will lead to the promotion of osteoblast differentiation (Bellavia et al., 2019).

1.7.2 MicroRNA-21

MicroRNA-21 has a role in inducing osteoblast differentiation through BMP, TGF-β, and MAPK pathways, and also has a role in inhibiting osteoclast differentiation through the RANK pathway (Bellavia et al., 2019). In the BMP signaling pathway, the expression of miR-21 blocks the production of SMAD7, which is known to inhibit osteoblast differentiation (Bellavia et al., 2019). A study has shown that partial dysfunction of SMAD7 disturbs bone remodeling by impairing osteogenesis (Li et al., 2014). Moreover, SMAD7 is also blocked by the expression of miR-21 through the TGF-β pathway (Bellavia et al., 2019). Furthermore, the MAPK cascade activation is prevented by the expression of miR-21, and that leads to a decrease in the level of Sprouty homolog 1 [SPRY1] (Bellavia et al., 2019). In adipocytes, the SPRY1 is expressed to act as a protector from high-fat diet-induced obesity and associated bone loss (Urs et al., 2012). So, the decreased level of SPRY1 will promote osteoclastogenesis by inhibiting the RANKL level and promoting the OPG level (Hu et al., 2017). Receptor activator of nuclear factor κB ligand (RANKL) is known to induce expression of miR-21, and its silencing suppresses

osteoclastogenesis (Sugatani et al., 2011). In the RANK pathway, the mRNA of c-FOS and its protein phosphorylation level is down-regulated; because of the inhibited expression of Programmed Cell Death Protein 4 [PDCD4] by the expression of miR-21, which results in promoting bone resorption (Hu et al., 2017).

1.7.3 MicroRNA-29a

MicroRNA-29a has a role in promoting osteoblast differentiation through Wnt, Matrix mineralization, and RUNX2 pathways and has a protective role from osteoporosis by repressing osteoclast regulator RANKL (Bellavia et al., 2019; Lian et al., 2019). Past researchers stated that miR-29a negatively regulates the negative regulators of the osteoblasts: Dikkopf 1 [DKK1], Kringle Containing Transmembrane Protein 2 [KREMEN2], and Secreted Frizzled Related Protein 2 [SFRP2] of the Wnt signaling pathway (Alfaro et al., 2010; Bellavia et al., 2019; Pinzone et al., 2009; Schulze et al., 2010). The Osteonectin [ON], which is a non-collagenous matrix protein that plays a vital role in matrix mineralization during osteogenesis, it is shown to be targeted by miR-29a, leading to accelerating extracellular mineralization response (Bellavia et al., 2019). Another study suggests that the inhibition of miR-29a leads to overexpression of TGFB1 [Transforming Growth Factor Beta 1], which results in an increased level of ON (James et al., 2014). Also, miR-29a protects RUNX2, which is involved in bone development, from deacetylation, by down-regulating the levels of Histone Deacetylase 4 [HDAC4] (Jonason et al., 2009; Ko et al., 2015).

1.7.4 MicroRNA-31

Sequence-binding protein 2 [SATB2] has a role in the transcriptional regulation of osteoblast differentiation (Baglìo et al., 2013). MicroRNA-31 targets the

mRNA of SATB2 [involved in preventing the imperfection in the osteoblast function] as well as RUNX2, consequently blocking osteoblast differentiation, and that effectively reduces the stability of the osteoblast-specific transcription factor Osterix (SP7) (Baglìo et al., 2013; Jin Zhang et al., 2011). This reduction in SP7 expression implicates the expression of osteoblast effector genes (Baglìo et al., 2013). In the literature review, the inhibition of miR-31 is determined to increase the expression of SP7, which promotes osteoblast differentiation (Baglìo et al., 2013). In addition, another research describes the considerable fall in the number of tartrate-resistant acid phosphatase [TRAP]-positive multinucleated osteoblastic cells upon suppression of miR-31 via specific antagomirs under receptor activator of NF-κB ligand (RANKL) treatment (Loh et al., 2018). Moreover, in osteoclastogenesis, Ras homolog family member A [RhoA] activates migration of osteoclast, actin polymerization and podosome turnover (Georgess et al., 2014). Studies suggest that miR-31 down-regulates RhoA which affects osteoclast formation and bone resorption (Mizoguchi et al., 2013). On the contrary, inhibition of miR-31 promotes the expression of the RhoA gene, which suppresses osteoclastogenesis and bone resorption (Mizoguchi et al., 2013). Also, the thyroid gland has parafollicular cells that synthesize calcitonin-related polypeptide alpha [CALCA] (Palmieri et al., 2007). This protein is a direct effector of osteogenesis (Palmieri et al., 2007). MiR-31 targets the mRNA of CALCA, and that signals for blocking osteogenesis (Palmieri et al., 2007).

1.7.5 MicroRNA-155

MicroRNA-155 has a role in suppressing osteoblast differentiation through TNF-α and BMP pathways, whereas it involves suppressing osteoclast differentiation through the RANK pathway (Bellavia et al., 2019). In a murine arthritis model, the

deficiency of miR-155 suppresses osteoclastogenesis (Blüml et al., 2011). In the TNF-α pathway, the Suppressor of Cytokine Signaling 1 [SOCS1] mRNA is inhibited by the expression of miR-155 (Wua et al., 2012). SOCS1 protein downregulates cytokine signal transduction involved in bone loss (Souza et al., 2017). Briefly, in the BMP signaling pathway, the expression of miR-155 down-regulates SMAD5 and inhibits osteoblast differentiation (Bellavia et al., 2019). SMAD5 is required for the formation of endochondral bone (Retting et al., 2009). One study suggests that the role of miR-155 in modulating the targets (Cathepsin K [CTSK] and Tartrate-resistant acid phosphatase [TRAP]) of Microphthalmia-Associated Transcription Factor [MITF] which are involved in the osteoclast activities, thereby reducing it (J. Zhang et al., 2012). Overexpression of miR-155 promotes cell proliferation and osteoclast activation, which works by decreasing the expression of OPG [Osteoprotegerin] and increasing the expression of RANK, RANKL, and TNF-α (Mao et al., 2019).

1.7.6 Summary of the Literature Review

A summary of the literature review stating the expression of miR-20a, miR-21, miR-29a, miR-31, and miR-155, their target genes expression, and their possible effects on the bone remodeling cycle is shown in Table 1.

Table 1: The target genes of miR-20a, miR-21, miR-29a, miR-31, and miR-155, their expression and effect on the bone remodeling cycle.

MicroRNA	MicroRNA Expression	Target Gene Expression	Effect on the Bone Remodeling Cycle	References
MiR-20a	Upregulation	↓ ATG16L1	Suppress osteoclast differentiation	Sun et al., 2015
		↓ PPARG ↓ BAMBI ↓ CRIM1 ↓ TGRBR2 ↓ KDM6B	Promote osteoblast differentiation	Bellavia et al., 2019
MiR-21	Upregulation	↓ SMAD7	Promote osteoblast differentiation	Bellavia et al., 2019
		↓ SPRY1	Promote osteoclastogenesis	Hu et al., 2017
		↓ PDCD4	Promote bone resorption	Hu et al., 2017

↓ = The expression of the target gene is downregulated

↑ = The expression of the target gene is upregulated

Table 1: The target genes of miR-20a, miR-21, miR-29a, miR-31, and miR-155, their expression, and effect on the bone remodeling cycle (continued).

MicroRNA	MicroRNA Expression	Target Gene Expression	Effect on the Bone Remodeling Cycle	References
MiR-29a	Upregulation	↓ DKK1 ↓ KREMEN2 ↓ SFRP2	Promote osteoblast differentiation	Bellavia et al., 2019
		↓ HDAC4	Promote osteoblast differentiation	Ko et al., 2015
		↓ ON	Accelerate extracellular mineralization	Bellavia et al., 2019
	Downregulation	↑ TGFB1	Increased level of ON	James, Delany, & Nair, 2014
MiR-31	Upregulation	↓ SATB2 ↓ RUNX2 ↓ SP7	Suppress osteoblast differentiation	Baglìo et al., 2013
		↓ CALCA	Suppress osteogenesis	Palmieri et al., 2007
	Downregulation	↑ RhoA	Suppress osteoclastogenesis & bone resorption	Mizoguchi et al., 2013
MiR-155	Upregulation	↓ SOCS1	Suppress osteoblast differentiation	Wua et al., 2012
		↓ SMAD5	Suppress osteoblast differentiation	Bellavia et al., 2019
		↓ MITF	Suppress bone resorption	Zhang et al., 2012
		↓ OPG ↑ RANK ↑ RANKL ↑ TNF-α	Promote bone resorption	Mao, Zhu, Hao, Chu, & Su, 2019

↓ = The expression of the target gene is downregulated

↑ = The expression of the target gene is upregulated

1.8 Research Hypothesis

The existing evidence indicates that short non-coding RNAs known as microRNAs (miRNAs), are the key post-transcriptional repressors of gene expression, and growing numbers of novel miRNAs have been verified to play vital roles in the regulation of osteogenesis, osteoclastogenesis, and adipogenesis, revealing how they interact with signaling molecules to control these processes. The study aims to identify the changes in miRNAs levels related to the bone remodeling cycle in bones and sera of type 2 diabetic rats. Previous studies have shown that some microRNAs are responsible for regulating the bone remodeling cycle, and changes in the expression of those microRNAs will result in osteoporosis.

1.9 Aims and Objectives

Aim:

The aim of this study is to identify the changes in microRNAs expression that are associated with the bone remodeling cycle in type 2 diabetes. Investigate the mechanism of osteoporosis in type 2 diabetes mellitus through MicroRNAs with the potential to be used as diagnostic biomarkers to assess fracture risk or therapeutic targets for type 2 diabetic osteopathy.

Objective:

1. Establish a type 2 diabetic animal model.

2. Investigate the expression of miR-20a, miR-21, miR-29a, miR-31, and miR-155 in the serum samples obtained from control and type 2 diabetic animal models.

3. Investigate the expression of miR-20a, miR-21, miR-29a, miR-31, and

miR-155 in the bone samples obtained from control and type 2 diabetic animal models.

4. Assess the expression of some of the target genes for the selected microRNAs in the bones of T2DM animal models.

5. Study the bone microstructure in control and diabetic bone samples using histological techniques.

6. Examine the bone biomarkers in the serum and bone samples obtained from control and diabetic animals using the ELISA technique.

Chapter 2: Methods

2.1 Animal Models

The design of this study consists of two independent groups of animal models. The three-month-old female Wistar rats were used as the proposed animal models in the experiments. They are closely related to humans in terms of behavioral, genetic, and biological characteristics (Bird & Parlee, 2000). From the animal house facility at United Arab Emirates University, those three-month-old female Wistar rats (n=96) were obtained. Under the standard conditions with a 12 h alternating light and dark cycle (22 – 24°C) in 50–60% humidity, the animals were individually housed in cages. During the two weeks of acclimatization, free access to standard rat chow and water ad libitum was provided to the animals. All efforts were made to reduce the suffering of the animal and to minimize the number of animals used. All animal procedures were approved by the animal ethical committee at United Arab Emirates University [ERA_2017_5597] (Mohsin et al., 2019).

The first group is the control group and the second group is the T2DM group. The control group contains normal three-month-old female Wistar rats (n=24) that have been fed with normal diet (D12492 diet; Research Diets, Inc., USA) for 21 days [during this period, the glucose test was performed for them, and they should maintain < 100 mg/dL]. On the 7th & 14th day, a saline injection is given to all the rats. After 10 days of the last saline injection, a blood glucose test was performed on their tail vein after fasting for 5 hours using a blood glucose meter (Accu-Chek Performa; Roche Diagnostics, USA); to check whether they have maintained a glucose level of < 100 mg/dL. Then, an insulin tolerance test was performed; to confirm that they lack insulin resistance. Lastly, they have been sacrificed at 8, 10, and 14 weeks (n = 8 for

each time interval) of the onset of being normal. All the bones have been dissected out, cleaned and fixed, and stored at –20°C for further analysis.

The T2DM group contains normal three-month-old female Wistar rats (n=24) that have been fed with a high-fat diet (D12492 diet; Research Diets, Inc., USA) for 21 days [during this period, the glucose test was performed for them, and the criteria was to maintain > 100 mg/dL of glucose in blood]. On the 7th & 14th day, a streptozocin (STZ) injection (30 mg/kg intraperitoneally) is given to all the rats. After 10 days of the last saline injection, a blood glucose test was performed on their tail vein after fasting for 5 hours using a blood glucose meter (Accu-Chek Performa; Roche Diagnostics, USA); to check their blood glucose levels. Those animals with glucose levels > 270 mg/dL were considered diabetic (M. Zhang et al., 2008). Then, an insulin tolerance test was performed; to confirm that they have insulin resistance. Lastly, they have been sacrificed at 8, 10, and 14 weeks (n = 8 for each time interval) of the onset of being type 2 diabetic. All the bones have been dissected out, cleaned and fixed, and stored at –20°C for further analysis. The serum samples were immediately withdrawn just before the animals were sacrificed, and kept in labeled Eppendorf tubes at room temperature for 30 minutes; to clot. Then, the tubes were centrifuged at 3,000 rpm for 10 minutes; to separate the clot from the serum. The serum samples were kept in fresh labeled Eppendorf tubes and stored at –80°C. In this study, the right and the left sides of the femur were used for histology, and the right and the left sides of the tibia along with the serum samples were used for molecular biology.

2.2 Preparation of Gelatin-Coated Microscopic Slides

The regular microscopic slides are uncoated, which means that the histological paraffin sections will detach from the slides during staining and washing steps. To

resolve this problem, those slides were coated with adhesive compounds, such as gelatin. To prepare gelatin-coated microscopic slides, a hot plate was used with a magnetic stirrer to heat 1 L of distilled water at a temperature of 45°C. With the aid of the magnetic stirrer, 3.0 g of gelatin was completely dissolved in the heated 1 L of distilled water (temperature = 45°C). Once the gelatin was completely dissolved, 0.5 g chromium potassium sulfate dodecahydrate $KCr(SO_4)_2·12(H_2O)$ [the color of the solution will be pale blue] was added. The purpose of the addition of chromium potassium sulfate dodecahydrate was to make the slides positively charged; to allow them to attract the tissue sections, which are negatively charged. The regular microscopic slides were cleaned by washing them in tap water and rinsing them in distilled water and lastly in absolute ethanol. Then, the cleaned slides were placed into the slide racks and dipped in the gelatin-coating solution 5 times. After that, the slides were drained from the excess solution by gently tapping the slide racks against a paper tissue. Finally, the slides were air-dried at room temperature for 24 hours by letting them stand on a cleaned laboratory bench covered with aluminum foil; to protect them from the dust. Those dried slides are now gelatin-coated microscopic slides, which can be stored in their original boxes [labeled as gelatin-coated slides] at room temperature until use.

2.3 Bone Histology

2.3.1 Procedure of Embedding Bones into Paraffin Blocks and Sectioning Them

The paraffin sections allowed the study of bone histology using a variety of staining techniques. The protocol consisted of fixation and decalcification of the bones, paraffin infiltration and embedding, and eventually sectioning them.

2.3.2 Fixation of the Bones

The proximal end of the femur [including the head of the femur] was used to study the histological changes. The specimens were 2 mm long, and they were kept in a small glass bottle containing 2 ml of 4% formaldehyde for 2 days. This step was important as the fixed bones prevent autolysis. Once the 48 hours of fixation was over, the fixed bones were washed in slowly running tap water for 30 minutes.

2.3.3 Decalcification of the Bones

The washed fixed bones were put into their separate small glass bottle containing 2 ml of 10% EDTA for 7 days. EDTA is a decalcifying solution that works by removing the calcium ions from the bones and making them soft and easy to section (Savi et al., 2017). It's been kept in mind that every day, the used decalcifying solution should be discarded and replaced with a fresh one. During that period, every two days a chemical test was performed for the residual calcium in the used decalcifying solution; to check whether the decalcification was completed (Rosen, 1981). The chemical test was done by preparing the ammonium hydroxide/ammonium oxalate working solution, and this was achieved by adding equal parts of 5% ammonium hydroxide solution and 5% ammonium oxalate solution (Rosen, 1981). Then, in a clean test tube, 5 ml of the used decalcifying solution was pipetted and added to it, and after that 10 ml of the ammonium hydroxide/ammonium oxalate working solution was added to the same test tube (Rosen, 1981). The test tube was mixed well and let stand for 5 minutes (Rosen, 1981). The lack of precipitate means that the decalcification was completed, and the presence of precipitate means that the decalcification was not completed (Rosen, 1981). To conclude that the decalcification was completed, the status of no precipitate was observed on two consecutive days of the testing. The bones

were washed in slowly running tap water for 30 minutes, once the decalcification was completed.

2.3.4 Paraffin Infiltration

The washed decalcified fixed bones were put into their cassettes and labeled those cassettes with pencil accordingly. After that, the bones were processed as follows:-

1. 70% Ethanol = 1 hour.

2. 95% Ethanol = 1 hour.

3. 100% Ethanol-I = 1 hour.

4. 100% Ethanol-II = 1 hour and 30 minutes.

5. 100% Ethanol-III = 1 hour and 30 minutes.

6. 100% Ethanol-IV = 2 hour.

7. 100% Xylene-I = 1 hour.

8. 100% Xylene-II = 1 hour.

9. Paraffin wax-I at 60°C = 1 hour.

10. Paraffin wax-II at 60°C = 1 hour.

Those processed bones in the cassettes can be stored at room temperature for an infinite time. In this step, the bones were dehydrated by series of ethanol baths; to displace the water from the bones, and then infiltrate them with paraffin wax.

2.3.5 Paraffin Embedding

Paraffin embedding is the step where the paraffin blocks of the processed bones can be created. It's been done according to the following steps:-

1. The cassette was opened by discarding the cassette lid.

2. The correct metal mold was chosen. The decision was made depending on the size of the tissue.

3. The mold, the forceps, and the opened cassette that contained the processed tissue with paraffin were placed on a hot plate at 60°C. Note that the paraffin in the opened cassette will be melted.

4. By using the forceps, the tissue was transferred to the center of the mold and oriented in a way that the face down tissue will be the cutting side.

5. The molten paraffin was dispensed in the mold.

6. As a support, the labeled tissue cassette was added to the top of the mold.

7. The molten paraffin was dispensed in the mold; to cover the face of the plastic cassette.

8. The mold was placed on a cold plate at – 4°C for 30 minutes.

9. The paraffin block was popped out of the metal mold.

   Those paraffin blocks can be stored at room temperature for an infinite time.

2.3.6 Sectioning of the Paraffin-Embedded Tissues

Once the paraffin blocks were made, sectioning and placing them on gelatin-coated microscopic slides were essential for staining them. The followings are the steps that have been used for sectioning the paraffin blocks:-

1. The station for sectioning was prepared by filling the water bath with distilled water, turning on the water bath and setting the temperature at 45°C, turning on the slide warmer and setting the temperature at 75°C, bringing a 25 ml glass breaker and placing on top of it a regular microscopic slide, making 30% ethanol and pouring it in a 300 ml plastic squeezing bottle, bringing a forceps, paintbrush, pencil, blades, a bucket filled with ice cubes, slide box and gelatin-

coated microscopic slides.

2. The paraffin block was placed face down on the ice cubes for 10 minutes.

3. A fresh blade was inserted in the microtome blade holder.

4. The paraffin block was inserted in the microtome block holder, and aligned in a way that the blade can create vertical planes of paraffin sections from the paraffin block.

5. The section thickness was set to 20 μm; to remove the extra paraffin to expose the tissue embedded inside it. Rotating the drive wheel was started to make the paraffin sections.

6. The paintbrush was used to remove the paraffin sections that don't contain the tissue out of the way.

7. The section thickness was changed to 5 μm, once the cutting came near to the tissue.

8. The forceps were used to pick up the paraffin sections that contain the tissue.

9. The paraffin sections were placed on the regular microscopic slide, and added to the few drops of 30% ethanol; to stretch them.

10. The sections were transferred to the water bath.

11. The gelatin-coated microscopic slides were used to pick up the floating sections from the water bath.

12. The pencil was used to label the gelatin-coated microscopic slides.

13. The labeled gelatin-coated microscopic slides that contain the sections were placed on the slide warmer for 10 minutes. This step was done to make sure that the tissue will bind to the slide.

14. The slides were stored in the slide box at room temperature for an infinite time. Those slides now can be used for staining.

2.4 Hematoxylin & Eosin [H&E] Staining

This kind of staining contains a basic dye, which is the hematoxylin, and an acidic dye, which is the eosin (Batra, 2018). The hematoxylin is a combination of hematein and a mordant, which is the aluminum salts (Batra, 2018). The mordant binds to basophilic or acidic structures of the tissue, then the hematein binds to the mordant, making a tissue-mordant-hematein linkage, and that is the hematoxylin dye (Batra, 2018). This dye stains the structures as purplish-blue (Batra, 2018). On the other hand, the eosin binds to acidophilic or basic structures of the tissue, which stains them pinkish-red (Batra, 2018). The acidic structures are the anionic components of a cell, such as the nucleic acids that are basophilic, which will react with the basic dyes (Batra, 2018). The basic structures are the cationic components of a cell, like the cytoplasmic proteins that are acidophilic, which will react with the acidic dyes (Batra, 2018).

In this study, an H&E stain was used to visualize the internal structure of the bone. The sections were made from two groups, three animals in each group. From each animal, 10 -15 sections of 5 μm thickness, were made using a microtome.

The sections were stained with H&E, as described below:-

1. The slides containing the paraffin sections were incubated at 60°C for 15 minutes.

2. 100% Xylene-I [Dewaxing] = 3 minutes.

3. 100% Xylene-II [Dewaxing]= 3 minutes.

4. 100% Ethanol-I [Hydration] = 3 minutes.

5. 100% Ethanol-II [Hydration] = 3 minutes.

6. 95% Ethanol [Hydration] = 3 minutes.

7. 90% Ethanol [Hydration] = 3 minutes.

8. 70% Ethanol [Hydration] = 3 minutes.

9. 50% Ethanol [Hydration] = 3 minutes.

10. Distilled water-I = 5 minutes.

11. Distilled water-II = 5 minutes.

12. Distilled water-III = 5 minutes.

13. Encircle the tissue on the slide with a pap pen.

14. Mayer's Hematoxylin [mix A and B equal volumes = 100 μL / tissue] = 8 minutes.

15. Tap water wash = 10 minutes.

16. Distilled water wash = Rinse.

17. 95% Ethanol = 10 Dips.

18. Eosin Y [100 μL / tissue] = 30 Seconds.

19. 70% Ethanol [Dehydration] = 5 minutes.

20. 95% Ethanol [Dehydration] = 5 minutes.

21. 100% Ethanol-I [Dehydration] = 5 minutes.

22. 100% Ethanol-II [Dehydration] = 5 minutes.

23. 100% Xylene-I [Clearing] = 5 minutes.

24. 100% Xylene-II [Clearing] = 5 minutes.

25. The stained sections were mounted using DPX; to adhere to the coverslip to the slide.

26. The stained sections were visualized under a brightfield microscope.

2.5 Masson's Trichrome Staining

The principle of this stain is that the paraffin sections will be fixed by Bouin's solution, which will act as a retrieval of the binding sites for acidic dyes (Mokobi,

2020). The hematoxylin is a basic dye, which is a combination of hematein and aluminum salts that acts as a mordant (Mokobi, 2020). This mordant binds to the acidic structures of the tissue, then allowing the hematein to bind to it, creating a linkage of tissue-mordant-hematein, and that gives the acidic structures, which are the nuclei, its color as black or dark purple (Mokobi, 2020). The acid fuchsin is an acidic red dye that will stain the cytoplasm, which is a basic structure, red (Mokobi, 2020). The phosphomolybdic-phosphotungstic acid solution will specifically remove the red dye from the collagen (Mokobi, 2020). Aniline blue will stain all the structures that are no longer bound to the red dye, which is the collagen, as blue (Mokobi, 2020). Finally, acetic acid will remove the unbound aniline blue from the tissue section (Mokobi, 2020).

In this study, Masson's Trichrome stain was used to measure the trabecular measurements, which are consisting of trabecular bone volume (BV/TV), trabecular separation (Tb. Sp), trabecular thickness (Tb. Th), and trabecular number (Tb. N).

Staining interpretation:

Collagen → blue

Muscle fibers → red

Nuclei → dark red to black/blue

Reagents used:-

1. Bouin's solution.

2. Hematoxylin (A+B = Equally).

3. Acid fuchsin.

4. Aniline blue.

5. Phosphomolybdic-Phosphotungstic Acid Solution (Equal parts of the two acids + Distilled water = Equally).

6. 1% Acetic acid (100 μL of Acetic acid + 10 ml of Distilled Water).

The sections were made from two groups, three animals in each group. From each animal, 10 -15 sections of 5 μm thickness, were made using a microtome.

Protocol for Masson's Trichrome staining:-

1. The slides containing the paraffin sections were incubated at 60°C for 15 minutes.

2. 100% Xylene-I [Dewaxing] = 5 minutes.

3. 100% Xylene-II [Dewaxing] = 5 minutes.

4. 100% Ethanol-I [Hydration] = 5 minutes.

5. 100% Ethanol-II [Hydration] = 5 minutes.

6. 95% Ethanol [Hydration] = 3 minutes.

7. 90% Ethanol [Hydration] = 3 minutes.

8. 70% Ethanol [Hydration] = 3 minutes.

9. 50% Ethanol [Hydration] = 3 minutes.

10. Distilled Water-I = 5 minutes.

11. Distilled Water-II = 5 minutes.

12. Distilled Water-III = 5 minutes.

13. Oven the Bouin's solution at 56°C.

14. Preheated Bouin's solution = 60 minutes.

15. Tap water cooling = 30 minutes.

16. Wash in tap water until the yellow color is removed.

17. Hematoxylin = 20 minutes.

18. Running tap water = 10 minutes.

19. Rinse in Distilled water.

20. Acid Fuchsin = 20 minutes.

21. Rinse in Distilled water.

22. Phosphomolybdic-Phosphotungstic Acid Solution = 20 minutes.

23. Aniline blue = 20 minutes.

24. Acetic acid (1%) = 8 minutes.

25. Rinse in Distilled water.

26. 95% Ethanol [Dehydration] = 1 minute.

27. 100% Ethanol-I [Dehydration] = 2 minutes.

28. 100% Ethanol-II [Dehydration] = 2 minutes.

29. 100% Xylene-I [Clearing] = 10 minutes.

30. 100% Xylene-II [Clearing] = 10 minutes.

31. The stained sections were mounted using DPX; to adhere the coverslip to the slide.

32. The stained sections were visualized under a brightfield microscope.

2.6 TUNEL [Terminal deoxynucleotidyl transferase dUTP Nick End Labeling] Assay

The TUNEL staining was used to detect apoptotic nuclei in paraffin-embedded tissue sections (Gao et al., 2017). One of the biochemical hallmarks of apoptosis is the generation of free 3′-hydroxyl termini on DNA via cleavage of chromatin into single and multiple oligonucleosome-length fragments (Gao et al., 2017). The TdT-mediated dUTP-biotin nick end labeling (TUNEL) assay exploits this biochemical hallmark by labeling the exposed termini of DNA, thereby enabling visualization of nuclei containing fragmented DNA (Gao et al., 2017). Apoptosis was measured using

TUNEL Assay Kit - HRP-DAB (ab206386). In response to apoptotic signals, the assay uses Terminal deoxynucleotidyl Transferase (TdT) that will bind to the exposed 3'-OH ends of DNA fragments and catalyzes the addition of biotin-labeled deoxynucleotides. Then, the Streptavidin-Horseradish Peroxidase (HRP) conjugate detects the biotinylated nucleotides. After that, those HRP-labeled samples got reacted with diaminobenzidine (DAB) and stains those cells as dark brown.

<u>Reagents used:-</u>

1. 1x TBS [Tris-buffered Saline] (6.05 g of 50 mM Tris and 8.76 g of 150 NaCl were dissolved in 800 ml dH$_2$O, the pH was adjusted to 7.6 with 1M HCl, then made up the volume to 1L with dH$_2$O).

2. PAP pen.

3. Proteinase K.

4. 30% H$_2$O$_2$.

5. TdT Equilibration Buffer.

6. TdT enzyme.

7. TdT Labeling Reaction Mix.

8. Stop Buffer.

9. Blocking Buffer.

10. 25x Conjugate.

11. DAB Solution 1.

12. DAB Solution 2.

13. Methyl Green Counterstain solution.

The sections were made from two groups, three animals in each group. From each animal, 10 -15 sections of 5 μm thickness, were made using a microtome.

The protocol for TUNEL Assay Kit - HRP-DAB (ab206386) according to the manufacturer's instructions with some modification:-

Briefly, the paraffin sections were rehydrated and permeabilized with Proteinase K at room temperature for 20 minutes. Endogenous peroxidases were inactivated by 3% H_2O_2 at room temperature for 15 minutes. TdT Equilibration Buffer was added to sections for equilibration and incubated at room temperature for 30 minutes. The sections were labeled by TdT Labeling Reaction Mixture and incubated in a humidified chamber at 37°C for 1.5 hours. The Stop buffer was added and incubated at room temperature for 5 minutes; to terminate the labeling reaction. Blocking Buffer was added and incubated at room temperature for 10 minutes. Following the addition of 25x Conjugate and incubation in a humidified chamber at room temperature for 30 minutes; for detection. The sections were developed by DAB solution and counterstained by the Methyl Green Counterstain solution.

The following steps described the procedure that was performed for the slides containing the paraffin sections:

2.6.1 Rehydration

1. 100% Xylene-I = 5 minutes.
2. 100% Xylene-II = 5 minutes.
3. 100% Ethanol-I = 5 minutes.
4. 100% Ethanol-II = 5 minutes.
5. 90% Ethanol = 3 minutes.
6. 80% Ethanol = 3 minutes.
7. 70% Ethanol = 3 minutes.

8. 1x TBS = 5 minutes.

9. The glass slide around the paraffin-embedded tissue section was dried, and encircled using a PAP pen.

2.6.2 Permeabilization of Specimen

1. For each section, 100 µl of the diluted Proteinase [1:100 dilution, 1 µL of Proteinase K + 99 µL of dH_2O] was added. Then, incubated at room temperature for 20 minutes.

2. 1x TBS = 5 minutes.

3. The glass slide around the paraffin-embedded tissue section was dried.

2.6.3 Quenching: Inactivation of Endogenous Peroxidases

1. For each section, 100 µl of 3% H_2O_2 [1:10 dilution, 10 µL of 30% H_2O_2 + 90 µL of methanol] was added. Then, incubated at room temperature for 15 minutes.

2. 1x TBS = 5 minutes.

3. The glass slide around the paraffin-embedded tissue section was dried.

2.6.4 Equilibration

1. For each section, 100 µl of TdT Equilibration Buffer was added. Then, incubated at room temperature for 30 minutes.

2. At 25 minutes of incubation, the next step proceeded.

2.6.5 Labeling Reaction

1. Before opening the TdT enzyme tube, the TdT enzyme tube was pulse spined.

2. In an Eppendorf tube, the working TdT Labeling Reaction Mixture was

prepared by adding 1 µl of TdT enzyme and adding 39 µl of TdT Labeling

Reaction Mix [this is only for one section, the calculation was done according

to the number of sections]. It was gently mixed and kept on ice until use.

3. The TdT Equilibration Buffer was blotted from the section.

4. For each section, 40 µl of the working TdT Labeling Reaction Mixture was
   added.

5. The sections were covered with coverslips; to avoid evaporation during
   incubation.

6. The sections were incubated in a humidified chamber at 37°C for 1.5 hours.

2.6.6 Termination of the Labeling Reaction

1. The Stop Buffer was warmed to 37°C for 5 minutes.

2. The coverslips were removed from the sections.

3. 1x TBS = 5 minutes.

4. For each section, 100 µl of the Stop Buffer was added and incubated at room
   temperature for 5 minutes.

5. 1x TBS = 5 minutes.

6. The glass slide around the paraffin-embedded tissue section was dried.

2.6.7 Blocking

1. For each section, 100 µl of the Blocking Buffer was added. Then, incubated at
   room temperature for 10 minutes.

2. At 5 minutes of incubation, the next step was proceeded.

2.6.8 Detection

1. In an Eppendorf tube, the 25x Conjugate (1:25 dilution) was diluted by adding 4 µl of 25x Conjugate and adding 96 µl of the Blocking Buffer [this is only for one section, the calculation was done according to the number of sections]. It was gently mixed and kept on ice until use.

2. The Blocking Buffer was blotted from the section.

3. For each section, 100 µl of the diluted 25x Conjugate was added.

4. The sections were incubated in a humidified chamber at room temperature for 30 minutes.

5. 1x TBS = 5 minutes.

2.6.9 Development

1. The glass slide around the paraffin-embedded tissue section was dried.

2. In an Eppendorf tube, prepare the working DAB solution (1:30 dilution) was prepared by adding 4 µl of DAB Solution 1 and adding 116 µl of DAB Solution 2 [this is only for one section, the calculation was done according to the number of sections]. It was gently mixed and kept on ice until use.

3. For each section, 100 µl of the working DAB solution was added.

4. The sections were incubated at room temperature for 15 minutes.

5. Rinse in distilled water.

2.6.10 Counterstain

1. For each section, 100 µl of Methyl Green Counterstain solution was added.

2. The sections were incubated at room temperature for 3 minutes.

3. The counterstain was drawn off from the slide against an absorbent towel.

4. 100% Ethanol-I = Dip 4 times.

5. The slide was blotted on an absorbent towel.

6. 100% Ethanol-II = Dip 4 times.

7. The slide was blotted on an absorbent towel.

8. 100% Xylene = Dip 4 times.

9. The stained sections were mounted using DPX; to adhere to the coverslip to the slide.

10. The stained sections were visualized under a brightfield microscope.

2.7 Molecular Biology Experiments

2.7.1 RNA Extraction from Bones

The mirVanaTM miRNA Isolation Kit (Invitrogen by Thermo Fisher Scientific) was used to purify the total RNA containing the microRNAs from the shaft of the tibia of the control and T2DM groups. This isolation kit relies on the advantage of combing two methods of isolation: chemical extraction [inactivate Rnases and very pure preparations of RNA] and solid-phase extraction [decrease the affinity of RNA for water and increase its affinity for the solid support], which is producing high yields of ultra-pure and high-quality RNA molecules.

Reagents used:-

1. miRNA Wash Solution 1 [for the first time use, add 21 ml of 100% ethanol to it before use].

2. Wash Solution 2/3 [for the first time use, add 40 ml of 100% ethanol before use].

3. Acid-Phenol: Chloroform.

4. Lysis/Binding Buffer.

5. miRNA Homogenate Additive.

6. Elution Solution [nuclease-free 0.1 mM EDTA].

7. Collection tubes.

8. Filter Cartridges.

The protocol for miVana miRNA Isolation Kit according to the manufacturer's instructions:-

1. Bone samples were crushed into powder using the mortar and pestle with liquid nitrogen.

2. In an Eppendorf tube, the powdered bone was collected, and added 600 µl of Lysis/Binding Buffer to it and mixed rapidly.

3. To the same Eppendorf tube, 1/10 volume of miRNA Homogenate Additive [60 µl] was added. The tube was vortexed to mix well.

4. The tube was incubated on ice for 10 minutes.

5. To the same tube, 600 µl of Acid-Phenol: Chloroform was added [the volume of Acid-Phenol: Chloroform should be equal to the lysate volume before the addition of the miRNA Homogenate Additive].

6. Mixed by vortexing for 60 seconds.

7. Centrifuged at 10,000 rpm at room temperature for 5 minutes.

8. Without disturbing the lower phase, remove the upper phase was removed and transferred to a fresh tube. Record the volume of the removed upper phase was recorded.

9. The Elution Solution was preheated to 95°C.

10. 1.25 volumes of 100% ethanol were added to the removed upper phase [if the volume of the removed upper phase was 300 µl, 375 µl of 100% ethanol will

be added].

11. A collection tube was brought and placed a filter cartridge into it.

12. The lysate/ethanol mixture was added onto the filter cartridge [the addition of the mixture should be no more than 700 µl, and if the volume of the mixture was more than 700 µl, the mixture in successive applications will be applied to the same filter].

13. Centrifuged at 10,000 rpm at room temperature for 15 seconds; to let the mixture pass through the filter.

14. The flow-through was discarded from the collection tube. The same filter cartridge was placed into the same collection tube.

15. 700 µl of miRNA Wash Solution 1 was added onto the filter cartridge.

16. Centrifuged at 10,000 rpm at room temperature for 10 seconds; to let the miRNA Wash Solution 1 pass through the filter.

17. The flow-through was discarded from the Collection tube. The same filter cartridge was placed into the same collection tube.

18. 500 µl of Wash Solution 2/3 was added onto the filter cartridge.

19. Centrifuged at 10,000 rpm at room temperature for 10 seconds; to let the Wash Solution 2/3 pass through the filter.

20. The flow-through was discarded from the Collection tube. The same filter cartridge was placed into the same collection tube.

21. 500 µl of Wash Solution 2/3 was added onto the filter cartridge.

22. Centrifuged at 10,000 rpm at room temperature for 10 seconds; to let the Wash Solution 2/3 will through the filter.

23. The flow-through was discarded from the collection tube. The same filter cartridge was placed into the same collection tube.

24. To remove residual fluid from the filter, the assembly was spined for 1 minute.

25. The collection tube was discarded, and a new collection tube was brought and the same filter cartridge was placed into it.

26. 25 µl of the preheated Elution Solution was added to the filter cartridge.

27. Centrifuged at 14,000 rpm at room temperature for 30 seconds; to let the Elution Solution containing the RNA pass through the filter.

28. Another 25 µl of the preheated Elution Solution was added to the filter cartridge.

29. Centrifuged at 14,000 rpm at room temperature for 30 seconds; to let the Elution Solution containing the RNA pass through the filter.

30. The filter cartridge was discarded.

31. The collection tube that has the eluate, which contains the total RNA along with the microRNAs was stored at –80°C. The concentration of the total RNA (ng/µl) was measured by the NanoDrop 2000 spectrophotometer from Thermo Fisher Scientific.

2.7.2 RNA Extraction from Serum

The total RNA from the sera of the control and T2DM groups were isolated by performing the following steps:

1. The serum was centrifuged at 3000 rpm at 4°C for 10 minutes.

2. In an Eppendorf tube, the serum supernatant was transferred to it.

3. In the same Eppendorf tube, 1/10 volume of miRNA Homogenate Additive was added and mixed well.

4. The tube was incubated on ice for 10 minutes.

5. 3.0 volumes of Acid-Phenol: Chloroform was added.

6. Mixed by inverting it several times.

7. Centrifuged at 16,000 rpm at 4°C for 10 minutes.

8. Without disturbing the lower phase, the upper phase was removed and transferred to a fresh tube. The volume of the removed upper phase was recorded.

9. Equal to or more than the volume of the removed upper phase, the isopropanol was added.

10. Mixed by inverting it several times.

11. Centrifuged at 16,000 rpm at 4°C for 15 minutes.

12. The supernatant was removed by inverting it up-side-down.

13. To the same tube, 500 µl of the washing solution was added [35 ml of 70% ethanol + 15 ml of nuclease-free water].

14. Mixed by inverting it several times.

15. Centrifuged at 16,000 rpm at 4°C for 5 minutes.

16. The supernatant was removed by inverting it up-side-down.

17. The tube was centrifuged briefly and the supernatant was removed by using the pipette.

18. The pellet was resuspended in 20 µl of nuclease-free water.

19. The tube that has the total RNA along with the microRNAs was stored at – 80°C. The concentration of the total RNA (ng/µl) was measured by the NanoDrop 2000 spectrophotometer from Thermo Fisher Scientific.

2.8 Reverse Transcription

2.8.1 For the MicroRNAs

For reverse transcription, the TaqMan® Small RNA Assays (Applied

Biosystems by Thermo Fisher Scientific) was used to reverse transcribe cDNA from total RNA. The steps below were followed according to the manufacturer's instructions with some modification; to perform the reverse transcription:

1. The following components of the reverse transcription kit were thawed on ice:

    a. 100mM dNTPs (with dTTP).

    b. 10x Reverse Transcription Buffer.

    c. RNase Inhibitor, 20 U/μl.

2. The following RT primers were thawed on ice:

    d. miR-20a (Assay ID: 001336).

    e. miR-21 (Assay ID: 000397).

    f. miR-29a (Assay ID: 002447).

    g. miR-31 (Assay ID: 002495).

    h. miR-155 (Assay ID 002571).

    i. U6 snRNA [as an internal control for the microRNAs] (Assay ID: 001973).

3. For one reaction, 0.15 μl of 100mM dNTPs (with dTTP) + 1.50 μl of 10x Reverse Transcription Buffer + 4.16 μl of nuclease-free water + 0.19 μl of RNase Inhibitor, 20 U/μl + 1.00 μl of MultiScribe™ Reverse Transcriptase, 50 U/μl, were added to a microcentrifuge tube.

4. Mixed by inversion, and briefly centrifuged.

5. To the same microcentrifuge tube that contains the RT Reaction Mix, 3 μl of one of the RT primers was added. Note that for the other RT primers, each one should have its microcentrifuge tube containing the RT Reaction Mix.

6. According to the concentration of the sample, The volume (μl) that should be added to the same microcentrifuge tube that contains the RT Reaction Mix was

calculated (0.5 µg of the total RNA from the bones and 1 µg of the total RNA from the sera).

7. The total volume of the reaction was made up to 20 µl by the addition of nuclease-free water.

8. The reaction tube was briefly centrifuged.

9. The reaction tube was placed into the thermal cycler, and performed the standard cycling steps as follows:

    j. First reverse transcription at 16°C for 30 minutes.

    k. Second reverse transcription at 42°C for 30 minutes.

    l. Reaction was stopped at 85°C for 5 minutes.

    m. Lastly, hold at 4°C.

10. The product of the reverse transcription was stored at –20°C.

2.8.2 For the Target Genes of the MicroRNAs

For reverse transcription, the High-Capacity cDNA Reverse Transcription Kits (Applied Biosystems by Thermo Fisher Scientific) was used to reverse transcribe cDNA from total RNA. The steps below were followed according to the manufacturer's instructions with some modifications; to perform the reverse transcription:

1. The following components of the reverse transcription kit were thawed on ice:

a. 10x RT Buffer.

b. 25x dNTP Mix [100 mM].

c. 10x RT Random Primers.

d. RNase Inhibitor, 20 U/µl.

2. For one reaction, 0.8 µl of 25x dNTP Mix [100 mM] + 2.0 µl of 10x RT Buffer

+ 3. 2 µl of nuclease-free water + 2.0 µl of 10x RT Random Primers + 1.0 µl of RNase Inhibitor, 20 U/µl + 1.0 µl of MultiScribe™ Reverse Transcriptase, 50 U/µl, was added to a microcentrifuge tube.

3. Mixed by inversion and briefly centrifuged.

4. According to the concentration of the sample, the volume (µl) that should be added to the same microcentrifuge tube that contains the RT Master Mix was calculated (1 µg of the total RNA from the bones).

5. The total volume of the reaction was made up to 20 µl by the addition of nuclease-free water.

6. The reaction tube was briefly centrifuged.

7. The reaction tube was placed into the thermal cycler, and performed the standard cycling steps as follows:

a. First step at 25°C for 10 minutes.

b. Second step at 37°C for 120 minutes.

c. Third step at 85°C for 5 minutes.

d. Lastly, hold at 4°C.

8. The product of the reverse transcription was stored at –20°C.

2.9 Quantification Real-Time PCR

For quantification-Real Time PCR, the TaqMan® Small RNA Assays (Applied Biosystems by Thermo Fisher Scientific) was used to amplify the cDNA. The steps below were followed according to the manufacturer's instructions with some modifications; to perform the quantification-Real Time PCR:

1. The following primers were thawed on ice:

   a. miR-20a (Assay ID: 001336).

b. miR-21 (Assay ID: 000397).

c. miR-29a (Assay ID: 002447).

d. miR-31 (Assay ID: 002495).

e. miR-155 (Assay ID 002571).

f. U6 snRNA [as an internal control for the microRNAs] (Assay ID: 001973).

g. ACTB [Actin-Beta, as an internal control for the target genes of the microRNAs] (Assay ID: Rn00667869_m1).

h. ATG16L1 [Autophagy Related 16 Like 1] (Assay ID: Rn01400301_m1).

i. BAMBI [Bone Morphogenetic Protein and Activin Membrane-Bound Inhibitor] (Assay ID: Rn00594597_m1).

j. BMP2 [Bone Morphogenetic Protein 2] (Assay ID: Rn00567818_m1).

k. BMP3 [Bone Morphogenetic Protein 3] (Assay ID: Rn00567346_m1).

l. CALCA [Calcitonin Related Polypeptide Alpha] (Assay ID: Rn00569199_m1).

m. CRIM1 [Cysteine rich transmembrane BMP regulator 1] (Assay ID: Rn01232943_m1).

n. DKK1 [Dickkopf WNT Signaling Pathway Inhibitor 1] (Assay ID: Rn01501537_m1).

o. KREMEN2 [Kringle Containing Transmembrane Protein 2] (Assay ID: Rn01752365_m1).

p. MITF [Microphthalmia-associated transcription factor] (Assay ID: Rn01425766_m1).

q. PDCD4 [Programmed cell death protein 4] (Assay ID:

Rn00573954_m1).

r. PPARG [Peroxisome proliferator activated receptor gamma] (Assay ID: Rn00440945_m1).

s. RhoA [Ras homolog family member A] (Assay ID: Rn00589172_m1).

t. RUNX2 [Runt-related transcription factor 2 (CBFA1)] (Assay ID: Rn01512298_m1).

u. SATB2 [Special AT-Rich Sequence-Binding Protein 2] (Assay ID: Rn01438160_m1).

v. SFRP2 [Secreted frizzled-related protein 2] (Assay ID: Rn01458837_m1).

w. SMAD7 [*Caenorhabditis elegans* SMA ("small" worm phenotype) and Drosophila MAD ("Mothers Against Decapentaplegic") (Smad family member 7)] (Assay ID: Rn00578319_m1).

x. SOCS1 [Suppressor of cytokine signaling 1 (STAT-induced STAT inhibitor 1 (SSI))] (Assay ID: Rn00595838_s1).

y. SOST [Sclerostin] (Assay ID: Rn00577971_m1).

z. SP7 [Sp7 Transcription Factor (Osterix)] (Assay ID: Rn01761789_m1).

aa. SRF [Serum Response Factor] (Assay ID: Rn01757240_m1).

bb. TGFB1 [Transforming Growth Factor Beta 1] (Assay ID: Rn00572010_m1).

cc. TNFRSF11B [Tumor necrosis factor receptor superfamily member 11b (OPG)] (Assay ID: Rn00563499_m1).

dd. TNFSF11 [Tumor Necrosis Factor Ligand Superfamily Member 11 (RANKL)] (Assay ID: Rn00589289_m1).

2. In a microcentrifuge tube, PCR Reaction Mix was prepared by adding 7 µl of nuclease-free water, 10 µl of PCR Master Mix, and 1 µl of one of the primers. Note that for the other primers, each one should have its microcentrifuge tube containing the PCR Reaction Mix.

3. 1 µl of the cDNA was added, if the reaction was meant for determining microRNAs. 2 µl of the cDNA was added, if the reaction is meant for determining the target genes of the microRNAs.

4. The reaction tube was briefly centrifuged.

5. The reaction tube was placed into the QuantStudio^{TM} 7 Flex Real-Time PCR system (Applied Biosystems by Thermo Fisher Scientific), and programed the thermal-cycling conditions as follows for 50 cycles:

   ee. UNG activation at 50°C for 2 minutes.

   ff. Enzyme activation at 94°C for 10 minutes.

   gg. Denature at 95°C for 15 seconds.

   hh. Anneal/Extend at 60°C for 60 seconds.

The expression analysis, using TaqMan® Small RNA Assays, was performed using the comparative delta-delta Ct method. The internal controls used for the normalization of microRNAs was U6 snRNA and for target mRNAs was Actin-Beta. Each experiment was performed in duplicates and repeated three times.

2.10 Enzyme-linked Immunosorbent Assay [ELISA] Kit For Osteocalcin [OC]

The ELISA kit for osteocalcin (Cloud-Clone Corp. / SEA471Ra) is a quantitative measurement and a type of a sandwich enzyme immunoassay. The kit's microplate wells are coated with a biotin-conjugated antibody that is specific to osteocalcin. To each well, the serum samples are added along with Avidin that is conjugated to Horseradish Peroxidase (HRP). The TMB substrate solution is added

afterward. The wells that exhibit a change in color (blue) are the ones that contain osteocalcin, and it is measured (referring to the optical density of osteocalcin) spectrophotometrically at a wavelength of 450 nm.

Reagents used, which were supplied by the company in the kit:-

1. Standard and Standard Diluent.

2. Detection Reagent A and Assay Diluent A.

3. Detection Reagent B and Assay Diluent B.

4. TMB substrate and Stop solution.

5. 1x Wash solution.

6. Pre-coated 96-well strip plate and plate sealer.

The protocol for measuring osteocalcin in sera using ELISA kit (Cloud-Clone Corp. / SEA471Ra) was done according to the manufacturer's instructions:-

1. The following components of the ELISA kit were brought to room temperature:

    a. Serum samples of the control and T2DM groups.

    b. Standard and Standard Diluent.

    c. Detection Reagent A and Assay Diluent A.

    d. Detection Reagent B and Assay Diluent B.

    e. TMB substrate and Stop solution.

    f. 1x Wash solution.

2. 1 ml of Standard Diluent was added to the Standard, inverted gently, and kept for 10 minutes at room temperature.

3. The concentration of the Standard is 5000 pg/ml. 7 points of diluted standard were made as 1000 pg/ml, 500 pg/ml, 250 pg/ml, 125 pg/ml, 62.5 pg/ml, 31.2

pg/ml and 15.6 pg/ml.

4. The blank was made as 0 pg/ml by adding only the Standard Diluent.

5. A 100 fold dilution was made of Detection Reagent A with Assay Diluent A and Detection Reagent B with Assay Diluent B.

6. On the pre-coated 96-well strip plate, the wells were defined for the 7 diluted standards, the blank, and the serum samples.

7. 100 μl of the diluted standards, the blank, and the serum samples were added into their defined wells.

8. The wells were covered with a plate sealer and incubated for 1 hour at 37°C.

9. The content of each well was removed.

10. 100 μl of Detection Reagent A was added into each well.

11. The wells were covered with a plate sealer and incubated for 1 hour at 37°C.

12. The content of each well was removed.

13. 350 μl of 1x Wash solution was added into each well and stood for 2 minutes.

14. The content of each well was removed.

15. Step 13 and step 14 were performed three times.

16. 100 μl of Detection Reagent B was added into each well.

17. The wells were covered with a plate sealer and incubated for 30 minutes at 37°C.

18. Step 13 and step 14 were performed five times.

19. 90 μl of TMB substrate solution was added into each well.

20. The wells were covered with a new plate sealer and incubated for 20 minutes at 37°C in dark.

21. 50 μl of Stop solution was added into each well, mixed by tapping the side of the plate.

22. Bubbles were inspected and removed.

23. The bottom of the plate was cleaned.

24. The absorbance (optical density) was read at 450 nm wavelength for the diluted standards, the blank, and the serum samples by using the spectrophotometer.

25. The calibration curve was created; to measure the osteocalcin concentration of the samples.

2.11 Rat Osteocalcin ELISA Kit

The Rat Osteocalcin ELISA kit (Abbkine / KTE101053) is a quantitative measurement and a type of a sandwich enzyme immunoassay. The kit's microplate wells are coated with an immobilized antibody that is specific to osteocalcin. To each well, the bone samples [bone hydrolysate] are added along with Rat Osteocalcin detection antibody that is conjugated to Horseradish Peroxidase (HRP). The Chromogen solution is added afterward. The wells that exhibit a change in color (yellow) are the ones that contain osteocalcin, and it is measured (referring to the optical density of osteocalcin) spectrophotometrically at a wavelength of 450 nm.

Reagents used, which were supplied by the company in the kit:-

1. Standard diluent.

2. Sample diluent.

3. Chromogen solution A.

4. Chromogen solution B.

5. Stop solution.

6. 1x Wash Buffer.

7. Pre-coated 96-well Rat Osteocalcin microplate.

8. Plate covers.

9. Rat Osteocalcin standard.

10. HRP-Conjugated Rat Osteocalcin detection antibody.

<u>Sample preparation:</u>

The bones were cleaned and washed in 1x PBS. Then, dried on tissue paper and ground with liquid nitrogen. 10 volume of 2 M acetic acid was added to each of the bone powder. Boiled for 10 minutes. Centrifuged at 3000 g for 15 minutes. Lastly, the supernatant was taken from each sample and transferred to their labeled Eppendorf tubes. The bone hydrolysates were formed by the Acid-Resistant CentriVap Concentrator from LABCONCO and added 10 μl of PBS to the sample.

<u>The protocol for measuring osteocalcin in bones using Rat Osteocalcin ELISA kit (Abbkine / KTE101053) was done according to the manufacturer's instructions:-</u>

1. The following components of the ELISA kit were brought to room temperature:

    a. Bone hydrolysate samples of the control and T2DM groups.

    b. Standard diluent.

    c. Sample diluent.

    d. Chromogen solution A.

    e. Chromogen solution B.

    f. Stop solution.

    g. 1x Wash buffer.

    h. Rat Osteocalcin standard.

2. 150 μl of Standard Diluent was added to the Rat Osteocalcin standard, inverted gently.

3. The concentration of the Standard is 1600 ng/l. 5 points of diluted standard

were made (2-fold dilution) as 800 ng/l, 400 ng/l, 200 ng/l, 100 ng/l, 50 ng/l.

4. The blank was made as 0 pg/ml by adding only the Standard Diluent.

5. On the pre-coated 96-well strip plate, the wells were defined for the 5 diluted standards, the blank, and the bone hydrolysate samples.

6. 50 μl of the diluted standards were added into their defined wells.

7. 40 μl of sample diluent and 10 μl of bone hydrolysate samples were added into their defined wells.

8. The wells were covered with a plate cover and incubated for 45 minutes at 37°C.

9. The content of each well was removed.

10. 250 μl of 1x Wash solution was added into each well and stood for 2 minutes.

11. The content of each well was removed.

12. Step 10 and step 11 were performed five times.

13. 50 μl of HRP-Conjugated detection antibody was added to the wells of the 5 diluted standards and the bone hydrolysate samples.

14. The wells were covered with plate cover and incubated for 30 minutes at 37°C.

15. The content of each well was removed.

16. 250 μl of 1x Wash solution was added into each well and stood for 2 minutes.

17. The content of each well was removed.

18. Step 16 and step 17 were performed five times.

19. 50 μl of chromogen solution A and 50 μl of chromogen solution B were added into each well and mixed gently.

20. The wells were incubated for 15 minutes at 37°C in dark.

21. 50 μl of Stop solution was added into each well, mixed by tapping the side of the plate.

22. Bubbles were inspected and removed.

23. The bottom of the plate was cleaned.

24. The absorbance (optical density) was read at 450 nm wavelength for the diluted standards, the blank, and the bone samples by using the spectrophotometer.

25. The calibration curve was created; to measure the osteocalcin concentration of the samples.

2.12 Statistical Analysis

The data obtained from quantification Real-Time PCR were presented as mean relative expression and Standard Error of Mean (SEM), and the p values were achieved by using Student's t-test.

The data obtained from ELISA were presented as mean concentration and Standard Error of Mean (SEM), and the p values were achieved by using Student's t-test.

The data obtained from the TUNEL assay were presented as mean counts were achieved by using ImageJ and Standard Error of Mean (SEM), and the p values were achieved by using Student's t-test.

The data obtained from Masson's Trichrome staining were used to measure the TBV(%) and Tb. Sp (mm) using Image J. The calculation was made for Tb. Th (1/Tb. Sp) and Tb. N (TBV/Tb. Th). The data were presented as mean measured parameters [TBV, Tb. Sp, Tb. Th, and Tb. N] and Standard Error of Mean (SEM), and the p values were achieved by using Student's t-test.

Chapter 3: Results

3.1 Identification of MicroRNAs in Bones of 8 Weeks of the Onset of Type 2 Diabetes Mellitus

Five microRNAs were selected to study their expression in the bones of 8 weeks of the onset of type 2 diabetes mellitus, and those microRNAs were miR-20a, miR-21, miR-29a, miR-31, and miR-155. Quantification Real-Time PCR was performed to analyze their expression using the comparative delta-delta Ct method. U6 snRNA was used as an internal control for normalization. Each experiment was performed in duplicates and repeated three times. The following observations were recorded:

The expression of miR-31 and miR-29a were non-significantly increased in the bones of 8 weeks of the onset of type 2 diabetes mellitus, whereas the expression of miR-20a has non-significantly decreased in the bones of 8 weeks of the onset of type 2 diabetes mellitus as presented in Figure 3.

MiR-21 expression was non-significantly upregulated in 8 weeks of type 2 diabetic rat bone tissue (Figure 4).

MiR-155 expression was non-significantly downregulated in 8 weeks of type 2 diabetic rat bone tissue (Figure 5).
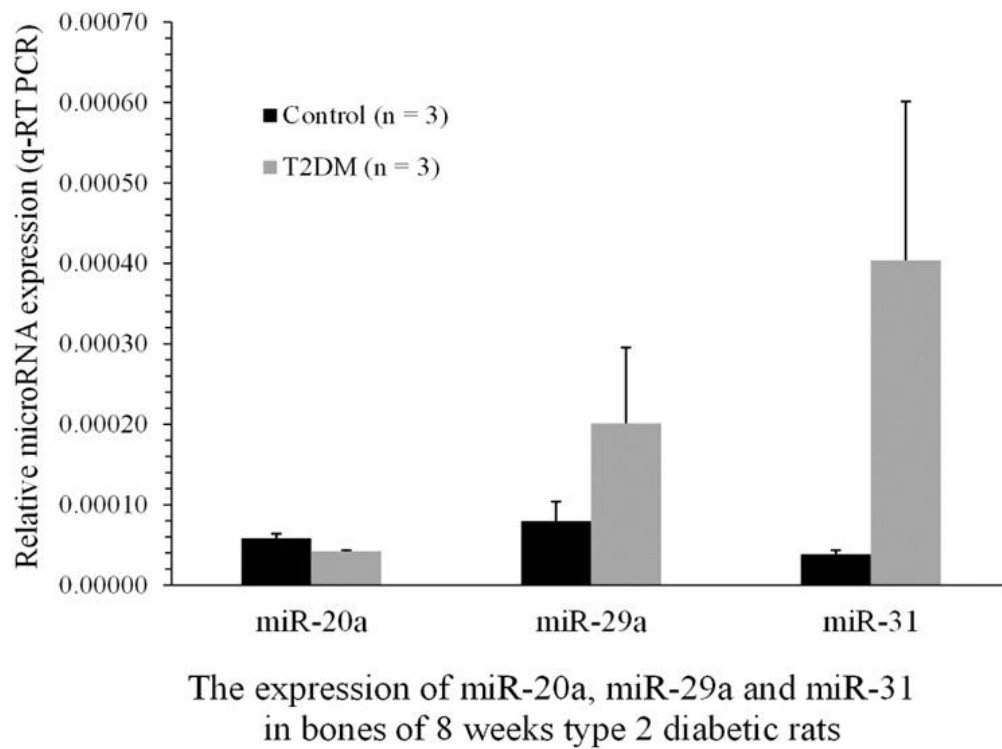
Figure 3: Upregulation of miR-31 and miR-29a, and downregulation of miR-20a in 8 weeks type 2 diabetic rat bone tissue.
Total RNA isolated from tibiae bone samples of control (n = 3) and T2DM (n = 3) rats were analyzed by q-RT PCR to quantify miR-31 (p = 0.1379), miR-29a (p = 0.3990) and miR-20a (p = 0.0614) and normalized against U6 snoRNA to plot the relative expression of miR-31, miR-29a and miR-20a. Student's t-test, error bars indicate Standard Error of Mean (SEM).
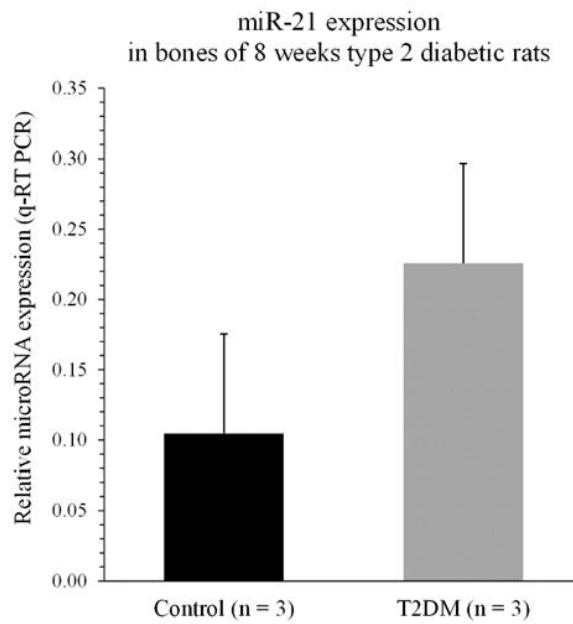
Figure 4: Upregulation of miR-21 in 8 weeks type 2 diabetic rat bone tissue. Total RNA isolated from tibiae bone samples of control (n = 3) and T2DM (n = 3) rats were analyzed by q-RT PCR to quantify miR-21 (p = 0.2359) and normalized against U6 snoRNA to plot the relative expression of miR-21. Student's t-test, error bars indicate Standard Error of Mean (SEM).
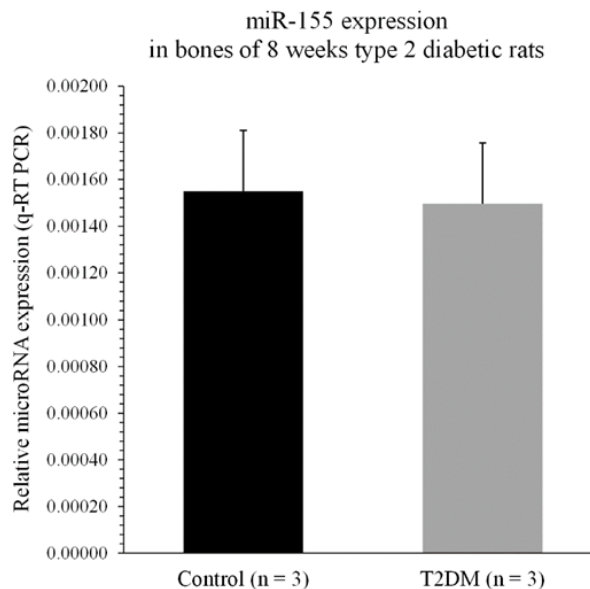

Figure 5: Downregulation of miR-155 in 8 weeks type 2 diabetic rat bone tissue. Total RNA isolated from tibiae bone samples of control (n = 3) and T2DM (n = 3) rats were analyzed by q-RT PCR to quantify miR-155 (p = 0.9126) and normalized against U6 snoRNA to plot the relative expression of miR-155. Student's t-test, error bars indicate Standard Error of Mean (SEM).

3.2 Identification of MicroRNAs in Bones of 10 Weeks of the Onset of Type 2 Diabetes Mellitus

The expression of miR-20a, miR-21, miR-29a, miR-31, and miR-155 was further examined in the bones of 10 weeks of the onset of type 2 diabetes mellitus. Quantification Real-Time PCR was performed to analyze their expression using the comparative delta-delta Ct method. U6 snRNA was used as an internal control for normalization. Each experiment was performed in duplicates and repeated three times. The following observations were recorded:

There was a significant reduction of miR-20a ($p < 0.05$) expression in 10 weeks type 2 diabetic rat bone tissue, as displayed in Figure 6.

The expression of miR-31 and miR-29a were non-significantly decreased in the bones of 10 weeks of the onset of type 2 diabetes mellitus as shown in Figure 6.

MiR-21 ($p < 0.05$) expression was significantly downregulated in 10 weeks type 2 diabetic rat bone tissue (Figure 7).

The expression of miR-155 ($p < 0.05$) expression was significantly declined in the bones of 10 weeks of the onset of type 2 diabetes mellitus (Figure 8).
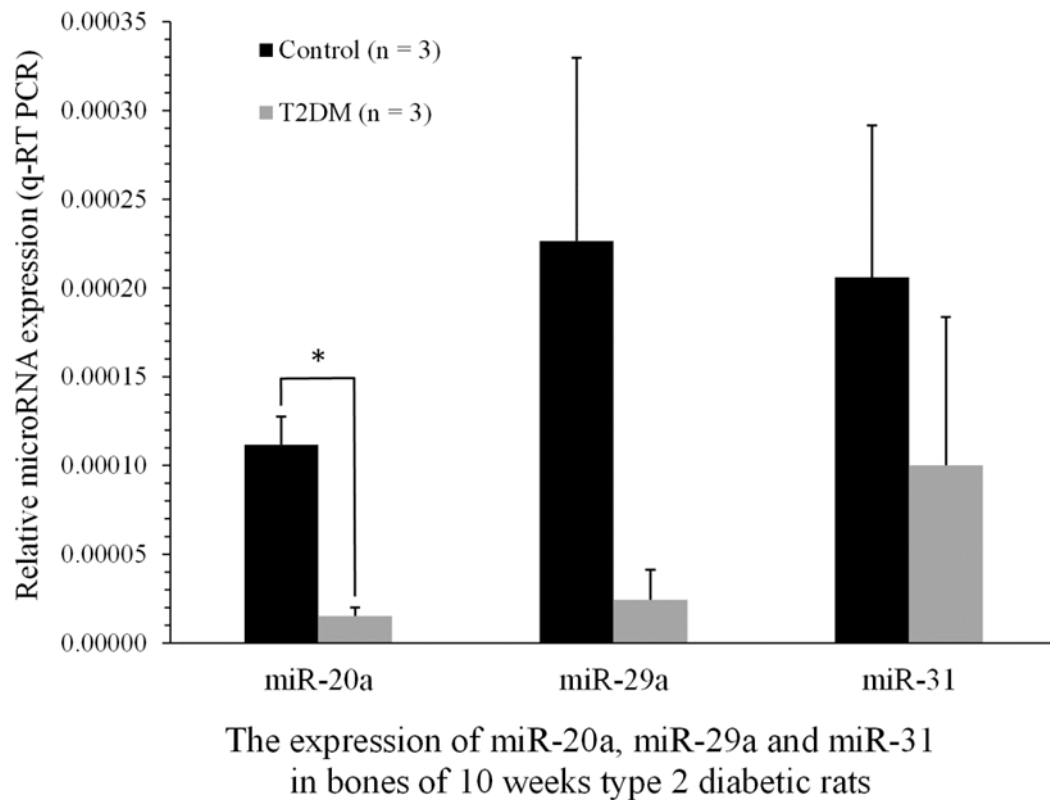
Figure 6: The expression of miR-29a and miR-31 is downregulated, the expression of miR-20a is significantly downregulated in 10 weeks type 2 diabetic rat bone tissue. Total RNA isolated from tibiae bone samples of control (n = 3) and T2DM (n = 3) rats were analyzed by q-RT PCR to quantify miR-20a (p = 0.0416), miR-29a (p = 0.2294), and miR-31 (p = 0.4845) and normalized against U6 snoRNA to plot the relative expression of miR-20a, miR-29a, and miR-31. (Student's t-test, error bars indicate Standard Error of Mean (SEM), * indicates significant differences at p < 0.05).

Figure 7: The expression of miR-21 is significantly downregulated in 10 weeks type 2 diabetic rat bone tissue.
Total RNA isolated from tibiae bone samples of control (n = 3) and T2DM (n = 3) rats were analyzed by q-RT PCR to quantify miR-21 (p = 0.0193) and normalized against U6 snoRNA to plot the relative expression of miR-21. (Student's t-test, error bars indicate Standard Error of Mean (SEM), * indicates significant differences at p < 0.05).
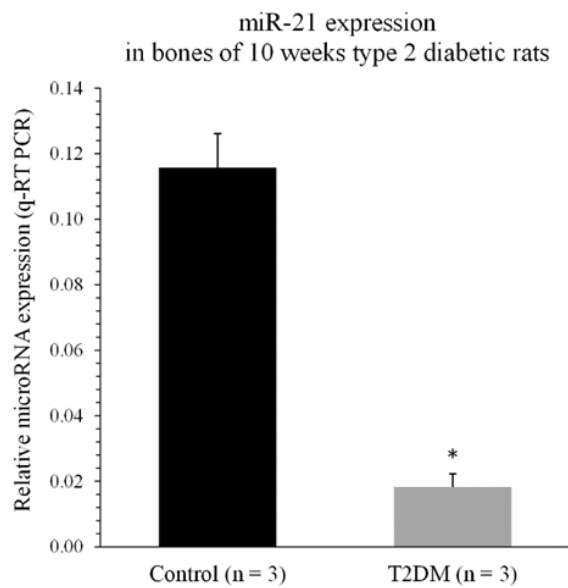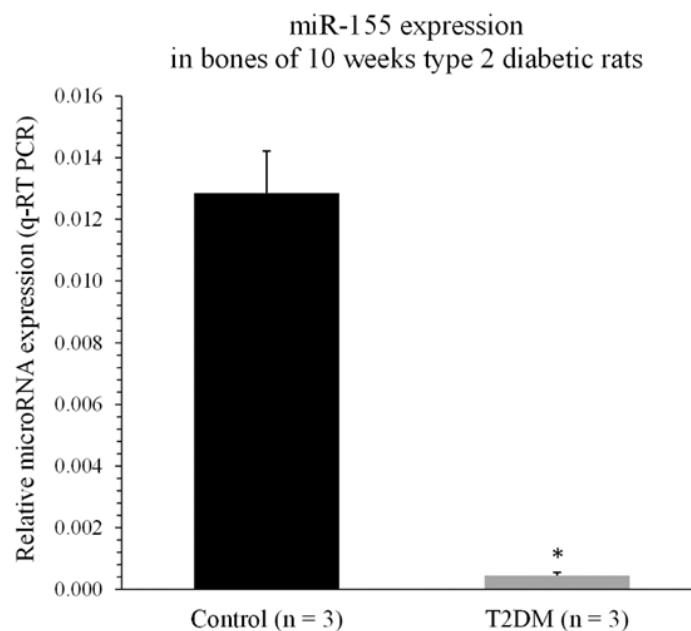

Figure 8: The expression of miR-155 is significantly downregulated in 10 weeks type 2 diabetic rat bone tissue.
Total RNA isolated from tibiae bone samples of control (n = 3) and T2DM (n = 3) rats were analyzed by q-RT PCR to quantify miR-155 (p = 0.0179) and normalized

against U6 snoRNA to plot the relative expression of miR-155. (Student's t-test, error bars indicate Standard Error of Mean (SEM), * indicates significant differences at $p < 0.05$).

3.3 Identification of MicroRNAs in Bones of 14 Weeks of the Onset of Type 2 Diabetes Mellitus

The expression of miR-20a, miR-21, miR-29a, miR-31, and miR-155 was determined in one more time point. Therefore, their expression have been studied in the bones of 14 weeks of the onset of type 2 diabetes mellitus. Quantification Real-Time PCR was performed to analyze their expression using the comparative delta-delta Ct method. U6 snRNA was used as an internal control for normalization. Each experiment was performed in duplicates and repeated three times. The following observations were recorded:

There was non-significant upregulation of miR-20a expression, and non-significant downregulation of the expression of miR-29a and miR-31 in 14 weeks type 2 diabetic rat bone tissue, as described in Figure 9.

MiR-21 expression was non-significantly lowered in 14 weeks type 2 diabetic rat bone tissue (Figure 10).

The expression of miR-155 was non-significantly raised in the bones of 14 weeks of the onset of type 2 diabetes mellitus (Figure 11).
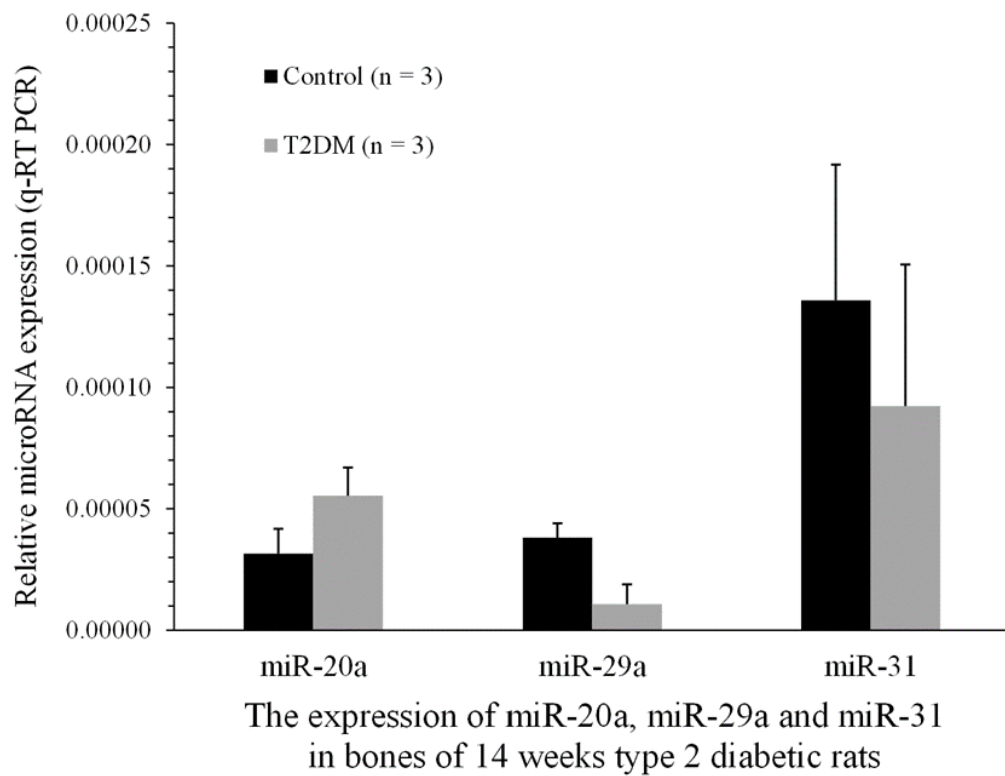
Figure 9: Upregulation of miR-20a, and downregulation of miR-29a and miR-31 in 14 weeks type 2 diabetic rat bone tissue.
Total RNA isolated from tibiae bone samples of control (n = 3) and T2DM (n = 3) rats were analyzed by q-RT PCR to quantify miR-20a (p = 0.2709), miR-29a (p = 0.1552), and miR-31 (p = 0.6650) and normalized against U6 snoRNA to plot the relative expression of miR-20a, miR-29a, and miR-31. Student's t-test, error bars indicate Standard Error of Mean (SEM).

Figure 10: Downregulation of miR-21 in 14 weeks type 2 diabetic rat bone tissue. Total RNA isolated from tibiae bone samples of control (n = 3) and T2DM (n = 3) rats were analyzed by q-RT PCR to quantify miR-21 (p = 0.4788) and normalized against U6 snoRNA to plot the relative expression of miR-21. Student's t-test, error bars indicate Standard Error of Mean (SEM).

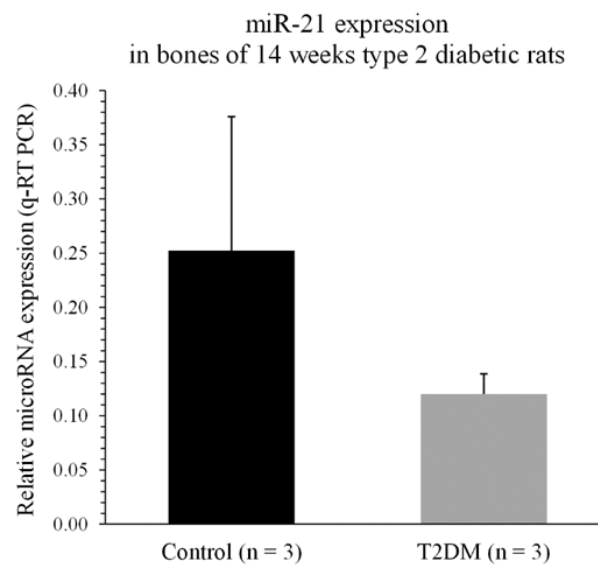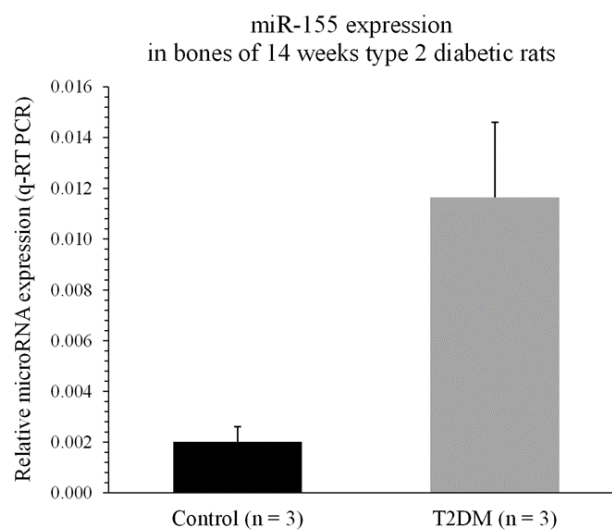Figure 11: Upregulation of miR-155 in 14 weeks type 2 diabetic rat bone tissue. Total RNA isolated from tibiae bone samples of control (n = 3) and T2DM (n = 3) rats were analyzed by q-RT PCR to quantify miR-155 (p = 0.1220) and normalized against U6 snoRNA to plot the relative expression of miR-155. Student's t-test, error bars indicate Standard Error of Mean (SEM).

3.4 Identification of MicroRNAs in Sera of 8 Weeks of the Onset of Type 2 Diabetes Mellitus

The expression of miR-20a, miR-21, miR-29a, miR-31, and miR-155 were further investigated in the sera of 8 weeks of the onset of type 2 diabetes mellitus; to know whether the results that were founded in the bones can be expressed in the sera as well. Quantification Real-Time PCR was performed to analyze their expression using the comparative delta-delta Ct method. U6 snRNA was used as an internal control for normalization. Each experiment was performed in duplicates and repeated three times. The following observations were recorded:

A total of 6 rats were assigned randomly to the Control group (n = 3) and T2DM group (n = 3). The serum samples were immediately withdrawn just before the animals were sacrificed, and kept in labeled Eppendorf tubes at room temperature for 30 minutes; to clot. Then, the tubes were centrifuged at 3,000 rpm for 10 minutes; to separate the clot from the serum. The serum samples were kept in fresh labeled Eppendorf tubes and stored at –80°C. From each serum sample, the total RNA was extracted and reverse transcribed to cDNA. The expression of miR-20a, miR-21, miR-29a, miR-31, and miR-155 in sera was determined by q-RT PCR.

There was a non-significant increase of miR-21 expression in the sera of 8 weeks of the onset of type 2 diabetes mellitus, as shown in Figure 12.

Figure 12: The expression of miR-21 is upregulated in the sera of 8 weeks type 2 diabetic rat models.
Total RNA isolated from serum samples of control (n = 3) and type 2 diabetic (n = 3) rats were analyzed by q-RT PCR to quantify miR-21 (p = 0.4140) and normalized against U6 snoRNA to plot the relative expression of miR-21. Student's t-test, error bars indicate Standard Error of Mean (SEM).

3.5 Identification of MicroRNAs in Sera of 10 Weeks of the Onset of Type 2 Diabetes Mellitus

The expression of miR-20a, miR-21, miR-29a, miR-31, and miR-155 was investigated in the sera of 10 weeks of the onset of type 2 diabetes mellitus. Quantification Real-Time PCR was performed to analyze their expression using the comparative delta-delta Ct method. U6 snRNA was used as an internal control for normalization. Each experiment was performed in duplicates and repeated three times. The following observations were recorded:

There was a significant reduction of miR-21 ($p < 0.05$) in the sera of 10 weeks of the onset of type 2 diabetes mellitus (Figure 13).
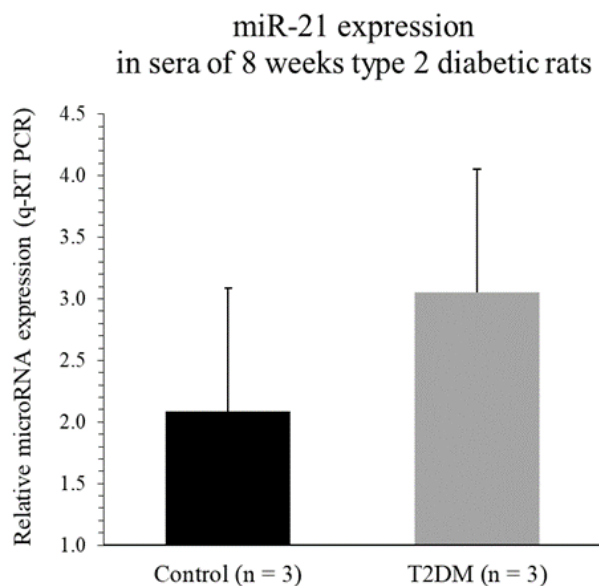
Figure 13: The expression of miR-21 is significantly downregulated in the sera of 10 weeks type 2 diabetic rat model.
Total RNA isolated from serum samples of control (n = 3) and type 2 diabetic (n = 3) rats were analyzed by q-RT PCR to quantify miR-21 (p = 0.0513) and normalized against U6 snoRNA to plot the relative expression of miR-21. (Student's t-test, error bars indicate Standard Error of Mean (SEM), * indicates significant differences at p < 0.05).

3.6 Identification of MicroRNAs in Sera of 14 Weeks of the Onset of Type 2 Diabetes Mellitus

The expression of miR-20a, miR-21, miR-29a, miR-31, and miR-155 in the sera of 14 weeks of the onset of type 2 diabetes mellitus were studied. Quantification Real-Time PCR was performed to analyze their expression using the comparative delta-delta Ct method. U6 snRNA was used as an internal control for normalization. Each experiment was performed in duplicates and repeated three times. The following observations were recorded:

There was a significant elevation of miR-155 (p < 0.01) expression in the sera of 14 weeks of the onset of type 2 diabetes mellitus, as displayed in Figure 14.
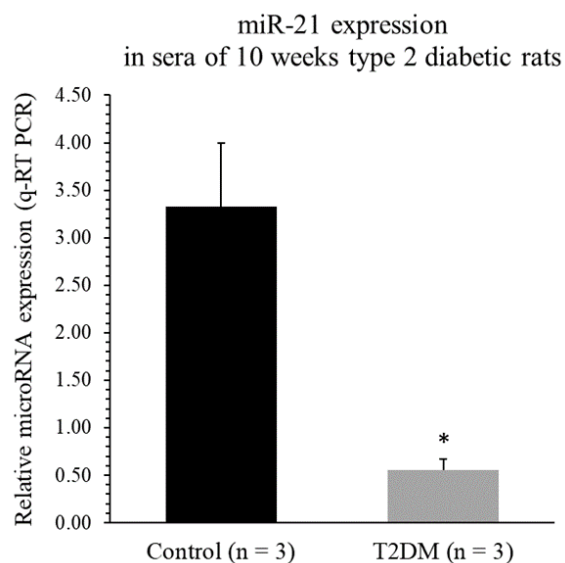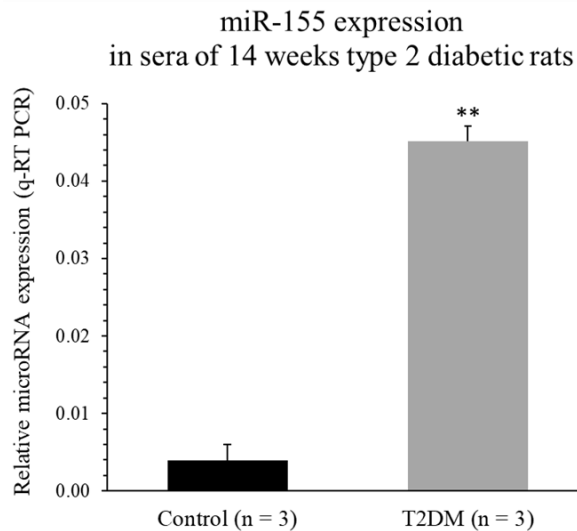
Figure 14: The expression of miR-155 is significantly upregulated in the sera of 14 weeks type 2 diabetic rat model.
Total RNA isolated from serum samples of control (n = 3) and type 2 diabetic (n = 3) rats were analyzed by q-RT PCR to quantify miR-155 (p = 0.0102) and normalized against U6 snoRNA to plot the relative expression of miR-155. (Student's t-test, error bars indicate Standard Error of Mean (SEM), ** indicates significant differences at p < 0.01).

3.7 Identification of MicroRNA Target Genes in Bones of 8 Weeks of the Onset of Type 2 Diabetes Mellitus

In the bones of 8 weeks of the onset of type 2 diabetes mellitus, 23 target genes that are known by the literature review to be controlled by miR-20a, miR-21, miR-29a, miR-31, and miR-155 were examined. The 23 target genes are as follows:

1. ATG16L1→ Autophagy Related 16 Like 1.

2. Bambi → Bone Morphogenetic Protein and Activin Membrane-Bound Inhibitor.

3. BMP2→ Bone Morphogenetic Protein 2.

4. BMP3 → Bone Morphogenetic Protein 3.

5. CALCA → Calcitonin Related Polypeptide Alpha.

6. CRIM1→ Cysteine-rich transmembrane BMP regulator 1.

7. DKK1→ Dickkopf WNT Signaling Pathway Inhibitor 1.

8. KREMEN2 → Kringle Containing Transmembrane Protein 2.

9. MITF → Microphthalmia-associated transcription factor.

10. PDCD4 → Programmed cell death protein 4.

11. PPARG → Peroxisome proliferator-activated receptor gamma.

12. RhoA → Ras homolog family member A.

13. RUNX2 → Runt-related transcription factor 2 [CBFA1].

14. SATP2 → Special AT-Rich Sequence-Binding Protein 2.

15. SFRP2 → Secreted frizzled-related protein 2.

16. SMAD7 → *Caenorhabditis elegans* SMA ("small" worm phenotype) and Drosophila MAD ("Mothers Against Decapentaplegic") [Smad family member 7].

17. SOCS1→ Suppressor of cytokine signaling 1 [STAT-induced STAT inhibitor 1 (SSI)].

18. SOST → Sclerostin.

19. SP7 → Sp7 Transcription Factor [Osterix].

20. SRF → Serum Response Factor.

21. TGFB1 → Transforming Growth Factor Beta 1.

22. TNFRSF11P → Tumor necrosis factor receptor superfamily member 11b [OPG].

23. TNFSF11 → Tumor Necrosis Factor Ligand Superfamily Member 11 [RANKL].

Quantification Real-Time PCR was performed to analyze their expression using the comparative delta-delta Ct method. Actin-Beta was used as an internal control for normalization. Each experiment was performed in duplicates and repeated three times. The following observations were recorded:

Among the 23 target genes, the expression of the RhoA gene and SOCS1 gene were detected.

RhoA (p < 0.05) gene expression was significantly lowered in 8 weeks type 2 diabetic rat bone tissue (Figure 15).

SOCS1 (p < 0.05) gene expression was significantly decreased in the bones of 8 weeks of the onset of type 2 diabetes mellitus (Figure 16).

Figure 15: The expression of the RhoA gene is significantly downregulated in 8 weeks type 2 diabetic rat bone tissue.
Total RNA isolated from tibiae bone samples of control (n = 3) and T2DM (n = 3) rats were analyzed by q-RT PCR and normalized against Actin-Beta to plot the relative expression of RhoA (p = 0.0425) gene. (Student's t-test, error bars indicate Standard Error of Mean (SEM), * indicates significant differences at p < 0.05).

SOCS1 gene expression
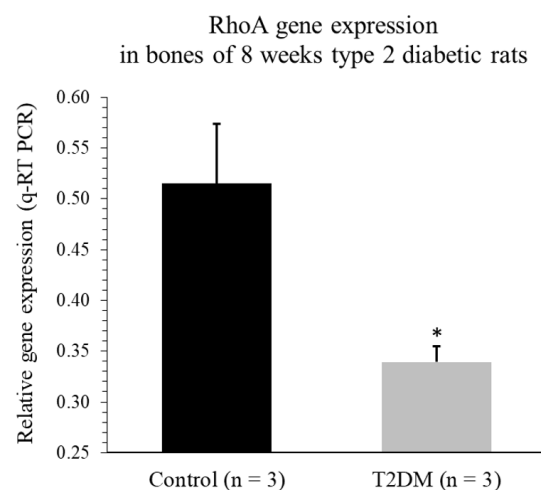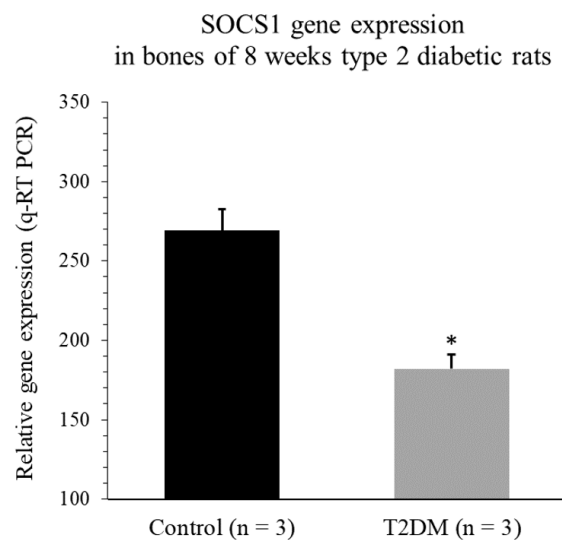in bones of 8 weeks type 2 diabetic rats

Figure 16: The expression of the SOCS1 gene is significantly downregulated in 8 weeks type 2 diabetic rat bone tissue.
Total RNA isolated from tibiae bone samples of control (n = 3) and T2DM (n = 3) rats were analyzed by q-RT PCR and normalized against Actin-Beta to plot the relative expression of SOCS1 (p = 0.0260) gene. (Student's t-test, error bars indicate Standard Error of Mean (SEM), * indicates significant differences at $p < 0.05$).

3.8 Identification of MicroRNA Target Genes in Bones of 10 Weeks of the Onset of Type 2 Diabetes Mellitus

The 23 target genes were studied in the bones of 10 weeks of the onset of type 2 diabetes mellitus. Quantification Real-Time PCR was performed to analyze their expression using the comparative delta-delta Ct method. Actin-Beta was used as an internal control for normalization. Each experiment was performed in duplicates and repeated three times. The following observations were recorded:

From the 23 target genes, the expression of the RhoA gene, SOCS1 gene, and PDCD4 gene was successfully detected.

There was a significant increase in the expression of the RhoA ($p < 0.05$) gene in 10 weeks type 2 diabetic rat bone tissue, as shown in Figure 17.

There was a non-significant increase in the expression of the SOCS1 gene in the bones of 10 weeks of the onset of type 2 diabetes mellitus (Figure 18).

There was a non-significant elevation in the expression of PDCD4 gene in 10 weeks type 2 diabetic rat bone tissue (Figure 19).

RhoA gene expression
in bones of 10 weeks type 2 diabetic rats
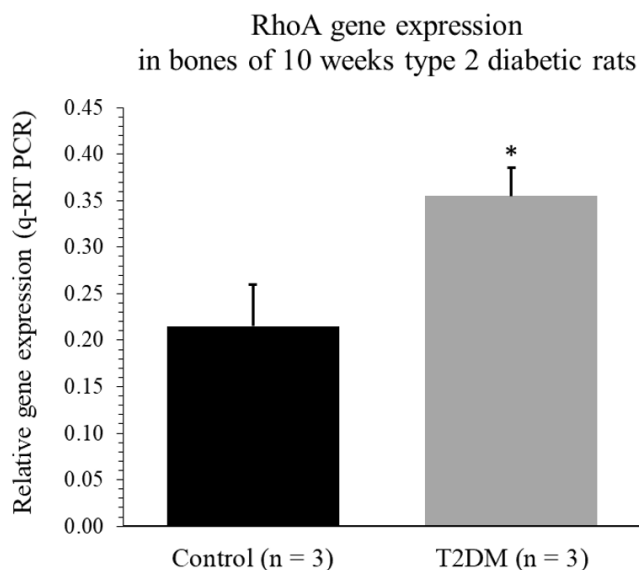
Figure 17: The expression of the RhoA gene is significantly upregulated in 10 weeks type 2 diabetic rat bone tissue.
Total RNA isolated from tibiae bone samples of control (n = 3) and T2DM (n = 3) rats were analyzed by q-RT PCR and normalized against Actin-Beta to plot the relative expression of RhoA (p = 0.047) gene. (Student's t-test, error bars indicate Standard Error of Mean (SEM), * indicates significant differences at $p < 0.05$).
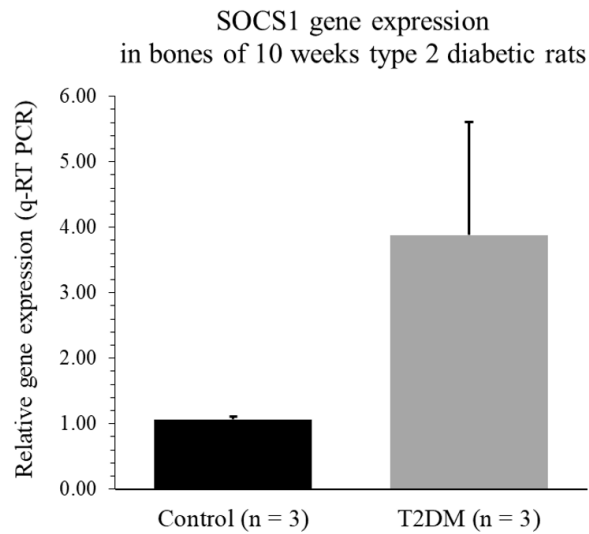
Figure 18: Upregulation of the SOCS1 gene expression in 10 weeks type 2 diabetic rat bone tissue.
Total RNA isolated from tibiae bone samples of control (n = 3) and T2DM (n = 3) rats were analyzed by q-RT PCR and normalized against Actin-Beta to plot the relative expression of SOCS1 ($p = 0.226$) gene. Student's t-test, error bars indicate Standard Error of Mean (SEM).
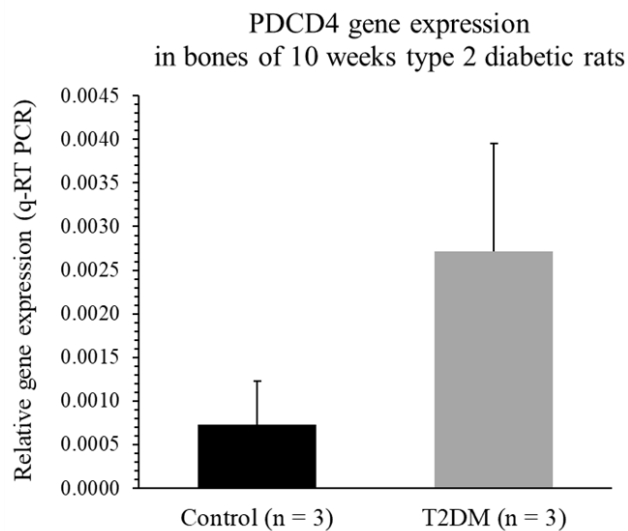
Figure 19: Upregulation of the PDCD4 gene expression in 10 weeks type 2 diabetic rat bone tissue.
Total RNA isolated from tibiae bone samples of control (n = 3) and T2DM (n = 3) rats were analyzed by q-RT PCR and normalized against Actin-Beta to plot the relative expression of the PDCD4 ($p = 0.3483$) gene. Student's t-test, error bars indicate Standard Error of Mean (SEM).

3.9 Identification of MicroRNA Target Genes in Bones of 14 Weeks of the Onset of Type 2 Diabetes Mellitus

The 23 target genes were studied in the bones of 14 weeks of the onset of type 2 diabetes mellitus. Quantification Real-Time PCR was performed to analyze their expression using the comparative delta-delta Ct method. Actin-Beta was used as an internal control for normalization. Each experiment was performed in duplicates and repeated three times. The following observations were recorded:

Among the 23 target genes, the expression of the RhoA gene and the SOCS1 gene were detected.

The expression of the RhoA gene was non-significantly decreased in 14 weeks type 2 diabetic rat bone tissue, as displayed in Figure 20.

The expression of the SOCS1 ($p < 0.05$) gene was significantly lowered in the bones of 14 weeks of the onset of type 2 diabetes mellitus (Figure 21).
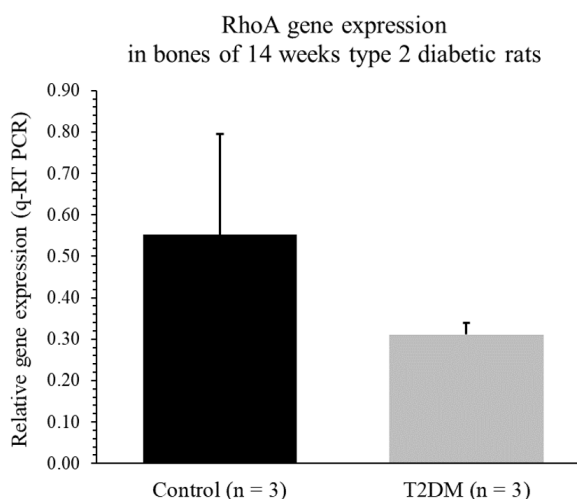
Figure 20: Downregulation of the RhoA gene expression in 14 weeks type 2 diabetic rat bone tissue.
Total RNA isolated from tibiae bone samples of control (n = 3) and T2DM (n = 3) rats were analyzed by q-RT PCR and normalized against Actin-Beta to plot the relative expression of the RhoA ($p = 0.3609$) gene. Student's t-test, error bars indicate Standard Error of Mean (SEM).
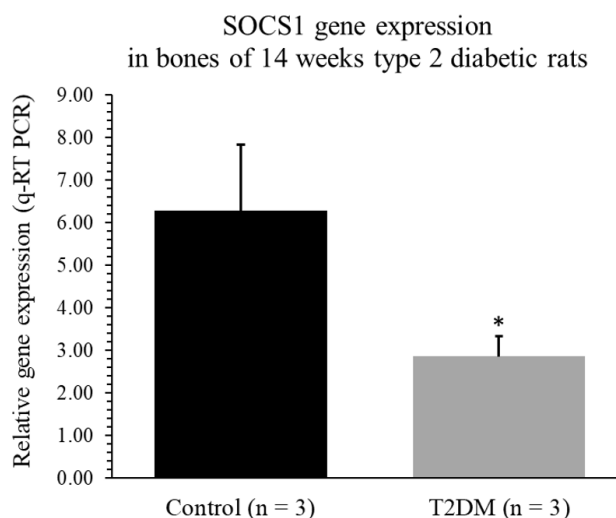
Figure 21: The expression of the SOCS1 gene is significantly downregulated in 14 weeks type 2 diabetic rat bone tissue.
Total RNA isolated from tibiae bone samples of control (n = 3) and T2DM (n = 3) rats were analyzed by q-RT PCR and normalized against Actin-Beta to plot the relative expression of SOCS1 (p = 0.0442) gene. (Student's t-test, error bars indicate Standard Error of Mean (SEM), * indicates significant differences at $p < 0.05$).

3.10 Measurement of Osteocalcin Level in Sera and Bones of 8, 10, and 14 Weeks of the Onset of Type 2 Diabetes Mellitus

The bone turnover rate of the 8, 10, and 14 weeks of the duration of type 2 diabetes mellitus was studied by checking their serum and bone osteocalcin level, which is a biomarker for the process of bone formation. The serum osteocalcin level was performed using an ELISA kit for osteocalcin (Cloud-Clone Corp. / SEA471Ra), and the bone osteocalcin level was performed using Rat Osteocalcin ELISA kit (Abbkine / KTE101053). The following observations were recorded:

The serum osteocalcin level in the sera of 8 weeks of the duration of type 2 diabetes mellitus was dropped significantly ($p < 0.05$) (Figure 22).

There was a non-significant increase in the serum osteocalcin level in the sera of 10 weeks of the duration of type 2 diabetes mellitus (Figure 22).

In the sera of 14 weeks of the duration of type 2 diabetes mellitus, the difference in the osteocalcin levels was non-significant and not much difference (Figure 22).

The bone osteocalcin levels in 8 weeks of the duration of T2DM were decreased, and in 10 and 14 weeks were increased. However, the results obtained were not significant (Figure 23).
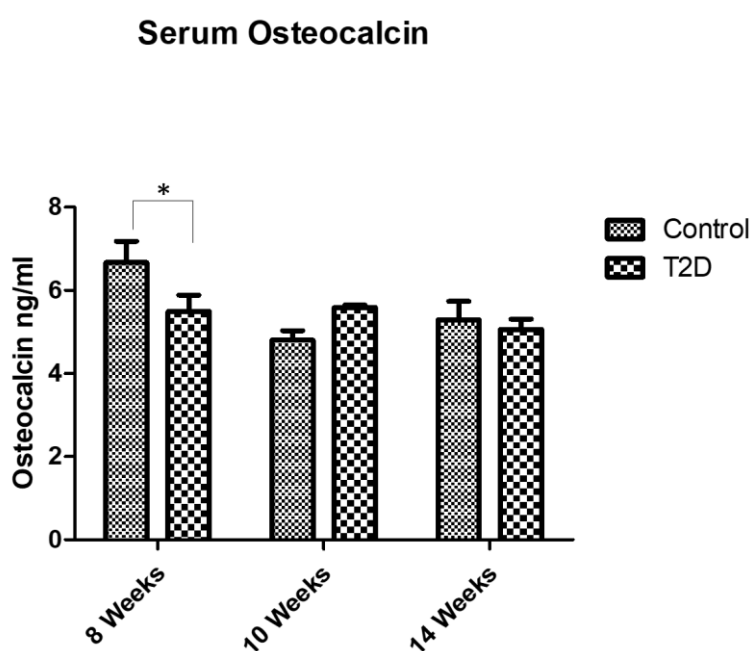
Serum Osteocalcin

Figure 22: Osteocalcin level is significantly decreased in the sera of 8 weeks, increased in the sera of 10 weeks, and no change in the sera of 14 weeks. Serum samples of control (n = 3) and T2DM (n = 3) rats in the duration of 8, 10, and 14 weeks were analyzed by Enzyme-linked Immunosorbent Assay [ELISA] Kit For Osteocalcin [OC] (Cloud-Clone Corp. / SEA471Ra) to plot the level of serum osteocalcin (ng/ml). (Student's t-test, error bars indicate Standard Error of Mean (SEM), * indicates significant differences at $p < 0.05$).

Osteocalcin in bone hydrolysate
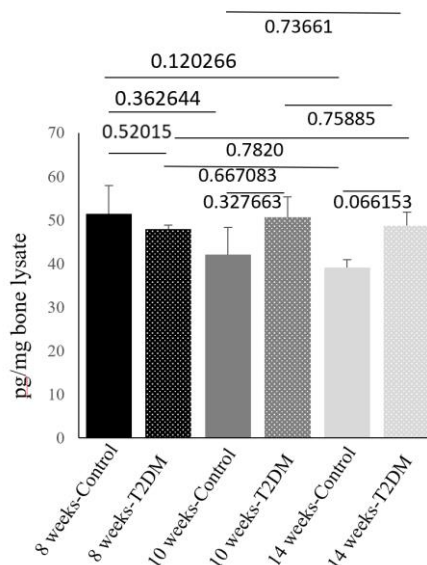
Figure 23: Osteocalcin level is decreased in the bones of 8 weeks, increased in the bones of 10 weeks, and increased in the bones of 14 weeks.
Bone samples of control (n = 3) and T2DM (n = 3) rats in the duration of 8 (p = 0.5201), 10 (p = 0.3276), and 14 (p = 0.0661) weeks were analyzed by Rat Osteocalcin ELISA Kit (Abbkine / KTE101053) to plot the level of bone osteocalcin (pg/mg). Student's t-test, error bars indicate Standard Error of Mean (SEM).

3.11 Summary of the Results

All the results that were achieved in this study from Sections 3.1 – 3.10 were summarized in Figure 24 and Tables 2, 3 and 4. In this study, the bones of type two diabetic rats were observed at week 8, 10 and 14, the expression of miR-20a, miR-21, miR-29a, miR-31, and miR-155 were altered. The log2 fold changed expression of miR-20a, miR-21, miR-29a, miR-31, and miR-155 in the bones of type 2 diabetic rats at 8 weeks, 10 weeks, and 14 weeks duration is displayed in Figure 24. The expression of miR-20a, miR-21, miR-29a, miR-31, and miR-155 in the bones and sera of 8 weeks of the duration of T2DM, as well as, the expression of the detected target genes and the serum and bone osteocalcin level is shown in Table 2. The expression of the five selected microRNAs in the bones and sera of 10 weeks of the duration of T2DM and

the expression of the detected target genes and the serum and bone osteocalcin level is shown in Table 3. The expression of the five selected microRNAs in the bones and sera of 14 weeks of the duration of T2DM and the expression of the detected target genes and the serum and bone osteocalcin level are presented in Table 4.

Figure 24: Schematic overview of the expression of miR-20a, miR-21, miR-29a, miR-31, and miR-155 in bones of type 2 diabetic rats at 8 weeks, 10 weeks, and 14 weeks duration.
The bars represent the log2 fold change of each microRNA at each of the three time points. The log2 fold change was calculated by using this formula: [Log ((T2DM/Control), 2)]. (Student's t-test, * indicates significant differences at $p < 0.05$).

Table 2: The expression of miR-20a, miR-21, miR-29a, miR-31, and miR-155 in bones and sera of 8 weeks of the onset of T2DM, the expression of the detected target genes and the serum and bone osteocalcin level.

microRNA	T2DM (8 weeks duration) Bone samples	T2DM (8 weeks duration) Serum samples	Target Genes	Serum OC	Bone OC
miR-20a	Decreased	(N/D)	▪ ATG16L1 (N/D) ▪ BAMBI (N/D) ▪ BMP2 (N/D) ▪ BMP3 (N/D) ▪ CALCA (N/D) ▪ CRIM1 (N/D) ▪ DKK1 (N/D) ▪ KREMAN2 (N/D) ▪ MITF (N/D) ▪ PDCD4 (N/D) ▪ PPARG (N/D) ✓ RhoA [Decreased]* ▪ RUNX2 (N/D) ▪ SATB2 (N/D) ▪ SFRP2 (N/D) ▪ SMAD7 (N/D) ✓ SOCS1 [Decreased]* ▪ SOST (N/D) ▪ SP7 (N/D) ▪ SRF (N/D) ▪ TGFB1(N/D) ▪ TNFRSF11B [OPG] (N/D) ▪ TNFSF11 [RANKL] (N/D)	Decreased*	Decreased
miR-21	Increased	Increased			
miR-29a	Increased	(N/D)			
miR-31	Increased	(N/D)			
miR-155	Decreased	(N/D)			

* = indicates significant differences at p < 0.05 (Student's t-test)

(N/D) = Not Detected

Table 3: The expression of miR-20a, miR-21, miR-29a, miR-31, and miR-155 in bones and sera of 10 weeks of the onset of T2DM, the expression of the detected target genes and the serum and bone osteocalcin level.

microRNA	T2DM (10 weeks duration) Bone samples	T2DM (10 weeks duration) Serum samples	Target Genes	Serum OC	Bone OC
miR-20a	Decreased*	(N/D)	▪ ATG16L1 (N/D) ▪ BAMBI (N/D) ▪ BMP2 (N/D) ▪ BMP3 (N/D) ▪ CALCA (N/D) ▪ CRIM1 (N/D) ▪ DKK1 (N/D) ▪ KREMAN2 (N/D) ▪ MITF (N/D) ✓ PDCD4 [Increased] ▪ PPARG (N/D) ✓ RhoA [Increased]* ▪ RUNX2 (N/D) ▪ SATB2 (N/D) ▪ SFRP2 (N/D) ▪ SMAD7 (N/D) ✓ SOCS1 [Increased] ▪ SOST (N/D) ▪ SP7 (N/D) ▪ SRF (N/D) ▪ TGFB1 (N/D) ▪ TNFRSF11B [OPG] (N/D) ▪ TNFSF11 [RANKL] (N/D)	Increased	Increased
miR-21	Decreased*	Decreased*			
miR-29a	Decreased	(N/D)			
miR-31	Decreased	(N/D)			
miR-155	Decreased*	(N/D)			

* = indicates significant differences at p < 0.05 (Student's t-test)

(N/D) = Not Detected

Table 4: The expression of miR-20a, miR-21, miR-29a, miR-31, and miR-155 in bones and sera of 14 weeks of the onset of T2DM, the expression of the detected target genes and the serum and bone osteocalcin level.

microRNA	T2DM (14 weeks duration) Bone samples	T2DM (14 weeks duration) Serum samples	Target Genes	Serum OC	Bone OC
miR-20a	Increased	(N/D)	▪ ATG16L1(N/D) ▪ BAMBI (N/D) ▪ BMP2 (N/D) ▪ BMP3 (N/D) ▪ CALCA (N/D)	No change	Increased
miR-21	Decreased	(N/D)	▪ CRIM1 (N/D) ▪ DKK1 (N/D) ▪ KREMAN2 (N/D) ▪ MITF (N/D) ▪ PDCD4 (N/D)		
miR-29a	Decreased	(N/D)	▪ PPARG (N/D) ✓ RhoA [Decreased] ▪ RUNX2 (N/D) ▪ SATB2 (N/D)		
miR-31	Decreased	(N/D)	▪ SFRP2 (N/D) ▪ SMAD7 (N/D) ✓ SOCS1 [Decreased]* ▪ SOST (N/D) ▪ SP7 (N/D)		
miR-155	Increased	Increased**	▪ SRF (N/D) ▪ TGFB1 (N/D) ▪ TNFRSF11B [OPG] (N/D) ▪ TNFSF11 [RANKL] (N/D)		

** = indicates significant differences at $p < 0.01$ (Student's t-test)

* = indicates significant differences at $p < 0.05$ (Student's t-test)

(N/D) = Not Detected

3.12 Analysis of Histological Changes in Bones of 8, 10, and 14 Weeks of the Onset of Type 2 Diabetes Mellitus

The proximal head of the femur is used for histologic analysis. In Figure 25, it illustrates an example of the proximal head of a femur and the region of interest [ROI] that is used for histologic examination in this study.

In subsection 3.12.1, the results of the trabecular measurements are explained. In Figure 26, it identifies the main features of a bone section (proximal head of the femur).

In subsection 3.12.2, the results of the quantitative analysis of apoptotic and live cells are explained. In Figure 27, it's pointing the live and apoptotic cells.
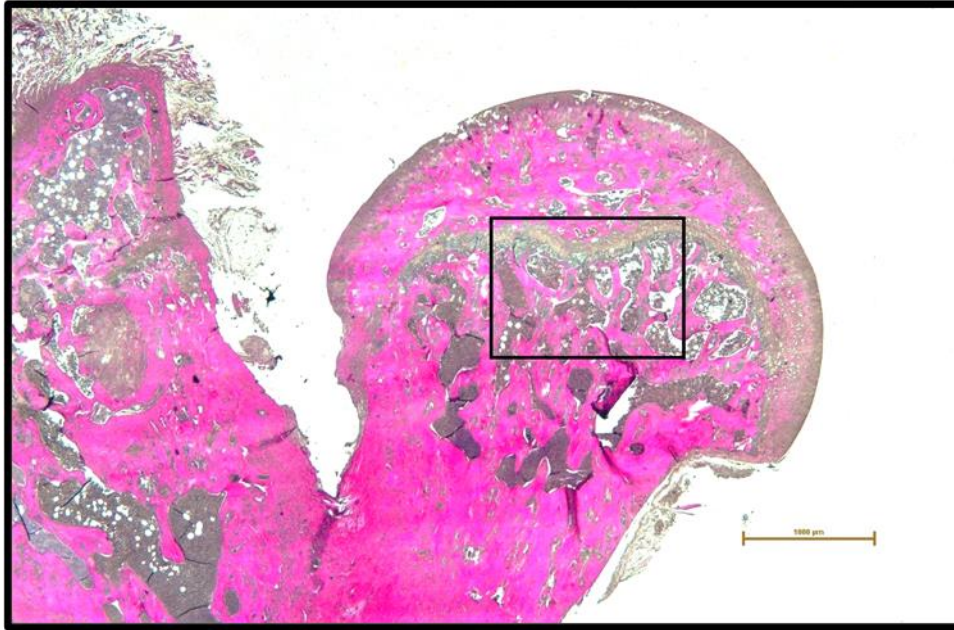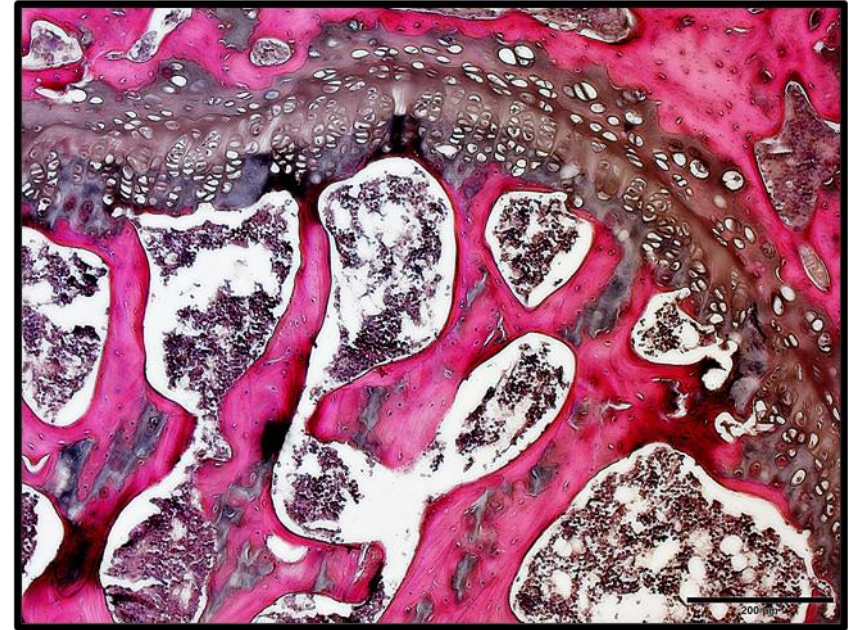
(a)   (b)

Figure 25: Histologic examination of the proximal head of a control femur.
Hematoxylin & Eosin staining, (a) Proximal head of a femur (Scale bar = 1000 µm), showing the region of interest (ROI) [the selected area] that is used for histologic analysis, (b) Example of a histologic section (Scale bar = 200 µm).
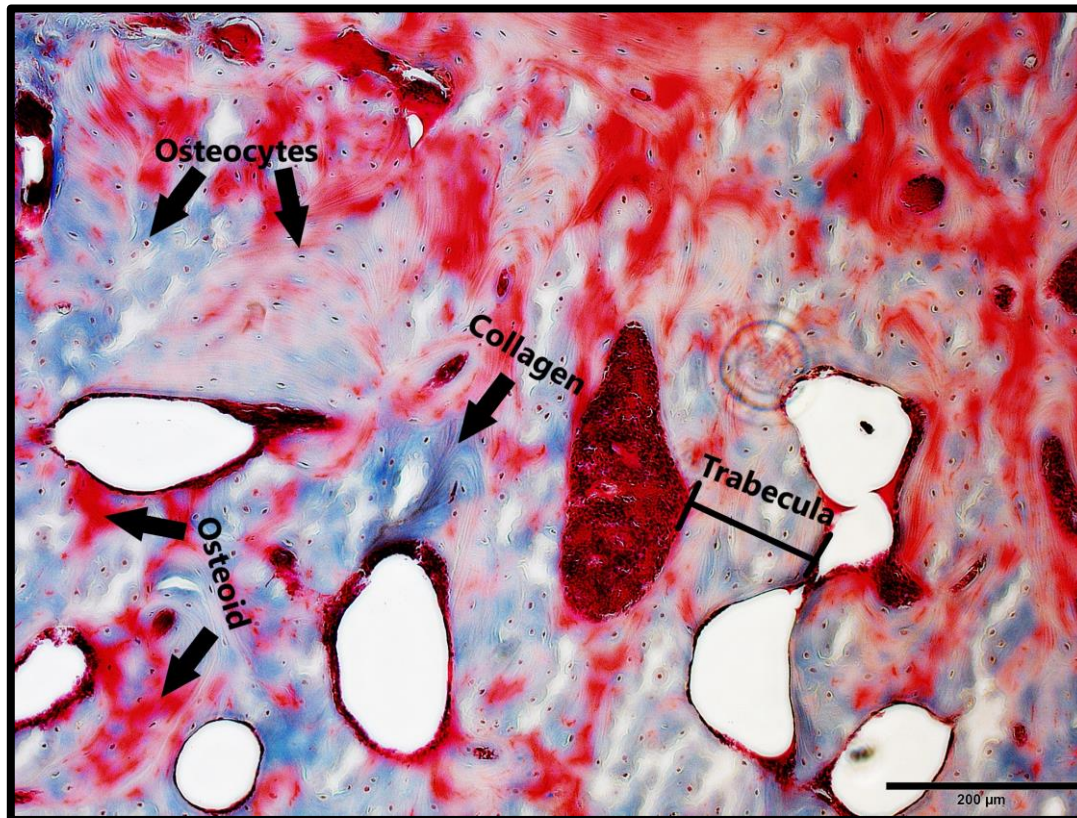
Figure 26: Masson's Trichrome staining of a control bone (proximal head of the femur).
Masson's Trichrome staining identifies collagen (blue), osteoid (red), osteocytes (dark blue dots). Scale bar = 200 μm.
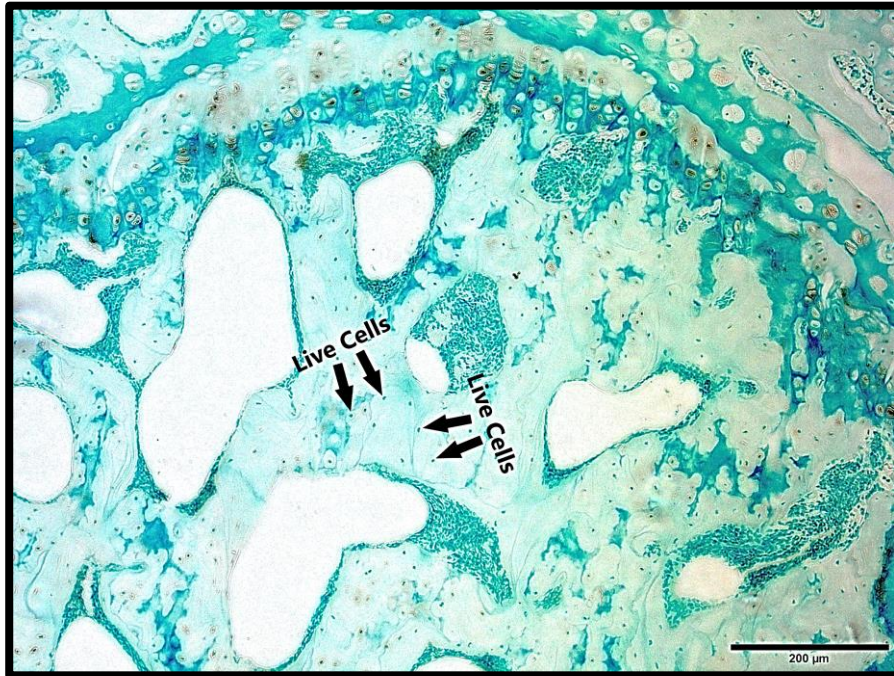
(a)
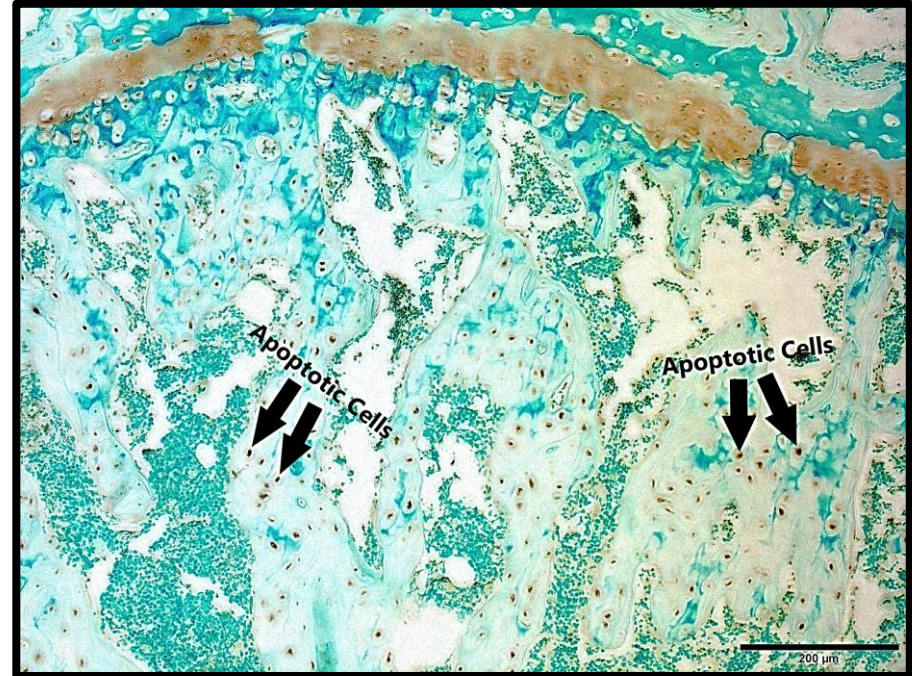
(b)

Figure 27: TUNEL staining of a bone section (proximal head of the femur).
TUNEL staining, (a) Control, showing live cells (blue dots), (b) T2DM, showing apoptotic cells (brown dots). Scale bar = 200 µm.

3.12.1 Trabecular Measurements

The trabecular measurements consist of trabecular bone volume (BV/TV), trabecular separation (Tb. Sp), trabecular thickness (Tb. Th), and trabecular number (Tb. N). Trabecular bone volume is expressed as a %, it is defined as the relative volume of the total trabecular bone. Trabecular separation is the mean distance between the trabecular plates (Figure 28). Trabecular thickness is the mean distance of the trabecular structure, and it is calculated as (1/Tb.Sp) (Figure 28). The trabecular number is the number of trabeculae per lineal mm, it is calculated as ([BV/TV]/Tb.Th).
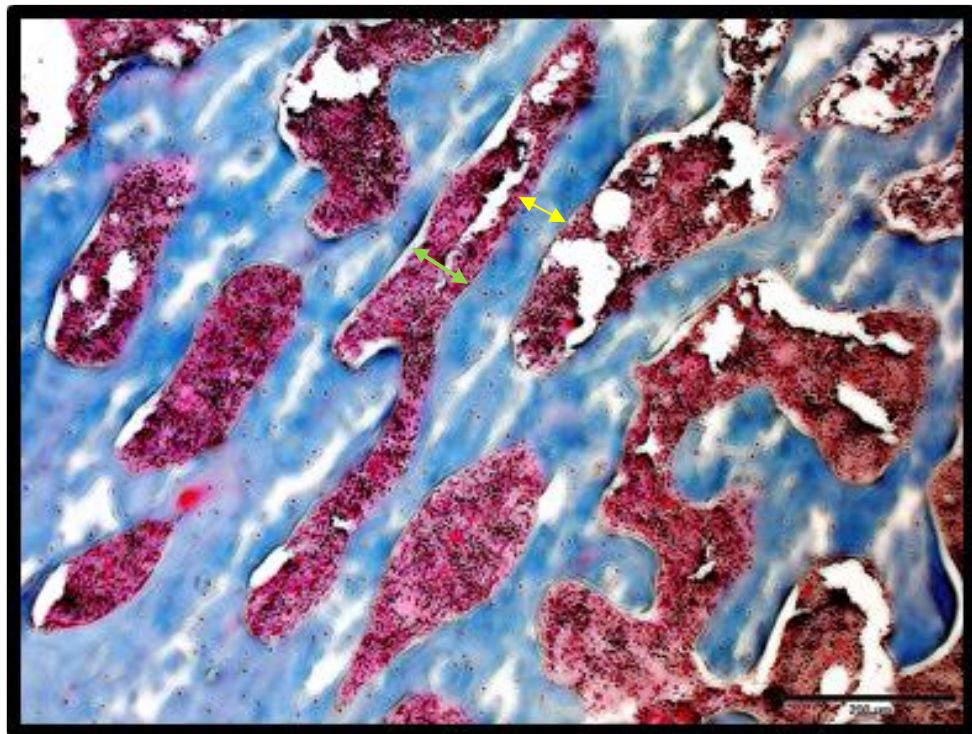
Figure 28: Definition of the two of the trabecular measurements (trabecular thickness and separation).
Trabecular thickness (Tb. Th), shown in the yellow arrow, is the distance measurement of the trabecula, and trabecular separation (Tb. Sp), shown in the green arrow, is the distance measurement between trabecular plates.

The bone sections of the control rats at 8, 10, 14 weeks duration, and as well as the bone sections of the T2DM rats at 8, 10, and 14 weeks duration, which was used

to perform the trabecular measurements are presented in Figure 29.

The BV/TV was significantly reduced in 8 ($p < 0.05$), 10 (< 0.0001), and 14 ($p < 0.05$) of the duration of T2DM (Figure 30).

The Tb. Sp of 14 ($p < 0.001$) weeks of the duration of T2DM were significantly raised, the Tb. Sp was non-significantly increased in 10 weeks of the duration of T2DM, and there was no notable change of Tb.Sp in 8 weeks of the duration of T2DM from the 8 weeks control (Figure 31).

The Tb. Th of 14 ($p < 0.01$) weeks of the duration of T2DM was significantly dropped, the Tb. Th was non-significantly reduced in 10 weeks of the duration of T2DM, and there was no notable change of Tb. Th in the 8 weeks of the duration of T2DM from the 8 weeks control (Figure 32).

The Tb. N of 10 ($p < 0.05$) weeks of the duration of T2DM was significantly decreased, and there was a non-significant decrease in the Tb. N of 8 and 14 weeks of the duration of T2DM (Figure 33).
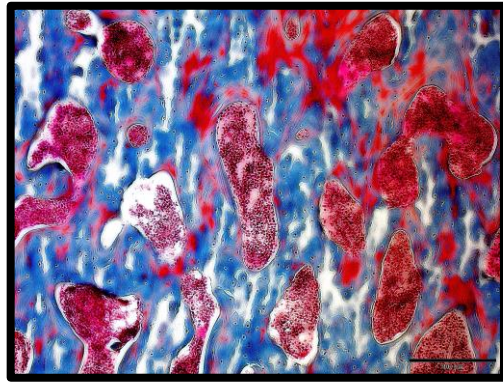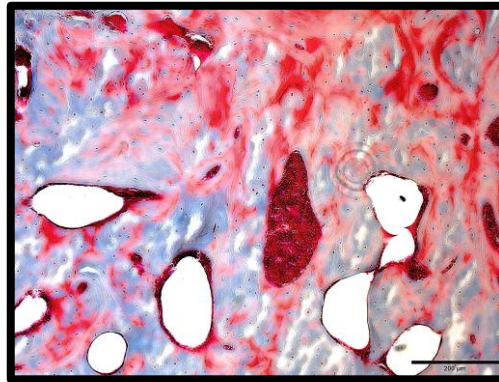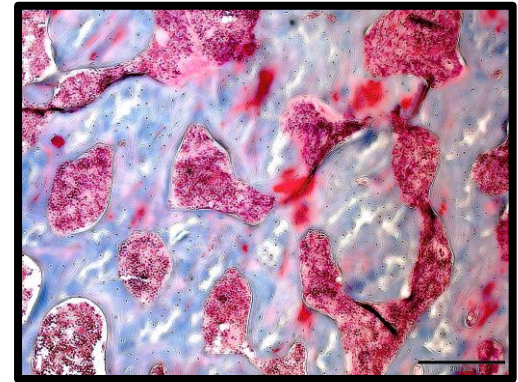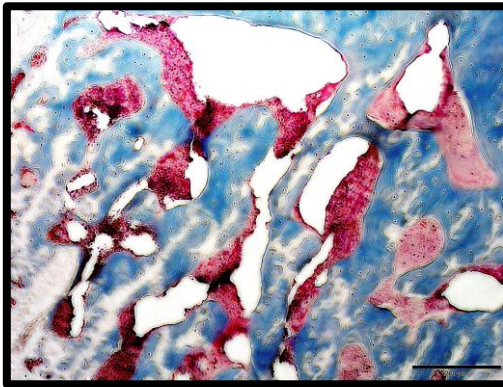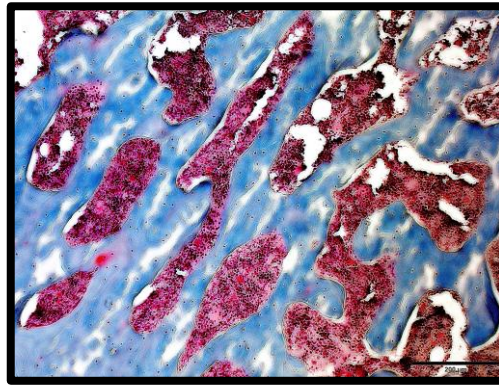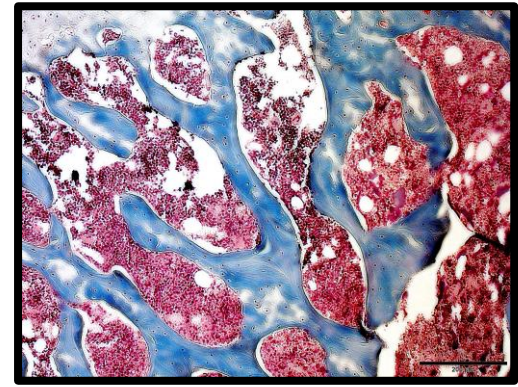
Figure 29: Masson's Trichrome staining of the bone sections (proximal head of the femur).
Masson's Trichrome staining, (a) Control [8 weeks duration], (b) Control [10 weeks duration], (c) Control [14 weeks duration], (d) T2DM [8 weeks duration], (e) T2DM [10 weeks duration], and (g) T2DM [14 weeks duration]. Scale bar = 200 μm.

Trabecular bone volume (BV/TV)
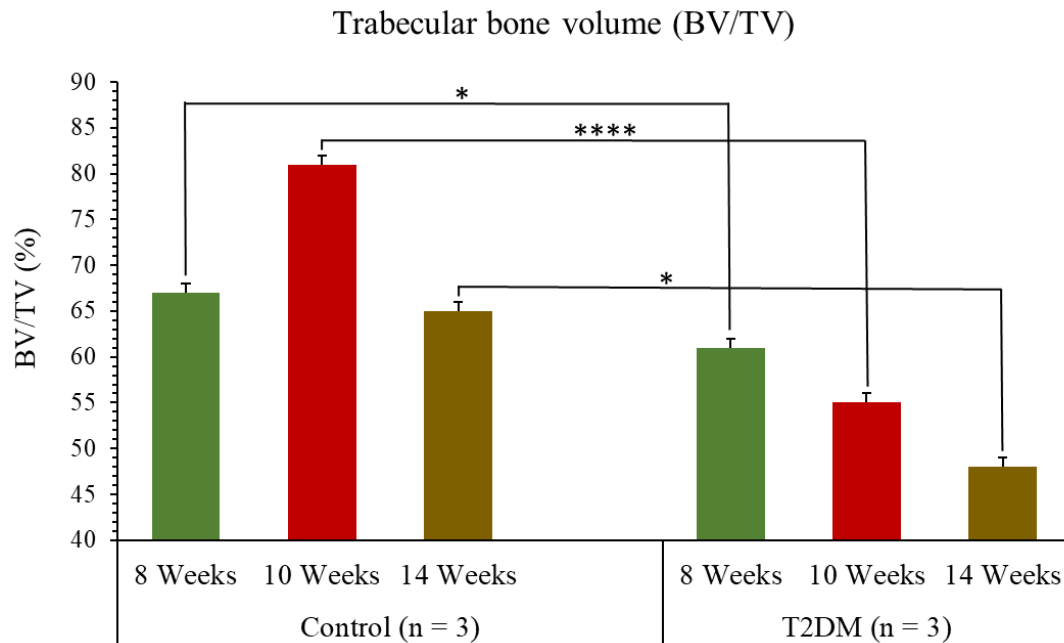
Figure 30: Significant decrease in BV/TV of T2DM rats at 8, 10, and 14 weeks duration.
Masson's Trichrome stained bone sections (proximal head of the femur) of control (n = 3) and T2DM (n = 3) rats in the duration of 8 (p = 0.0286), 10 (p = 0.000015), and 14 (p = 0.0423)weeks were analyzed by using the application Image J to plot the trabecular bone volume [BV/TV] (%). (Student's t-test, Error bars indicate Standard Error of Mean (SEM), * indicates significant differences at p < 0.05, **** indicates significant differences at p < 0.0001).

Trabecular separation (Tb.Sp)
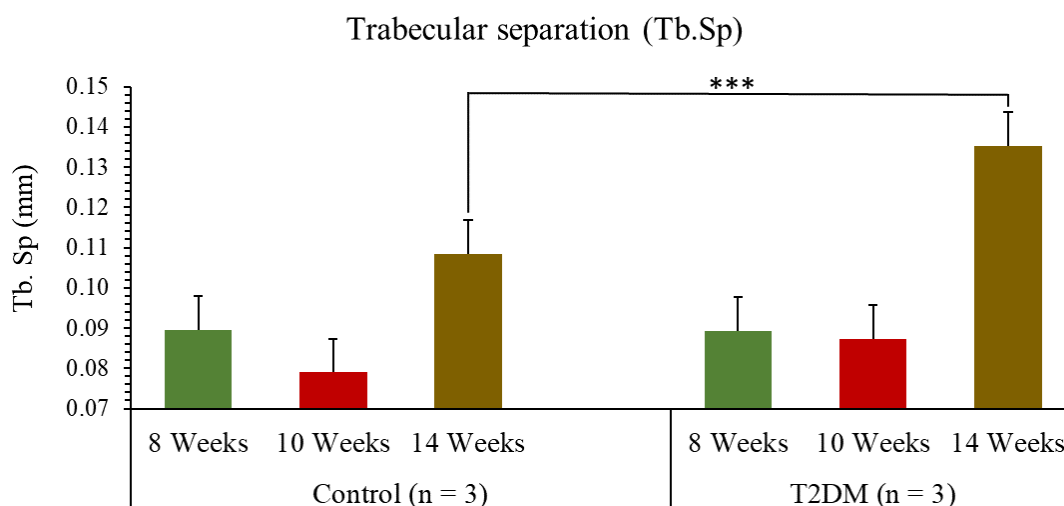
Figure 31: Tb.Sp in 14 weeks is significantly increased, increased in 10 weeks, and no change in 8 weeks.
Masson's Trichrome stained bone sections (proximal head of the femur) of control (n = 3) and T2DM (n = 3) rats in the duration of 8 (p = 0.4957), 10 (p =

0.140), and 14 (p = 0.0011) weeks were analyzed by using the application ImageJ to plot the trabecular separation [Tb.Sp] (mm). (Student's t-test, Error bars indicate Standard Error of Mean (SEM), *** indicates significant differences at p < 0.001).

Trabecular thickness (Tb.Th)

Figure 32: Tb.Th in 14 weeks is significantly decreased, decreased in 10 weeks, and no change in 8 weeks.

Masson's Trichrome stained bone sections (proximal head of the femur) of control (n = 3) and T2DM (n = 3) rats in the duration of 8 (p = 0.4589), 10 (p = 0.1544), and 14 (p = 0.0029) weeks were analyzed by calculating 1/Tb.Sp to plot the trabecular thickness [Tb. Th] (mm). (Student's t-test, Error bars indicate Standard Error of Mean (SEM), ** indicates significant differences at p < 0.01).

Trabecular number (Tb. N)

Figure 33: Significant decrease in Tb. N of 10 weeks of the onset of T2DM, and decrease in Tb. N of 8 and 14 weeks of the onset of T2DM.

Masson's Trichrome stained bone sections (proximal head of the femur) of control (n = 3) and T2DM (n = 3) rats in the duration of 8 (p = 0.1796), 10 (p = 0.0398) and 14 (p = 0.2964) weeks were analyzed by calculating [BV/TV]/Tb.Th to plot the trabecular number [Tb. N] (1/mm). (Student's t-test, Error bars indicate Standard Error of Mean (SEM), * indicates significant differences at p < 0.05).

3.12.2 Quantitative Analysis of Apoptotic and Live Cells

The bone sections were taken from the proximal femur of the control rats at 8, 10, 14 weeks duration, and as well as the bone sections were taken from the proximal femur of the T2DM rats at 8, 10, and 14 weeks duration, which was used to count the apoptotic and live cells, as shown in Figure 34.

The number of apoptotic cells (p < 0.05) was significantly elevated in 8 weeks of the duration of T2DM, while the number of live cells was non-significantly reduced (Figure 35).

There was a significant increase in the number of apoptotic cells (p < 0.05) in 10 weeks of the duration of T2DM, whereas there was a significant drop in the number of live cells (p < 0.001) in 10 weeks of T2DM (Figure 36).

The number of apoptotic cells (p < 0.05) was significantly raised in 14 weeks of the duration of T2DM, while the number of live cells (p < 0.05) was significantly decreased (Figure 37).
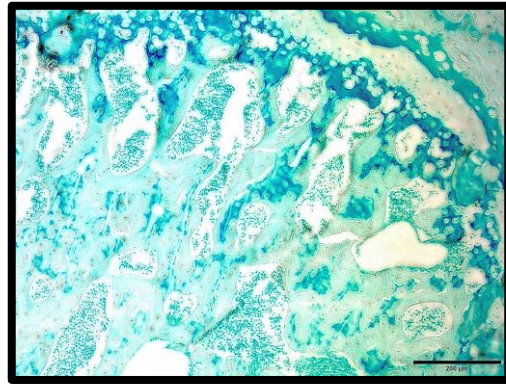
(a)
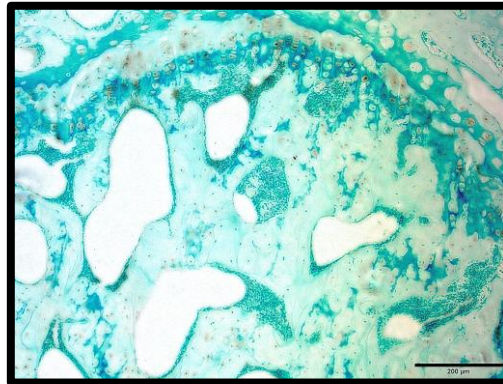
(b)
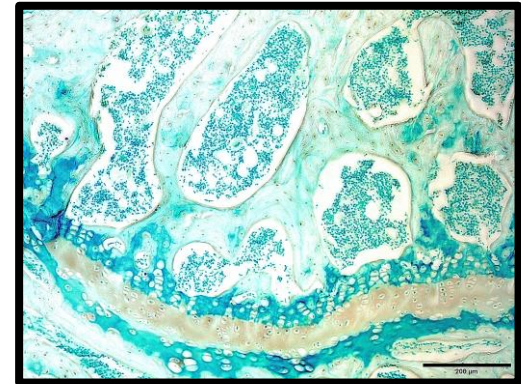
(c)
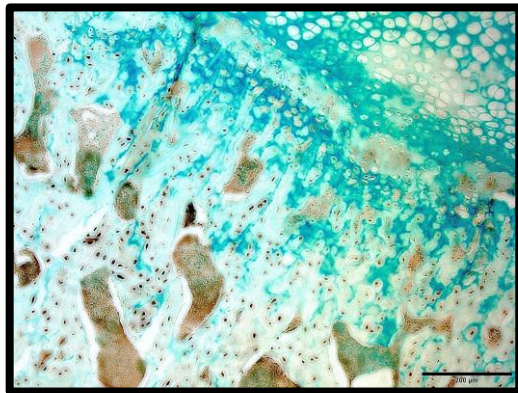
(d)
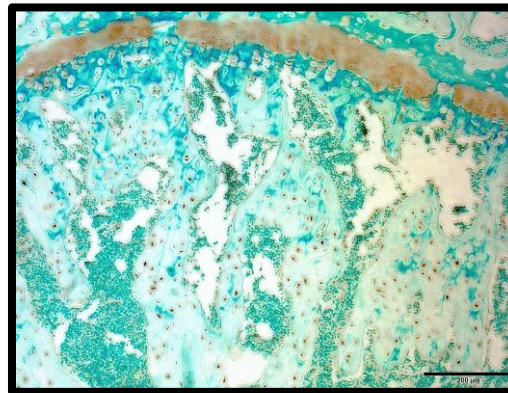
(e)
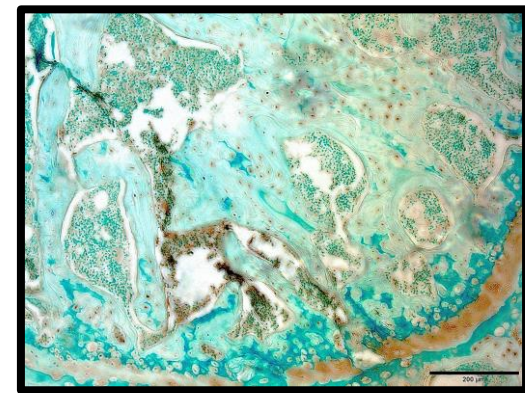
(g)

Figure 34: TUNEL staining of the bone sections (proximal head of the femur).
TUNEL staining, (a) Control [8 weeks duration], (b) Control [10 weeks duration], (c) Control [14 weeks duration], (d) T2DM [8 weeks duration], (e) T2DM [10 weeks duration], and (g) T2DM [14 weeks duration]. Scale bar = 200 μm.

TUNEL assay − 8 weeks
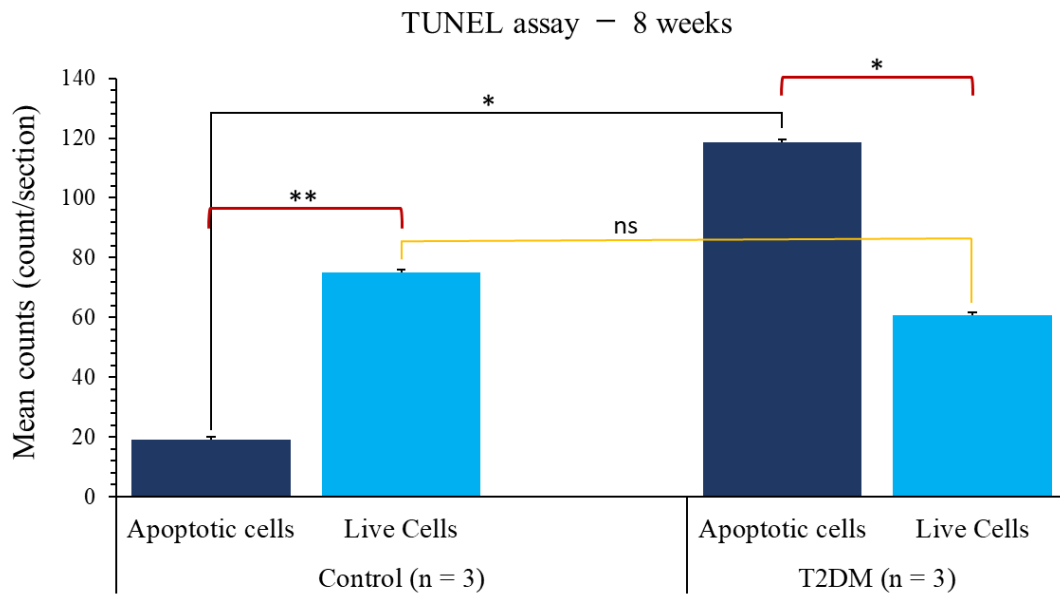
Figure 35: Significant increase of apoptotic cells in 8 weeks of the onset of T2DM, and a decrease of live cells in 8 weeks of the onset of T2DM.
TUNEL stained bone sections (proximal head of the femur) of control (n = 3) and T2DM (n = 3) rats in the duration of 8, 10, and 14 weeks were analyzed by counting the apoptotic cells and the live cells per section to plot the mean counts (count/section). (Student's t-test, Error bars indicate Standard Error of Mean (SEM), * indicates significant differences at p < 0.05, ** indicates significant differences at p < 0.01). (Apoptotic cells-Control vs Apoptotic cells-T2DM, p = 0.0139), (Live cells-Control vs Live cells, p = 0.1702), (Control-Apoptotic vs Live cells, p = 0.0096), (T2DM-Apoptotic vs Live cells, p = 0.0463).

TUNEL assay − 10 weeks
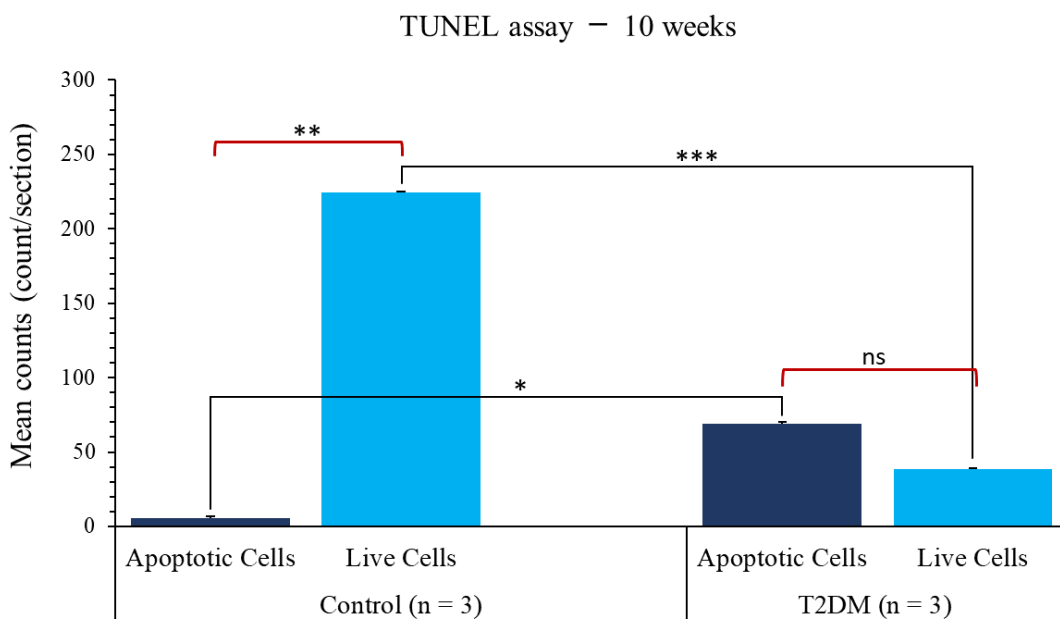
Figure 36: Significant increase of apoptotic cells in 10 weeks of the onset of T2DM, and a significant decrease in live cells in 10 weeks of the onset of T2DM.

TUNEL stained bone sections (proximal head of the femur) of control (n = 3) and T2DM (n = 3) rats in the duration of 8, 10, and 14 weeks were analyzed by counting the apoptotic cells and the live cells per section to plot the mean counts (count/section). (Student's t-test, Error bars indicate Standard Error of M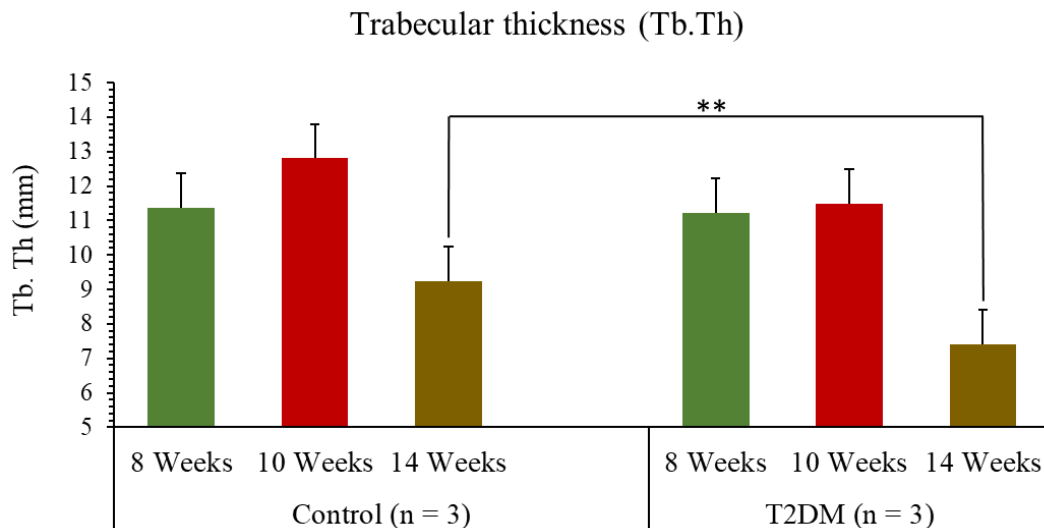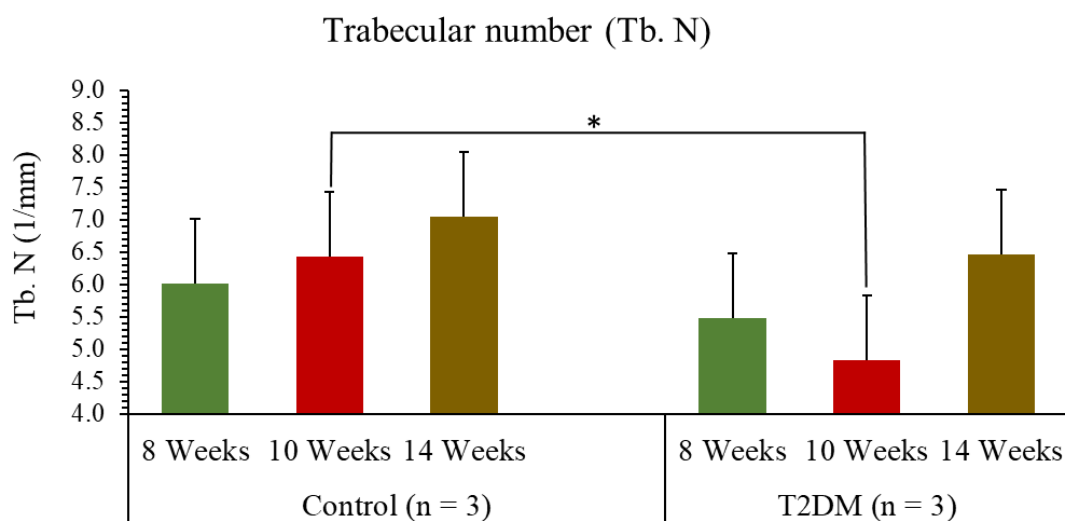ean (SEM), * indicates significant differences at $p < 0.05$, ** indicates significant differences at $p < 0.01$, *** indicates significant differences at $p < 0.001$). (Apoptotic cells-Control vs Apoptotic cells-T2DM, $p = 0.0330$), (Live cells-Control vs Live cells, $p = 0.00095$), (Control-Apoptotic vs Live cells, $p = 0.0018$), (T2DM-Apoptotic vs Live cells, $p = 0.1104$).
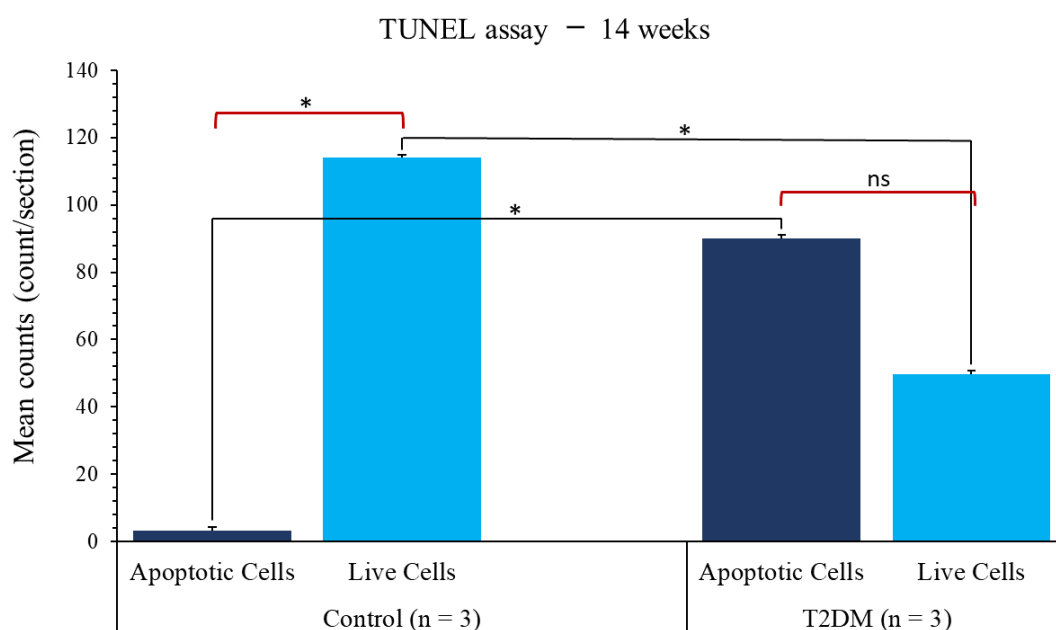
Figure 37: Significant increase of apoptotic cells in 14 weeks of the onset of T2DM, and a significant decrease in live cells in 14 weeks of the onset of T2DM.
TUNEL stained bone sections (proximal head of the femur) of control (n = 3) and T2DM (n = 3) rats in the duration of 8, 10, and 14 weeks were analyzed by counting the apoptotic cells and the live cells per section to plot the mean counts (count/section). (Student's t-test, Error bars indicate Standard Error of Mean (SEM), * indicates significant differences at $p < 0.05$). (Apoptotic cells-Control vs Apoptotic cells-T2DM, $p = 0.0213$), (Live cells-Control vs Live cells, $p = 0.0418$), (Control-Apoptotic vs Live cells, $p = 0.0157$), (T2DM-Apoptotic vs Live cells, $p = 0.0796$).

3.13 Significant Results

The significant results were gathered in Table 5.

Table 5: The significant results.

T2DM (8 weeks duration) Bone samples	1. Decreased expression of RhoA gene. 2. Decreased expression of SOCS1 gene.
T2DM (10 weeks duration) Bone samples	1. Decreased expression of miR-20a. 2. Decreased expression of miR-21. 3. Decreased expression of miR-155. 4. Increaed expression of RhoA gene.
T2DM (14 weeks duration) Bone samples	1. Decreased expression of SOCS1 gene.
T2DM (8 weeks duration) Serum samples	1. Decreased osteocalcin level.
T2DM (10 weeks duration) Serum samples	1. Decreased expression of miR-21.
T2DM (14 weeks duration) Serum samples	1. Increased expression of miR-155.

Chapter 4: Discussion

The constant status of elevated blood glucose level is one of the characteristics of non-insulin-dependent [type 2] diabetes mellitus (Hurtado & Vella, 2018). Insulin resistance and impaired secretion of insulin are the mechanisms by which this metabolic disorder is posing (Hurtado & Vella, 2018). One of the complications of having the onset of type 2 diabetes mellitus is encountering osteoporosis (Zhao et al., 2019). The most recognized definition of osteoporosis is a disorder that leads to fracture susceptibility and accelerated levels of bone fragility observed by the decreased levels of bone mass and the deterioration of the microarchitecture of the bone tissue (Compston et al., 2019). Normally, gene expression is controlled through a process called RNA interference by a small endogenous non-coding RNA molecule called microRNAs (Bellavia et al., 2019). MicroRNA works by targeting the mRNA of a gene and results in gene silencing (Bellavia et al., 2019). Therefore, an increased level of microRNAs inhibits gene expression and decreased levels of microRNAs promote gene expression (Bellavia et al., 2019). Current studies have revealed that the levels of microRNAs are varied between diseases, as a consequence, those microRNAs could be used as diagnostic biomarkers for certain diseases like osteoporosis (Bellavia et al., 2019). Based on that the study aimed to investigate the bone remodeling cycle modulators in type 2 diabetes mellitus through microRNAs.

In this study, the mode of modulation in the bone remodeling cycle was investigated by testing the expression of miR-20a, miR-21, miR-29a, miR-31, and miR-155 in the bones and sera of 8, 10, and 14 weeks of the onset of T2DM. Furthermore, some of their possible target genes were tested as well in the bones of 8, 10, and 14 weeks of the onset T2DM. The serum osteocalcin level was tested in the

sera of 8, 10, and 14 weeks of the onset of T2DM. In addition to that, the bone osteocalcin level was tested in the bones of 8, 10, and 14 weeks of the onset of T2DM. The bone microstructure was analyzed using histological techniques for the bones of 8, 10, and 14 weeks of the onset of T2DM.

According to the literature review, downregulation of miR-20a increases the expression of a gene essentially involved in autophagy, ATG16L1 (Autophagy related 16 like 1), which, promotes osteoclast differentiation (Sun et al., 2015). The maintenance of osteocyte homeostasis is regulated by autophagy (Yin et al., 2019). High reactive oxygen species (ROS) and hypoxia are the adverse factors that threats osteocytes survival (Yin et al., 2019). Osteocytes depend on autophagy to sustain their survival (Yin et al., 2019). Under high oxidative stress, the elevated autophagic activity led to reduced osteocyte apoptosis (Yin et al., 2019). Osteocyte apoptosis is linked with local bone resorption (Plotkin, 2014). The apoptotic osteocytes are devoured by osteoclasts (Plotkin, 2014). Using caspase inhibitors, the osteocyte apoptosis was stopped, which results in a decrease in bone resorption (Plotkin, 2014). In this study, it's have been observed that in the bones of 8 weeks of the onset of type 2 diabetes mellitus, the expression of miR-20a was non-significantly decreased, the expression of its target gene ATG16L1 was not detected, and the apoptotic cells were significantly ($p < 0.05$) increased. This suggests that the increased apoptosis at 8 weeks of the onset of T2DM could be the reason for enhanced bone resorption and osteoclastogenesis.

Previous studies have shown that the overexpression of miR-21 promotes osteoblast differentiation by downregulating the SMAD7 gene, and promotes bone resorption by downregulating PDCD4 (Bellavia et al., 2019; Hu et al., 2017). In this study, the bones of 8 weeks of the onset of type 2 diabetes mellitus were analyzed, it

revealed that the expression of miR-21 was non-significantly increased, the expression of SMAD7 and PDCD4 however were not detected. The osteocalcin levels measured in samples obtained from bone and serum showed decreased osteocalcin levels. The data obtained from the serum osteocalcin was significant ($p < 0.05$). These results speculate that miR-21 functions in suppressing osteoblast differentiation maybe acting on other target genes; since the serum osteocalcin levels were significantly decreased, which might suggest a reduced bone formation. Moreover, these results also suggest that miR-21 functions in promoting bone resorption; since the samples showing a trend towards increased miR-21, which most likely increasing bone resorption. But, in the future, the need to investigate the biomarkers for bone resorption is necessary to back up this suggestion.

The expression of miR-29a, miR-29b and miR-29c induces apoptosis by upregulating p53 [tumor suppressor gene] (Park et al., 2009). Earlier researches investigated that upregulation of miR-29a expression promotes osteoblast differentiation (Bellavia et al., 2019; Ko et al., 2015). Moreover, the upregulation of miR-29a expression also decreases non-collagenous matrix proteins such as osteocalcin and osteonectin [ON], which leads to speeding up the extracellular mineralization (Bellavia et al., 2019; Kapinas et al., 2009). A previous study has shown that reduced non-collagenous matrix proteins indicate reduced osteoblast numbers (Delany et al., 2003). Furthermore, many studies support the idea that the rate of extracellular mineralization is controlled by apoptosis (An et al., 2015; Roy et al., 2010). For example, if apoptosis is high, the rate of extracellular mineralization is accelerated (Roy et al., 2010). In this study, it's have been noticed that in the bones of 8 weeks of the onset of type 2 diabetes mellitus, the expression of miR-29a was increased (non-significantly), suggesting that it might be affecting the bone

remodeling cycle by accelerating extracellular mineralization; since the apoptosis cells were significantly ($p < 0.05$) elevated. However, osteocalcin levels measures in bone and serum showed decreased osteocalcin levels. The data obtained from the serum osteocalcin was significant ($p < 0.05$). Reduced bone formation is indicated by the reduced osteocalcin, which declares that the increased expression of miR-29a in the bones of 8 weeks of the onset of T2DM could be through decreasing non-collagenous matrix protein. In addition, reduced non-collagenous matrix protein means that there are decreased number of osteoblasts, and that triggers the rate of extracellular mineralization to be fast by differentiating those osteoblasts to osteocytes, and that's approved by the significant increase of apoptotic cells in 8 weeks of the onset of T2DM.

A previous study has shown that in osteoclast cells, the miR-31 target gene is RhoA (Mizoguchi et al., 2013). The same previous study examined the underexpression of RhoA by the overexpression of miR-31 induces osteoclastogenesis (Mizoguchi et al., 2013). Equivalently, in this study, it's have been observed that in the bones of 8 weeks type 2 diabetic rats, the expression of miR-31 was non-significantly increased, and the expression of RhoA was significantly ($p < 0.05$) decreased, indicating a possibility of induction in osteoclastogenesis. Bone resorption markers will be measured to confirm osteoclast activity.

As shown in an earlier study, in osteoblast cells, the miR-155 target gene is SOCS1 (Wua et al., 2012). An earlier study investigated that the underexpression of SOCS1 by the overexpression of miR-155 suppresses osteoblast differentiation, whereas the overexpression of SOCS1 by the underexpression of miR-155 partially reduces the suppression of osteoblast differentiation (Wua et al., 2012). In this study,

it's have been noticed that in the bones of 8 weeks of the onset of type 2 diabetes mellitus, the change in the expression of miR-155 was non-significant, but the expression of SOCS1 was significantly ($p < 0.05$) decreased. The mode of modulation in the bone remodeling cycle is more probably toward suppressing osteoblast differentiation; because of the significant reduction in SOCS1 expression. This suggestion was backed up by looking at the serum and bone osteocalcin level in 8 weeks of the onset of T2DM, which implies a reduced bone formation; since they were decreased, the mode of modulation is probably going toward suppressing osteoblast differentiation.

It's been examined in a past study that the downregulation of miR-20a causes suppression of osteoblast differentiation (Jin-fang Zhang et al., 2011). In line with this, it's been found in this study that in the bones of 10 weeks of the duration of type 2 diabetes mellitus, the expression of miR-20a was significantly ($p < 0.05$) decreased. These findings directs that the modulation of the bone remodeling cycle by the decreased miR-20a is probably on the osteoblast, not the osteoclast.

A study has suggested that the PDCD4 gene is one of the miR-21 target genes (Hu et al., 2017). It's been reported that the overexpression of the PDCD4 gene by the underexpression of miR-21 causes suppression of osteoclastogenesis (Sugatani et al., 2011). In this study, similarly it's been observed that in the bones of 10 weeks of the onset of type 2 diabetes mellitus, the expression of miR-21 was significantly ($p < 0.05$) decreased, and the expression of PDCD4 was non-significantly increased, suggesting a possibility of suppressing osteoclastogenesis.

The increased expression of miR-29a downregulates the negative regulators of Wnt signaling [DKK1, KREMEN2, and SFRP2], which results in promoting

osteoblast differentiation (Kapinas et al., 2010). Furthermore, the expression of miR-29a reduces non-collagenous matrix proteins, which leads to acceleration in extracellular mineralization (Kapinas et al., 2009). It's been investigated that apoptosis controls the rate of extracellular mineralization, the higher the apoptosis, the higher the rate of extracellular mineralization (Roy et al., 2010). In this study, it's has been seen that in the bones of 10 and 14 weeks of the duration of type 2 diabetes mellitus, the expression of miR-29a was non-significantly decreased, the expression of the target genes, DKK1, KREMEN2, and SFRP2 were not detected in the samples. Previous studies have shown miR-29a is necessary for human osteoblast differentiation and decreased miR-29a levels increases in DKK1 levels and suppresses the bone formation (Kapinas et al., 2010).

The apoptotic cells were significantly ($p < 0.05$) increased at the 10th and 14th week of onset of T2DM. Although there was a significant increase of apoptotic cells in 10th and 14th week of the onset of T2DM when compared with controls, there was no significant difference between the apoptotic cells and the live cells within the group of 10th and 14th week of the onset of T2DM. This means that the rate of extracellular mineralization is not high, instead, it triggers the start of extracellular mineralization.

This study found that in the bones of 10 weeks of the onset of type 2 diabetes mellitus, the expression of miR-31 was non-significantly decreased and the expression of RhoA was significantly ($p < 0.05$) increased. The RhoA gene is one of the miR-31 target genes (Mizoguchi et al., 2013). The literature review suggested that the inhibition of miR-31 leads to raised expression of the RhoA gene, which affects the bone remodeling cycle by suppressing osteoclastogenesis and bone resorption (Mizoguchi et al., 2013). Correspondingly in this study, indicating a possibility of

suppression in osteoclastogenesis and bone resorption at 10 weeks of the onset of type 2 diabetes mellitus.

Osteoblast differentiation is inhibited by the expression of miR-155 through downregulating SMAD proteins (Gu et al., 2017). SMAD7 is one the proteins involved in Smad signaling (Xu et al., 2016). In this study, it's been observed that in the bones of 10 weeks of the onset of type 2 diabetes mellitus, the expression of miR-155 was significantly ($p < 0.05$) decreased, and the expression of SMAD7 was not detected. Decreased expression of miR-155 causes hyperglycemia, impaired glucose tolerance, and insulin resistance (Lin et al., 2016).

As previous studies mentioned that the upregulation of miR-20a could affect the osteoblasts by promoting their differentiation by downregulating the expression of the PPARG gene, BAMBI gene, and CRIM1gene, which involved in differentiation and developmental processes (Bellavia et al., 2019; Jin-fang Zhang et al., 2011). In this study, a significant difference was not found in the expression of miR-20a levels between control and diabetic bone samples with 14 weeks of the onset of type 2 diabetes mellitus, and the target gene PPARG, BAMBI, and CRIM1 were not detected. PPARγ2 gene is linked to a genetic risk factor for type 2 diabetes mellitus and its effect becomes more manifest when diabetes is accompanied by obesity (Pattanayak et al., 2014).

It's been investigated in the literature review that the silencing of miR-21 affects the bone remodeling cycle by impairing osteoclastogenesis through overexpression of PDCD4 (Sugatani et al., 2011). Equivalently, in this study, it's been noticed that in the bones of 14 weeks of the onset of type 2 diabetes mellitus, the expression of miR-21 was non-significantly decreased, and the expression of the target

gene PDCD4 was not detected. These results suggest a possible impairment of osteoclastogenesis.

The overexpression of the RhoA gene by the inhibition of miR-31 leads to the suppression of osteoclastogenesis and bone resorption, whereas the overexpression of miR-31 downregulates the RhoA gene, which leads to the promotion of osteoclastogenesis (Mizoguchi et al., 2013). In this study, it's been noticed that in the bones of 14 weeks of the onset of type 2 diabetes mellitus, the expression of miR-31 was non-significantly decreased, and the expression of RhoA was non-significantly decreased as well; could be due to less number of samples. It is hard to claim which mode of modulation in the bone remodeling cycle is miR-31 posing in 14 weeks of the onset of T2DM. MiR-31 is a positive regulator of osteoclast formation and bone resorption.

The overexpression of miR-155 downregulates the SOCS1 gene, which results in suppressing osteoblast differentiation (Wua et al., 2012). Thus in this study, it's been found out that in the bones of 14 weeks of the onset of type 2 diabetes mellitus, the expression of miR-155 was non-significantly increased, and the expression of miR-155 was significantly ($p < 0.01$) increased in the sera of 14 weeks of the onset of T2DM. Moreover, the expression of SOCS1 was significantly ($p < 0.05$) decreased, indicating a possible suppression of osteoblast differentiation.

Clinically, microRNA drugs can be used to treat certain diseases through suppressing or promoting the levels of mRNA based on recent in-vivo studies (Roser et al., 2018). Based on that idea, it might be possible to detect the expression of the microRNAs in serum samples; to use them clinically for diagnosis. In this study, the expression of miR-21 in the sera of 8 weeks of the duration of T2DM was increased

non-significantly (p = 0.4140), which is matching with the result of the bones of 8 weeks of the duration of T2DM. In addition, the expression of miR-21 in the sera of 10 weeks of the duration of T2DM was significantly (p = 0.0513) decreased, and this result goes in line with the result of the bones of 10 weeks of the duration of T2DM. The expression of miR-155 in the sera of 14 weeks of the duration of T2DM was significantly (p = 0.0102) increased, and that's equivalent to the result of the bones of 14 weeks of the duration of T2DM. These findings suggest that those microRNAs could be highly expressed in sera compared to the other microRNAs and can be used as potential biomarkers.

By the use of a micro-CT, the previous study characterized the trabecular microarchitecture of the T2DM femoral head, the study stated a significant elevation in trabecular separation and a decrease in bone volume, trabecular number, and thickness (Mohsin et al., 2019). In addition to that, the study suggested that the trabecular structure was affected negatively by the onset of T2DM, and that increases the risk of hip fractures (Mohsin et al., 2019). The data obtained in this study using the histological techniques is consistent with an earlier study (Mohsin et al., 2019). It was found that there was a significant decrease (p <0.05) in trabecular bone volume in 10 and 14 weeks of the onset of T2DM. For the trabecular separation, there was a significant (p < 0.001) increase in 14 weeks of the onset of T2DM, an non-significant increase in 10 weeks of the onset of T2DM and no change in 8 weeks of the onset of T2DM. For the trabecular thickness, there was a significant (p < 0.01) decrease in 14 weeks of the onset of T2DM, a non-significant decrease in 10 weeks of the onset of T2DM, and no change in 8 weeks of the onset of T2DM. For the trabecular number, there was a significant (p < 0.05) decrease in 10 weeks of the onset of T2DM, and a non-significant decrease in 8 and 14 weeks of the onset of T2DM. These trabecular

measurements indicate that type 2 diabetes mellitus have an adverse effect on the trabecular structure, suggesting increased susceptibility to hip fractures.

Chapter 5: Conclusion

To sum up, miR-20a, miR-21, miR-29a, miR-31, and miR-155 are known to be responsible to regulate the bone remodeling cycle, and their dysregulation has been described in bone disorders like osteoporosis.

The study 1) identified the changes in some miRNAs levels related to bone remodeling cycle in bones of type 2 diabetic rats, 2) measured the miRNAs in the sera to use them as a potential biomarker, and 3) investigated the target genes for those miRNAs to understand the mechanisms involved in skeletal fragility related to T2DM and their potential use in therapeutics.

This current study revealed that in 8 weeks of the duration of T2DM, the dysregulation of miR-20a, miR-21, miR-29a, miR-31, and miR-155 affects the bone remodeling cycle by promoting osteoclastogenesis, and suppressing osteoblast differentiation. In 10 weeks of the duration of T2DM, the dysregulation of miR-20a, miR-21, miR-29a, miR-31, and miR-155 affects the bone remodeling cycle by suppressing osteoclastogenesis, and suppressing bone formation. In 14 weeks of the duration of T2DM, the dysregulation of miR-20a, miR-21, miR-29a, miR-31, and miR-155 affects the bone remodeling cycle by suppressing osteoclastogenesis and suppressing osteoblast differentiation. T2DM is regarded as a disease of slow turnover (Purnamasari et al., 2017). In addition, the results also show that it suppresses osteoblast differentiation and at late stages of diabetes (10,14 weeks) also suppresses osteoclast activity. Moreover, miR-21 and miR-155 could be used as potential serum biomarkers. The study also suggests, the longer duration of T2DM affects adversely the bone microstructure, indicating an increased bone fragility.

5.1 Future Work

Many clinical studies have shown an increased cases of fracture or bone injuries in type 2 diabetic patients. This suggests a close relation between type 2 diabetes and osteopathies such as osteoporosis. Another group of researchers have shown certain alteration in the microRNAs expression in case of osteoporetic animal models. Therefore, in this study the interest was in finding the expression of those microRNAs which were seen to be altered in osteoporetic animal models. Hence, the expression of microRNAs were determined in type 2 diabetic rats. It's been found that certain miRNAs to be differrentially expressed in type 2 diabetics rats. These microRNAs target the key regulators of bone remodeling cycle. This gives an insight for the possible relation between type 2 diabetes and osteoporosis. For future studies, it would be fascinating to decode the possible association between type 2 diabetes and osteoporosis. It would be interesting to analyze the expression of the differentially dysregulated miroRNAs from this current study in the osteoporetic rat models. Furthermore, the effect of microRNAs can be studied further on protein level using western blotting and immunohistochemistry. This will give a functional understanding of each microRNAs and target genes. Addiotionally, analyzing the levels of bone resorption markers in order to understand the modulation of bone remodeling cycle is crucial to be further studied.

References

Alfaro, M. P., Vincent, A., Saraswati, S., Thorne, C. A., Hong, C. C., Lee, E., & Young, P. P. (2010). sFRP2 Suppression of Bone Morphogenic Protein (BMP) and Wnt Signaling Mediates Mesenchymal Stem Cell (MSC) Selfrenewal Promoting Engraftment and Myocardial Repair. *Journal of Biological Chemistry*, *285*(46), 35645–35653. https://doi.org/10.1074/jbc.M110.135335

An, S., Gao, Y., Huang, Y., Jiang, X., Ma, K., & Ling, J. (2015). Short-term effects of calcium ions on the apoptosis and onset of mineralization of human dental pulp cells in vitro and in vivo. *International Journal of Molecular Medicine*, *36*(1), 215–221.

Baglìo, S. R., Devescovi, V., Granchi, D., & Baldini, N. (2013). MicroRNA expression profiling of human bone marrow mesenchymal stem cells during osteogenic differentiation reveals Osterix regulation by miR-31. *Gene*, *527*(1), 321–331. https://doi.org/10.1016/j.gene.2013.06.021

Bandiera, S., Pfeffer, S., Baumert, T. F., & Zeisel, M. B. (2015). miR-122 – A key factor and therapeutic target in liver disease. *Journal of Hepatology*, *62*(2), 448–457. https://doi.org/10.1016/j.jhep.2014.10.004

Batra, S. (2018). *Hematoxylin and Eosin (H&E) Staining Protocol – Principle, Procedure, Results*. Retrieved March 18, 2020, from https://paramedicsworld.com/histopathology-practicals/hematoxylin-eosin-staining-protocol-principle-procedure-results/medical-paramedical-studynotes#:~:text=Hematoxylin and Eosin are the,nucleus and the cytoplasmic inclusions.&text=Alum acts as a mordant,in the presence of alkali.

Bellavia, D., De Luca, A., Carina, V., Costa, V., Raimondi, L., Salamanna, F., & Giavaresi, G. (2019). Deregulated miRNAs in bone health: Epigenetic roles in osteoporosis. *Bone*, 52–75.

Berg, J. M., Tymoczko, J. L., Gatto, J. G., & Stryer, L. (2015). RNA Synthesis and Processing. In *Biochemistry* (8th ed., pp. 859–892). W. H. Freeman and Company.

Bhamb, N., Kanim, L. E. A., Maldonado, R. C., Nelson, T. J., Salehi, K., Glaeser, J. D., & Metzger, M. F. (2019). The impact of type 2 diabetes on bone metabolism and growth after spinal fusion. *The Spine Journal*, *19*, 1085–1093. https://doi.org/10.1016/j.spinee.2018.12.003

Bird, S. J., & Parlee, M. B. (2000). OF MICE AND MEN (AND WOMEN AND CHILDREN): SCIENTIFIC AND ETHICAL IMPLICATIONS OF ANIMAL MODELS. *Prog. Neuro-Psychopharmacol. & Biol. Psychiat.*, *24*, 1219–1227.

Blüml, S., Bonelli, M., Niederreiter, B., Puchner, A., Mayr, G., Hayer, S., Koenders, M. I., Berg, W. B. van den, Smolen, J., & Redlich, K. (2011). Essential role of microRNA-155 in the pathogenesis of autoimmune arthritis in mice. *Arthritis & Rheumatism*, *63*(5), 1281–1288. https://doi.org/10.1002/art.30281

Chatterjee, S., Khunti, K., & Davies, M. J. (2017). Type 2 diabetes. *The Lancet*, *389*, 2239–2251. https://doi.org/10.1016/S0140-6736(17)30058-2

Che, J., Wang, W., Huang, Y., Zhang, L., Zhao, J., Zhang, P., & Yuan, X. (2019). miR-20a inhibits hypoxia-induced autophagy by targeting ATG5/FIP200 in colorectal cancer. *Molecular Carcinogenesis*, 1234–1247.

Chung, D. J., Choi, H. J., Chung, Y.-S., Lim, S. K., Yang, S.-O., & Shin, C. S. (2013). The prevalence and risk factors of vertebral fractures in Korean patients with type 2 diabetes. *Journal of Bone and Mineral Metabolism*, *31*, 161–168. https://doi.org/10.1007/s00774-012-0398-5

Clarke, B. (2008). Normal Bone Anatomy and Physiology. *Clinical Journal of the American Society of Nephrology*, *3*(3), 131–139. https://doi.org/10.2215/CJN.04151206

Compston, J. E., Mcclung, M. R., & Leslie, W. D. (2019). Osteoporosis. *Lancet*, *393*, 364–376. https://doi.org/10.1016/S0140-6736(18)32112-3

Crockett, J. C., Michael, J., Coxon, F. P., Lynne, J., Helfrich, M. H., Crockett, J. C., Rogers, M. J., Coxon, F. P., Hocking, L. J., & Helfrich, M. H. (2011). Bone remodelling at a glance. *Journal of Cell Science*, *124*(7), 991–998. https://doi.org/10.1242/jcs.063032

Cui, H., Zhang, C., Zhao, Z., Zhang, C., Fu, Y., Li, J., Chen, G., Lai, M., Li, Z., & Dong, S. (2020). Identification of cellular microRNA miR-188-3p with broad-spectrum anti-influenza A virus activity. *Virology Journal*, *17*(1), 12. https://doi.org/10.1186/s12985-020-1283-9

Davegårdh, C., García-calzón, S., Bacos, K., & Ling, C. (2018). DNA methylation in the pathogenesis of type 2 diabetes in humans. *Molecular Metabolism*, *14*, 12–25. https://doi.org/10.1016/j.molmet.2018.01.022

Delaisse, J.-M. (2014). The reversal phase of the bone-remodeling cycle: cellular prerequisites for coupling resorption and formation. *International Bone & Mineral Society*, *3*(561), 1–8. https://doi.org/doi:10.1038/bonekey.2014.56

Delany, A. M., Kalajzic, I., Bradshaw, A. D., Sage, E. H., & Canalis, E. (2003). Osteonectin-Null Mutation Compromises Osteoblast Formation, Maturation, and Survival. *Endocrinology*, *144*(6), 2588–2596. https://doi.org/doi: 10.1210/en.2002-221044

Dougherty, G. (1996). Quantitative CT in the measurement of bone quantity and bone quality for assessing osteoporosis. *Medical Engineering & Physics*, *18*(7), 557–568. https://doi.org/10.1016/1350-4533(96)00011-2

Eastell, R. (2013). Osteoporosis. *Medicine*, *41*(10), 586–591. https://doi.org/10.1016/j.mpmed.2013.07.014

Feng, X., & McDonald, J. M. (2011). Disorders of Bone Remodeling. *Annual Review of Pathology*, *6*, 121–145. https://doi.org/10.1146/annurev-pathol-011110-130203

Foessl, I., Kotzbeck, P., & Obermayer-Pietsch, B. (2019). miRNAs as novel biomarkers for bone related diseases. *Journal of Laboratory and Precision Medicine*, *4*. http://dx.doi.org/10.21037/jlpm.2018.12.06

Gao, Y., Fang, X., Vincent, D. F., Threadgill, D. W., Bartholin, L., & Li, Q. (2017). Disruption of postnatal folliculogenesis and development of ovarian tumor in a mouse model with aberrant transforming growth factor beta signaling. *Reproductive Biology and Endocrinology*, *15*(94), 1–12. https://doi.org/10.1186/s12958-017-0312-z

Georgess, D., Machuca-Gayet, I., Blangy, A., & Jurdic, P. (2014). Podosome organization drives osteoclast-mediated bone resorption. *Cell Adhesion & Migration*, *8*(3), 191–204. https://doi.org/10.4161/cam.27840

Gokita, K., Inoue, J., Ishihara, H., Kojima, K., & Inazawa, J. (2020). Therapeutic Potential of LNP-Mediated Delivery of miR-634 for Cancer Therapy. *Molecular Therapy - Nucleic Acids*, *19*, 330–338. https://doi.org/10.1016/j.omtn.2019.10.045

Gu, Y., Ma, L., Song, L., Li, X., Chen, D., & Bai, X. (2017). miR-155 inhibits mouse osteoblast differentiation by suppressing SMAD5 expression. *BioMed Research International*, *2017*. https://doi.org/10.1155/2017/1893520

Hadjidakis, D. J., & Androulakis, I. I. (2006). Bone Remodeling. *ANNALS NEW YORK ACADEMY OF SCIENCES*, 385–396. https://doi.org/10.1196/annals.1365.035

Heinz, A. (1992). Osteoporosis. *The American Council on Science and Health*, 01–20. https://www.acsh.org/news/1992/08/01/osteoporosis

Hu, C.-H., Sui, B.-D., Du, F.-Y., Shuai, Y., Zheng, C.-X., Zhao, P., & Jin, Y. (2017). miR-21 deficiency inhibits osteoclast function and prevents bone loss in mice. *Scientific Reports*, 42191. https://doi.org/10.1038/srep43191

Huang, W. (2017). MicroRNAs: biomarkers, diagnostics, and therapeutics. In *Bioinformatics in MicroRNA Research* (pp. 57–67). Springer.

Humbel, R. (1966). Biosynthesis of insulin. *The American Journal of Medicine*, *40*(5), 672–675. https://doi.org/10.1016/0002-9343(66)90147-1

Hurtado, M. D., & Vella, A. (2018). What is type 2 diabetes ? *Medicine*, *47*(1), 10–15. https://doi.org/10.1016/j.mpmed.2018.10.010

James, E. N., Delany, A. M., & Nair, L. S. (2014). Post-transcriptional regulation in osteoblasts using localized delivery of miR-29a inhibitor from nanofibers to enhance extracellular matrix deposition. *Acta Biomaterialia*, *10*(8), 3571–3580. https://doi.org/10.1016/j.actbio.2014.04.026

Janghorbani, M., Dam, R. M. Van, Willet, W. C., & Hu, F. B. (2007). Systematic Review of Type 1 and Type 2 Diabetes Mellitus and Risk of Fracture. *American Journal of Epidemiology*, *166*(5), 495–505. https://doi.org/10.1093/aje/kwm106

Jonason, J. H., Xiao, G., Zhang, M., Xing, L., & Chen, D. (2009). Post-translational Regulation of Runx2 in Bone and Cartilage. *Journal of Dental Research*, *88*(8), 693–703. https://doi.org/10.1177/0022034509341629

Kapinas, K., Kessler, C. B., & Delany, A. M. (2009). miR-29 Suppression of Osteonectin in Osteoblasts: Regulation During Differentiation and by Canonical Wnt Signaling. *Journal of Cellular Biochemistry*, *108*(1), 216–224. https://doi.org/10.1002/jcb.22243

Kapinas, K., Kessler, C., Ricks, T., Gronowicz, G., & Delany, A. M. (2010). miR-29 modulates Wnt signaling in human osteoblasts through a positive feedback loop. *Journal of Biological Chemistry*, *285*(33), 25221–25231.

Kenkre, J. S., & Bassett, J. H. D. (2018). The bone remodelling cycle. *Annals of Clinical Biochemistry*, *0*(0), 1–20. https://doi.org/10.1177/0004563218759371

Ko, J.-Y., Chuang, P.-C., Ke, H.-J., Chen, Y.-S., S., Un, Y.-C., & Wang, F.-S. (2015). MicroRNA-29a mitigates glucocorticoid induction of bone loss and fatty marrow by rescuing Runx2 acetylation. *Bone*, 80–88.

Leidig-Bruckner, G., Grobholz, S., Bruckner, T., Scheidt-Nave, C., Nawroth, P., & Schneider, J. G. (2014). Prevalence and determinants of osteoporosis in patients with type 1 and type 2 diabetes mellitus. *BMC Endocrine Disorders*, *14*(33), 1–13. https://bmcendocrdisord.biomedcentral.com/articles/10.1186/1472-6823-14-33

Li, N., Lee, W. Y.-W., Lin, S.-E., Ni, M., Zhang, T., Huang, X.-R., Lan, H.-Y., & Li, G. (2014). Partial loss of Smad7 function impairs bone remodeling, osteogenesis and enhances osteoclastogenesis in mice. *Bone*, *67*, 46–55. https://doi.org/10.1016/j.bone.2014.06.033

Lian, W.-S., Ko, J.-Y., Chen, Y.-S., Ke, H.-J., Hsieh, C.-K., Kuo, C.-W., Wang, S.-Y., Huang, B.-W., Tseng, J.-G., & Wang, F.-S. (2019). MicroRNA-29a represses osteoclast formation and protects against osteoporosis by regulating PCAF-mediated RANKL and CXCL12. *Cell Death & Disease Volume*, *10*(705), 1–14. https://doi.org/10.1038/s41419-019-1942-1

Lin, X., Qin, Y., Jia, J., Lin, T., Lin, X., Chen, L., Zeng, H., Han, Y., Wu, L., & Huang, S. (2016). MiR-155 enhances insulin sensitivity by coordinated regulation of multiple genes in mice. *PLoS Genetics*, *12*(10), e1006308. https://doi.org/10.1371/journal.pgen.1006308

Ling, C., & Ronn, T. (2019). Epigenetics in Human Obesity and Type 2 Diabetes. *Cell Metabolism*, *29*, 1028–1044. https://doi.org/10.1016/j.cmet.2019.03.009

Lodish, H., Berk, A., Kaiser, C. A., Krieger, M., Bretscher, A., Ploegh, H., & Scott, M. P. (n.d.). Signaling Pathways that Control Gene Expression. In *Molecular Cell Biology* (7th ed., p. 752). W. H. Freeman and Company.

Loh, H.-Y., Lau, Y.-Y., Lai, K.-S., & Osman, M. A. (2018). MicroRNAs in Bone Diseases: Progress and Prospects. In *Transcriptional and Post-transcriptional Regulation* (pp. 77–100). IntechOpen. http://dx.doi.org/10.5772/intechopen.79275

Lorentzon, M., & Cummings, S. R. (2015). Osteoporosis: the evolution of a diagnosis. *Journal of Internal Medicine*, *277*, 650–661. https://doi.org/10.1111/joim.12369

Mao, Z., Zhu, Y., Hao, W., Chu, C., & Su, H. (2019). MicroRNA-155 inhibition up-regulates LEPR to inhibit osteoclast activation and bone resorption via activation of AMPK in alendronate-treated osteoporotic mice. *International Union of Biochemistry and Molecular Biology Life*, *71*, 1916–1928. https://doi.org/DOI: 10.1002/iub.2131

Melton, L. J., Leibson, C. L., Achenbach, S. J., Therneau, T. M., & Khosla, S. (2008). Fracture Risk in Type 2 Diabetes: Update of a Population-Based Study. *Journal of Bone and Mineral Research*, *23*(8), 1334–1342. https://doi.org/10.1359/JBMR.080323

Mizoguchi, F., Murakami, Y., Saito, T., Miyasaka, N., & Kohsaka, H. (2013). miR-31 controls osteoclast formation and bone resorption by targeting RhoA. *Arthritis Research & Therapy*, *15*(R102), 1–7. https://doi.org/10.1186/ar4282

Moayeri, A., Mohamadpour, M., Mousavi, S. F., Shirzadpour, E., Mohamadpour, S., & Amraei, M. (2017). Fracture risk in patients with type 2 diabetes mellitus and possible risk factors: a systematic review and meta-analysis. *Therapeutics and Clinical Risk Management*, *13*, 455–468. https://doi.org/10.2147/TCRM.S131945

Mohsin, S., Kaimala, S., Sunny, J. J., Adeghate, E., & Brown, E. M. (2019). Type 2 Diabetes Mellitus Increases the Risk to Hip Fracture in Postmenopausal Osteoporosis by Deteriorating the Trabecular Bone Microarchitecture and Bone Mass. *Journal of Diabetes Research*, *2019*(3876957), 10 pages. https://doi.org/10.1155/2019/3876957

Mokobi, F. (2020). *Masson's Trichrome Staining*. Retrieved March 10, 2020, from https://microbenotes.com/massons-trichrome-staining/#principle-of-the-massons-trichrome-staining

Monami, M., Cresci, B., Colombini, A., Pala, L., Balzi, D., Gori, F., Chiasserini, V., Marchionni, N., Rotella, C. M., & Mannucci, E. (2008). Bone Fractures and Hypoglycemic Treatment in Type 2 Diabetic Patients. *Diabetes Care*, *31*(2), 199–203. https://doi.org/10.2337/dc07- 1736

Mukaiyama, K., Kamimura, M., Uchiyama, S., Ikegami, S., Nakamura, Y., & Kato, H. (2015). Elevation of serum alkaline phosphatase (ALP) level in postmenopausal women is caused by high bone turnover. *Aging Clinical and Experimental Research*, *27*(4), 413–418. https://doi.org/10.1007/s40520-014-0296-x

Nelson, D. L., & Cox, M. L. (2005). Regulation of Gene Expression. In *Lehninger Principles of Biochemistry* (4th ed., pp. 1081–1119). W. H. Freeman and Company.

OpenStax. (2013a). Bone Tissue and the Skeletal System. In *Anatomy and Physiology*. Retrieved May 9, 2020, from https://opentextbc.ca/anatomyandphysiology/chapter/6-3-bone-structure/

OpenStax. (2013b). The Endocrine Pancreas. In *Anatomy and Physiology*. Retrieved May 9, 2020, from https://opentextbc.ca/anatomyandphysiology/chapter/17-9-the-endocrine-pancreas/

Palmieri, A., Pezzetti, F., Brunelli, G., Scapoli, L., Muzio, L. Lo, Scarano, A., Martinelli, M., & Carinci, F. (2007). Calcium Sulfate Acts on the miRNA of MG63E Osteoblast-Like Cells. *Journal of Biomedical Materials Research Part B: Applied Biomaterials*, 369–374. https://doi.org/DOI: 10.1002/jbm.b.30880

Park, S.-Y., Lee, J. H., Ha, M., Nam, J.-W., & Kim, V. N. (2009). miR-29 miRNAs activate p53 by targeting p85α and CDC42. *Nature Structural & Molecular Biology*, *16*(1), 23–29.

Pattanayak, A. K., Bankura, B., Balmiki, N., Das, T. K., Chowdhury, S., & Das, M. (2014). Role of peroxisome proliferator-activated receptor gamma gene polymorphisms in type 2 diabetes mellitus patients of W est B engal, I ndia. *Journal of Diabetes Investigation*, *5*(2), 188–191.

Pinzone, J. J., Hall, B. M., & Shaughnessy, J. D. (2009). The role of Dickkopf-1 in bone development, homeostasis, and disease. *Blood*, *113*(3), 517–525. https://doi.org/10.1182/blood-2008-03-145169

Plotkin, L. I. (2014). Apoptotic osteocytes and the control of targeted bone resorption. *Current Osteoporosis Reports*, *12*(1), 121–126.

Purnamasari, D., Puspitasari, M. D., Setiyohadi, B., Nugroho, P., & Isbagio, H. (2017). Low bone turnover in premenopausal women with type 2 diabetes mellitus as an early process of diabetes-associated bone alterations: a cross-sectional study. *BMC Endocrine Disorders*, *17*(72), 1–8. https://doi.org/10.1186/s12902-017-0224-0

Retting, K. N., Song, B., Yoon, B. S., & Lyons, K. M. (2009). BMP canonical Smad signaling through Smad1 and Smad5 is required for endochondral bone formation. *Development*, *136*(7), 1093–1104. https://doi.org/10.1242/dev.029926

Rosen, A. D. (1981). Notes on technic: end-point determination in EDTA decalcification using ammonium oxalate. *Stain Technology*, *56*(1), 48–49.

Roser, A., Gomes, L. C., Schünemann, J., & Maass, F. (2018). Circulating miRNAs as Diagnostic Biomarkers for Parkinson ' s Disease. *Frontiers in Neuroscience*, *12*(625), 1–9. https://doi.org/10.3389/fnins.2018.00625

Rossini, M., Adami, S., Bertoldo, F., Diacinti, D., Gatti, D., Giannini, S., Giusti, A., Malavolta, N., Minisola, S., Osella, G., Pedrazzoni, M., Sinigaglia, L., Viapiana, O., & Isaia, G. C. (2016). Guidelines for the diagnosis, prevention and management of osteoporosis. *Reumatismo*, *68*(1), 1–39. https://doi.org/10.4081/reumatismo.2016.870

Roy, R., Kudryashov, V., Binderman, I., & Boskey, A. L. (2010). The Role of Apoptosis in Mineralizing Murine vs. Avian Micromass Culture Systems. *Journal of Cellular Biochemistry*, *111*(3), 653–658. https://doi.org/doi:10.1002/jcb.22748.

Savi, F. M., Brierly, G. I., Baldwin, J., Theodoropoulos, C., & Woodruff, M. A. (2017). Comparison of Different Decalcification Methods Using Rat Mandibles as a Model. *Journal of Histochemistry & Cytochemistry*, *65*(12), 705–722. https://doi.org/10.1369/0022155417733708

Schulze, J., Seitz, S., Saito, H., Schneebauer, M., Marshall, R. P., Baranowsky, A., Busse, B., Schilling, A. F., Friedrich, F. W., Albers, J., Spiro, A. S., Zustin, J., Streichert, T., Ellwanger, K., Niehrs, C., Amling, M., Baron, R., & Schinke, T. (2010). Negative Regulation of Bone Formation by the Transmembrane Wnt Antagonist Kremen-2. *PLoS ONE*, *5*(4), e10309. https://doi.org/10.1371/journal.pone.0010309

Singh, S., Kumar, D., & Lal, A. K. (2015). Serum Osteocalcin as a Diagnostic Biomarker for Primary Osteoporosis in Women. *Journal of Clinical and Diagnostic Research*, *9*(8), 4–7. https://doi.org/10.7860/JCDR/2015/14857.6318

Souza, J. A. C. de, Nogueira, A. V. B., Souza, P. P. C. de, Oliveira, G. J. P. L. de, Medeiros, M. C. de, Garlet, G. P., Cirelli, J. A., & Junior, C. R. (2017). Suppressor of cytokine signaling 1 expression during LPS-induced inflammation and bone loss in rats. *Brazilian Oral Research*, *31*(e75). https://doi.org/10.1590/1807-3107bor-2017.vol31.0075

Sugatani, T., Vacher, J., & Hruska, K. A. (2011). A microRNA expression signature of osteoclastogenesis. *Blood*, *117*(13), 3648–3657. https://doi.org/10.1182/blood-2010-10-311415.The

Sun, K.-T., Chen, M., Tu, M.-G., Wang, I.-K., Chang, S.-S., & Li, C.-Y. (2015). MicroRNA-20a regulates autophagy related protein-ATG16L1 in hypoxia-induced osteoclast differentiation. *Bone*, 145–153.

Taylor, R., Al-mrabeh, A., & Sattar, N. (2019). Personal Review Understanding the mechanisms of reversal of type 2 diabetes. *THE LANCET Diabetes & Endocrinology*, *8587*(19), 1–11. https://doi.org/10.1016/S2213-8587(19)30076-2

Torbati, P. M., Asadi, F., & Fard-Esfahani, P. (2019). Circulating miR-20a and miR-26a as Biomarkers in Prostate Cancer. *Asian Pacific Journal of Cancer Prevention*, 1453–1456.

Urs, S., Henderson, T., Le, P., Rosen, C. J., & Liaw, L. (2012). Tissue-specific expression of Sprouty1 in mice protects against high-fat diet-induced fat accumulation, bone loss and metabolic dysfunction. *British Journal of Nutrition*, *108*(6), 1025–1033. https://doi.org/10.1017/S0007114511006209

Walsh, J. S. (2017). Normal bone physiology , remodelling and its hormonal regulation. *Surgery*, *36*(1), 1–6. https://doi.org/10.1016/j.mpsur.2017.10.006

Watson, J. D., Gann, A., Baker, T. A., Levine, M., Bell, S. P., Losick, R., & Harrison, S. C. (2014). Regulatory RNAs. In *Molecular Biology of the Gene* (pp. 701–732). Pearson Education, Inc.

Wua, T., Xie, M., Wang, X., Jiangb, X., Li, J., & Huang, H. (2012). miR-155 modulates TNF-α-inhibited osteogenic differentiation by targeting SOCS1 expression. *Bone*, *51*(3), 498–505. https://doi.org/10.1016/j.bone.2012.05.013

Xu, F., Liu, C., Zhou, D., & Zhang, L. (2016). TGF-β/SMAD pathway and its regulation in hepatic fibrosis. *Journal of Histochemistry & Cytochemistry*, *64*(3), 157–167.

Yalochkina, T. O., Belaya, Z. E., Rozhinskaya, L. Y., Antsiferov, M. B., Dzeranova, L. K., & Melnichenko, G. A. (2016). Bone fractures in patients with type 2 diabetes mellitus: prevalence and risk factors. *Diabetes Mellitus*, *19*(5), 359–365. https://doi.org/10.14341/DM7796

Yin, X., Zhou, C., Li, J., Liu, R., Shi, B., Yuan, Q., & Zou, S. (2019). Autophagy in bone homeostasis and the onset of osteoporosis. *Bone Research*, *7*(1), 1–16.

Zaitseva, O. V., Shandrenko, S. G., & Veliky, M. M. (2015). Biochemical markers of bone collagen type I metabolism. *Ukrainian Biochemical Journal*, *87*(1), 21–32. https://doi.org/UDC 577.11:611.018.43

Zhang, J., Zhao, H., Chena, J., Xia, B., Jin, Y., Wei, W., & Huang, Y. (2012). Interferon-β-induced miR-155 inhibits osteoclast differentiation by targeting SOCS1 and MITF. *FEBS Letters*, 3255–3262.

Zhang, Jin-fang, Fu, W., He, M., Xie, W., Lv, Q., Li, G., Wang, H., Lu, G., Hu, X., Jiang, S., Li, J., Marie, C. M., Zhang, Y., & Kung, H. (2011). MiRNA-20a promotes osteogenic differentiation of human mesenchymal stem cells by co-regulating BMP signaling. *RNA Biology*, *8*(5), 829–838. https://doi.org/10.4161/rna.8.5.16043

Zhang, Jin, Tu, Q., Grosschedl, R., Kim, M. S., Griffin, T., Drissi, H., Yang, P., & Chen, J. (2011). Roles of SATB2 in Osteogenic Differentiation and Bone Regeneration. *Tissue Engineering: Part A*, *17*(13–14), 1767–1776. https://doi.org/10.1089/ten.tea.2010.0503

Zhang, M., Lv, X.-Y., Li, J., Xu, Z.-G., & Chen, L. (2008). The Characterization of High-Fat Diet and Multiple Low-Dose Streptozotocin Induced Type 2 Diabetes Rat Model. *Journal of Diabetes Research*, *2008*(Article ID 704045), 9 pages. https://doi.org/10.1155/2008/704045

Zhao, W., Zhang, W., Yang, B., Sun, J., & Yang, M. (2019). NIPA2 regulates osteoblast function via its effect on apoptosis pathways in type 2 diabetes osteoporosis. *Biochemical and Biophysical Research Communications*, *513*(4), 883–890. https://doi.org/10.1016/j.bbrc.2019.04.030

Zoch, M. L., Clemens, T. L., & Riddle, R. C. (2016). New insights into the biology of osteocalcin. *Bone*, *82*, 42–49. https://doi.org/10.1016/j.bone.2015.05.046

Appendix

8 weeks - Control		
Animal Assigned No.	Weight (g)	Blood Glucose Level
Animal #6	328.5	109
Animal #7	217.5	114
Animal #8	247.5	113

8 weeks – T2DM		
Animal Assigned No.	Weight (g)	Blood Glucose Level
Animal #23	435	435
Animal #24	308.5	558
Animal #25	262.5	428

10 weeks - Control		
Animal Assigned No.	Weight (g)	Blood Glucose Level
Animal #9	263	127
Animal #10	209	107
Animal #11	230	113

10 weeks – T2DM		
Animal Assigned No.	Weight (g)	Blood Glucose Level
Animal #12	172	458
Animal #13	224	499
Animal #14	228	447

14 weeks - Control		
Animal Assigned No.	Weight (g)	Blood Glucose Level
Animal #1	250	119
Animal #2	220	131
Animal #16	252	117

14 weeks – T2DM		
Animal Assigned No.	Weight (g)	Blood Glucose Level
Animal #13	235	123
Animal #15	187	457
Animal #23	282.5	493